



# THE EFFECTS OF ADDITION OF COPPER ON THE STRUCTURE AND ANTIBACTERIAL PROPERTIES OF BIOMEDICAL GLASSES

Leyla Mojtabavi<sup>[a]</sup> and Amir Razavi<sup>[a]\*</sup>

**Keywords:** Biomedical glasses, copper, structure, XPS, antibacterial.

The properties of 3 and 6 mol % copper-containing bioactive glasses have been evaluated. The structure of the doped glass has been studied by X-ray diffraction (XRD), X-ray photoelectron survey (XPS), high-resolution scans and NMR spectroscopy. The results indicated that copper acts as a network modifier in the glass composition and copper-containing glasses show a less connected microstructure. Differential Thermal Analysis (DTA) showed that the copper addition in the glass lowers the glass transition temperature. Antibacterial studies showed that doping with copper enhances the antibacterial effect of the bioglass.

\* Corresponding Authors

Tel: +989147560142

Email: amir.rzv87@gmail.com

[a] University of Tehran, Department of Engineering Science, Enghelab Ave, Tehran, Iran 111554563

## INTRODUCTION

Bioglass®, also known as 45S5 glass, was first discovered by Larry Hench in the late 1960s in order to develop a material to fill bone voids without being rejected by the body.<sup>1</sup> The initial 45S5 Bioglass® that was introduced by Hench was a silicate-based glass with a composition of 45SiO<sub>2</sub>-24.5Na<sub>2</sub>O-24.5CaO-6P<sub>2</sub>O<sub>5</sub> in weight percent.<sup>2</sup> Early studies on this composition showed its capacity to form a chemical bond with living tissue.<sup>3</sup> As a biodegradable material, the bioglass degrades slowly in an aqueous solution and stimulates new bone formation and growth through a chemical bond to the existing bone tissue.<sup>4</sup> The dissolution of the glass and formation of the calcium phosphate layer on the surface of glass initiates the osteogenesis mechanism. Besides, the release of dissolution products from the glass into surrounding physiological solutions can provide therapeutic effects to adjacent tissue.<sup>5</sup>

In the past few years, different compositions of bioactive glasses have been developed to improve the properties and take full advantage of these glasses for biomedical applications. The bioactive glasses have been used in dental applications, applied as bioactive coatings on the surface of metal implants, used as bioactive components of composites and have been made into synthetic bone scaffolds.<sup>2,3,6-8</sup> The diversity of their applications comes from the glass composition and how the incorporation of new elements can modify it and therefore changing the glass structure.<sup>2</sup>

The atomic structure of the glass significantly affects its properties and in particular, the bioactivity and degradation rate, which directly influences the formation of calcium phosphate surface layer and cell viability.<sup>9</sup> The key compositional factor in the determination of the bioactivity

of these glasses is the SiO<sub>2</sub> content.<sup>10</sup> The bioactive glass composition consists of relatively low amounts of silica and high concentrations of network modifiers such as Ca and Na to facilitate its dissolution in the physiological solutions.<sup>8,10</sup> The structure of bioactive glasses can be described in the same way as other silicate glasses, which have been well characterized in terms of the arrangement of the SiO<sub>4</sub> tetrahedron coordination.<sup>11</sup> The number of tetrahedrons determines the size of the ring used to characterize the network. The structure of pure SiO<sub>2</sub> consists of a three-dimensional network of SiO<sub>4</sub> tetrahedra, and each tetrahedron is associated with bridging oxygen in the structure, through Si-O-Si bonding.<sup>12</sup> The addition of network modifying elements disrupt the linkage of SiO<sub>4</sub> tetrahedra and creates non-bridging oxygens.<sup>13</sup> As a result of incorporation of modifier ions, the disrupted glass network is now prone to hydrolysis in aqueous solutions, which is a critical step for the bioactivity of glass.<sup>5</sup>

Since the introduction of bioactive glass by Hench, a wide variety of chemical modifications have been proposed by the incorporation of different elements in the glass. Some of the ubiquitous elements are Zn, Ti, and Sr.<sup>14,15</sup> These elements have been added to the glass composition to improve its physical, mechanical and biological behaviour.<sup>9,16</sup> In this work, we have incorporated copper in bioactive glass composition. Copper is a monovalent/divalent cation acting as a network-modifier in the glass structure.<sup>17</sup> The addition of CuO at the expense of SiO<sub>2</sub> can make the glass composition more soluble in the physiological solution, which in turn can enhance the bioactivity. Irrespective of this role, copper may be beneficial to the biological properties associated with the resultant material as there are numerous reports on the positive antibacterial response associated with the use of copper.<sup>18,19</sup>

The main purpose of this study is to modify the glass composition with the incorporation of copper in the glass and to determine its structural effects on the glass network. Further, we aim to investigate any changes occurring in the antibacterial efficacy of the glass as a result of copper addition.

## EXPERIMENTAL

### Glass synthesis

Three different glass powders were synthesized, a control and two copper-containing glasses. The control glass (BG) was synthesized based on a  $\text{SiO}_2\text{-CaO-Na}_2\text{O-P}_2\text{O}_5$  composition. The copper-containing glasses contain 3 and 6 mol % of CuO at the expense of  $\text{SiO}_2$  (Table 1). The analytical grade reagents of  $\text{SiO}_2$ , CuO,  $\text{CaCO}_3$ ,  $\text{Na}_2\text{CO}_3$ ,  $\text{NH}_4\text{H}_2\text{PO}_4$  were mixed and milled for 30 min. The glass batch was then dried at 110 °C for 1 h and melted at 1400 °C for 5 h in a platinum crucible and shock quenched in water.

**Table 1.** Glass compositions (mol %) where  $\text{SiO}_2$  is substituted by CuO.

Bioglass	$\text{SiO}_2$	CaO	$\text{Na}_2\text{O}$	$\text{P}_2\text{O}_5$	CuO
BG	55	20	20	5	0
BG-3Cu	52	20	20	5	3
BG-6Cu	49	20	20	5	6

### X-Ray Diffraction

Synthesized glass powders were analyzed for their diffraction patterns using X-Ray Diffractometer (Shimadzu XRD-6100X) at 40 kV and 30 mA utilizing CuK $\alpha$  radiation. The range of angles was from 10° to 60°, at a step size of 0.03° and step time of 10 s.

### Differential Thermal Analysis

Differential Thermal Analysis (DTA) experiments were performed using an SDT Q600 DTA instrument. Around 25 mg of each of the glass powders were loaded in platinum pans, where one empty platinum pan was also used as a reference. DTA curves were collected in air from 25 °C to 1200 °C at the heating rate of 10 °C min<sup>-1</sup>.

### X-Ray Photoelectron Spectroscopy

X-Ray photoelectron spectroscopy (XPS) was performed using a VG-Microtech ESCA-2000 system with AlK $\alpha$  source ( $h\nu = 1486.6$  eV) at the output of 25.5 W. Before the sample loading, the glass powders were first kept in a vacuum oven at 90 °C for 30 min to dry the powders. During the test, the vacuum in the analysis chamber of the instrument was in the range of  $10^{-9}$ – $10^{-10}$  mBar. Survey scans and high-resolution spectra of glass powders were collected, and the binding energies referenced to the C1s at 284.6 eV.

### Magic Angle Spinning Nuclear Magnetic Resonance (MAS-NMR)

MAS-NMR was carried out on powdered glass samples using a DSX-200 FT-NMR. The measurements were conducted at a frequency of 39.77 MHz, with the spinning rate at the magic angle of 5 kHz for  $^{29}\text{Si}$  with a recycle time of 2.0 s. The reference material used to measure the chemical shift was tetramethylsilane (TMS).

### Antibacterial Agar Diffusion

The antibacterial efficacy of the glasses was tested using the agar diffusion test method. First, glass disks of the synthesized powders were prepared and kept under UV for 4 hours for sterilization. Bacteria were grown aerobically in liquid broth at 37 °C for 48 h. Glass disks were placed in petri-dish covered with bacterial agar. The agar plates were then inoculated with the bacteria solution using a sterile swab and kept in the incubator for 24 h at 37 °C. After 24 h, the samples were evaluated for their inhibition zone by measuring the size of the zone from the edge of the disk to the end of the inhibition zone.

## RESULTS AND DISCUSSION

In this study, a series of bioactive glass compositions were synthesized. BG is a bioactive control glass composed of  $\text{SiO}_2$ , CaO,  $\text{Na}_2\text{O}$ , and  $\text{P}_2\text{O}_5$ . BG-3Cu and BG-6Cu glasses contain incremental amounts of 3 and 6 mol % of CuO at the expense of  $\text{SiO}_2$ . The specific compositions are shown in table 1.

The initial characterization on glasses was to generate XRD patterns to identify if any crystalline phases were present in the glasses. XRD was performed on each glass composition (BG, BG-3Cu, and BG-6Cu), and results are presented in Figure 1. All three glasses show the characteristic amorphous curve for the silicate glasses at around 20 to 30 degrees. The amorphous hump arises from the glasses having no long-range atomic order in their molecular arrangement. The results from the diffractograms show that the glasses used for this study were predominantly amorphous in structure.

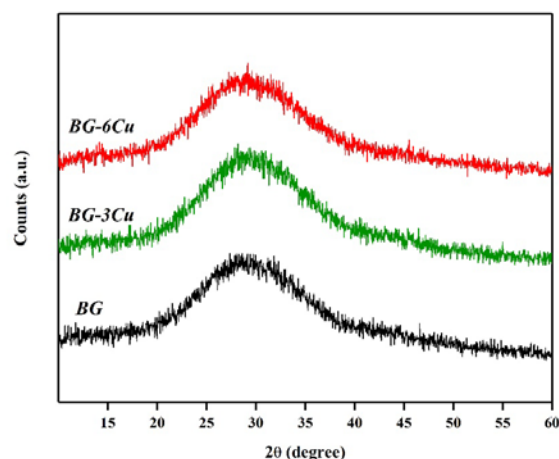


**Figure 1.** X-ray diffractograms of amorphous glass powders of BG, BG-3Cu, and BG-6Cu.

DTA was employed to measure the glass transition temperature ( $T_g$ ), and the glass crystallization temperature ( $T_c$ ), as a function of CuO addition. Figure 2 shows the DTA profiles of the glass series. The  $T_g$  of BG was found to be 646 °C, and the only  $T_c$  started at 936 °C. The  $T_g$  of BG-3Cu and BG-6Cu glasses were found to be at 611 °C and 590 °C, respectively. BG-3Cu showed two separate crystallization exotherm starting at 752 °C and 864 °C.

However, BG-6Cu had only one crystallization exotherm starting at 901 °C. Thus, it can be concluded that the CuO incorporation in the glass structure, shifts the glass transition to lower temperatures.  $T_g$  represents the temperature at which the glass begins the transformation from a solid material to a supercooled viscous liquid. Below  $T_g$ , the bonding in amorphous glass particles remains in a solid-state, however, as the temperature increases, the bonding within the glass becomes more mobile where the materials behave more like a liquid.  $T_g$  is a valuable material property as it represents the upper-temperature limit at which the glass can be used. In this case,  $T_g$  establishes the network disruption of the glass, where a more disrupted glass network has a lower  $T_g$ . Therefore, DTA is a useful technique, which can be used to determine if any differences in the glass structure exist between the glasses as a function of temperature. Preliminary analysis of the glass structure using DTA, suggests that the CuO addition decreases the network connectivity and hence increases its disruption. This was further investigated by XPS and NMR studies.

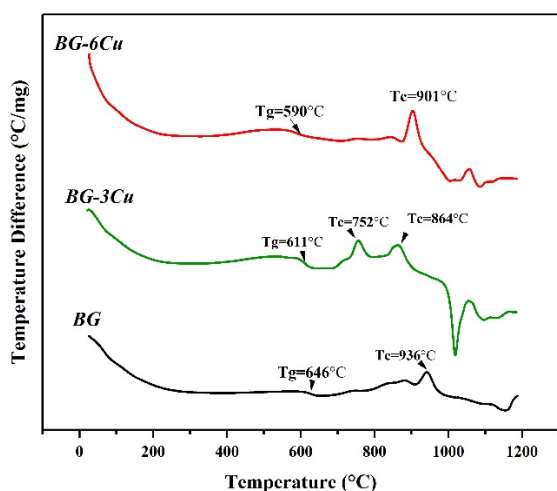


**Figure 2.** DTA profiles of BG, BG-3Cu, and BG-6Cu glasses.

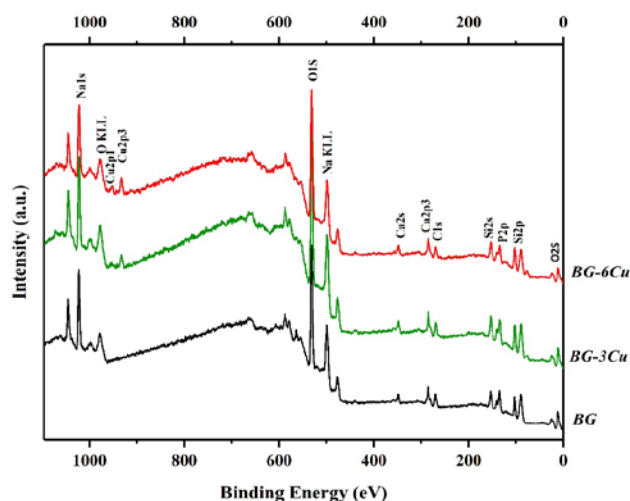


**Figure 3.** XPS survey scans of BG, BG-3Cu, and BG-6Cu glasses.

Compositional analysis of each glass was then determined using XPS survey scans, as shown in Figure 3. The survey scan of BG contains Na, O, Ca, P, and Si, with minor traces of carbon (C). Both BG-3Cu and BG-6Cu glasses show the

presence of Na, O, Cu, Ca, P, and Si with minor traces of carbon (C) as well, which corresponds with initial glass batch composition as shown in table 1. XPS survey scans were used to confirm the glass compositions and to find any possible contamination within the samples. High-resolution XPS was conducted on glasses to study the structure of glass as a function of CuO addition. The XPS O1s signals of glass series are shown in Figure 4. There is a compositional dependence on the binding energy of the O1s spectra of glasses when CuO is introduced in the composition. The peak for the control BG glass is centered at 532.93 eV. For the copper-containing glasses, the O1s binding energies were found to be at 532.71, and 532.59 eV for BG-3Cu, and BG-6Cu, respectively.

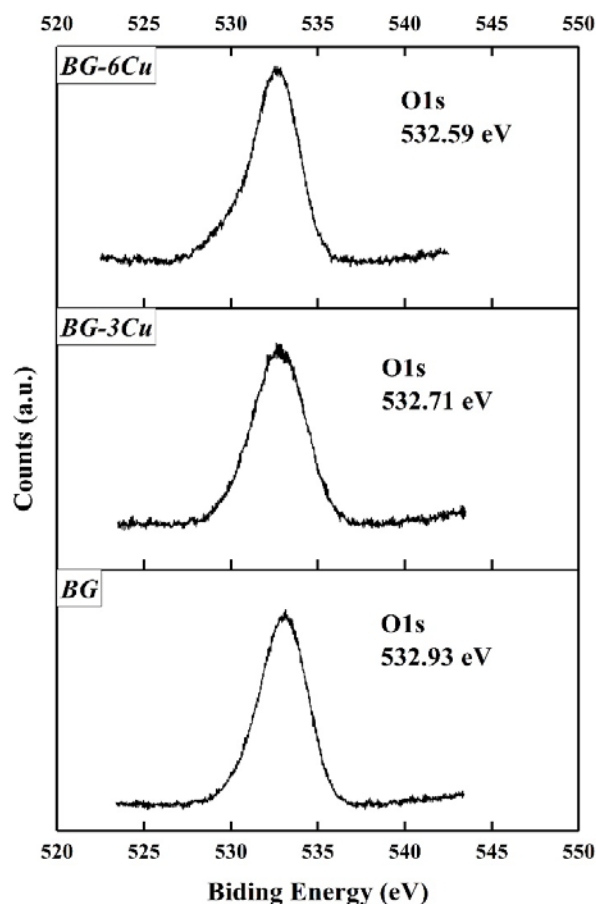


**Figure 4.** XPS O1s spectra of BG, BG-3Cu, and BG-6Cu glasses.

As can be seen from Figure 4, the incorporation of the Cu at the expense of Si shifts the O1s binding energy to lower values. Within the structure of oxide glasses, different oxygen species are present, as oxygen ions in the glass have different types of chemical bonding.<sup>20</sup> The bonding environment of the oxygen ions can be studied by analyzing the O1s spectrum of the glass. Therefore, XPS O1s is a very useful technique to study the contribution of bridging to non-bridging oxygens in the glass.<sup>21</sup> The lower binding energy peak of the O1s spectra is attributed to non-bridging oxygens, whereas the higher binding energy peak represents the bridging oxygens. The shift of the binding energies to lower values within the structure of copper glasses indicates an increase in the number of non-bridging oxygen at the expense of bridging oxygens.<sup>21</sup> This effect is suggesting that the Cu is acting as a network modifier in the glass by



breaking the Si-O-Si bonds and replacing them with Si-O-NBO. This is in agreement with the glass transition temperature studies observed with DTA. Glasses were further analyzed for their structure with  $^{29}\text{Si}$  MAS-NMR.

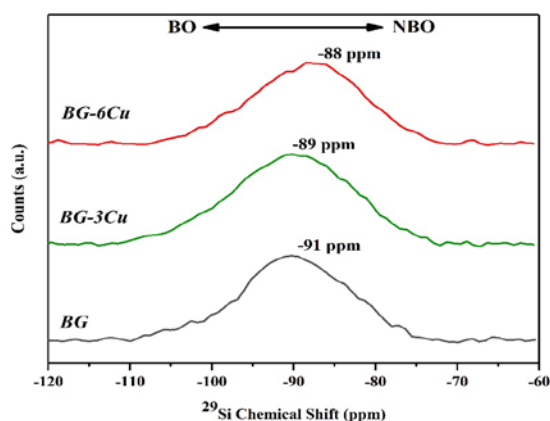


**Figure 5.**  $^{29}\text{Si}$  MAS-NMR spectra of glass series.

MAS-NMR was employed to analyze the structure of the glass series. Figure 5 shows the  $^{29}\text{Si}$  MAS-NMR spectra of the glass series, as  $\text{SiO}_2$  is the network former in the glass composition. The chemical shift indicates the local environment around the silicon atom. The silicon spectra in these glasses predominantly show a large, broad peak at around -75 to -105 ppm. The chemical shift in a four-coordinate silicon state is between -60 and -120 ppm.<sup>22</sup> The chemical shift of the spectra in the glass depends on the percentage of non-bridging, and bridging oxygens bound to the silicon. Increasing the number of non-bridging oxygens will increase the shielding of the nucleus of the atom, so the peak shifts to the positive direction. However, increasing the number of bridging oxygens moves the peak in a negative direction due to decreased shielding.<sup>23</sup>

The Q-structure of the glass relates to the number of BOs associated with the silicon atom. A silicon atom with 4-BOs can be assigned a Q-structure of  $\text{Q}^4$ , 3-BOs assumes a  $\text{Q}^3$ -structure, 2-BOs assumes a  $\text{Q}^2$ -structure etc.<sup>24</sup> MAS-NMR can be used to calculate the chemical shift position for identifying the Q-structure of silica glass. Chemical shifts have been identified at >-78ppm for  $\text{Q}^1$ , -80 ppm for  $\text{Q}^2$ , -90ppm for  $\text{Q}^3$  and -110ppm for  $\text{Q}^4$ .<sup>22</sup> The MAS-NMR spectra of the glasses tested in this work indicate predominant  $\text{Q}^3/\text{Q}^2$  structures due to the chemical shift occurring mostly between -85 and -95 ppm. However, the broadness of the peaks suggests that all Q-structures may be present in the glass. For BG, a high degree of asymmetry exists within the  $\text{Q}^4$  region of the spectra. The peaks obtained from the MAS-NMR spectra of the BG, BG-3Cu, and BG-6Cu glasses are centered at -91 ppm, -89 ppm and -88 ppm, respectively. It is evident with copper-containing glasses that their broad spectra predominantly occur at  $\text{Q}^3$  structure. However, a slight shift is happening towards the  $\text{Q}^2$  region of the spectra as they move more towards a positive direction. This suggests that copper glasses may contain higher quantities of  $\text{Q}^2$  structures and therefore contain a higher number of non-bridging oxygens compared to control.

The results obtained from DTA, XPS and NMR spectra suggest that the control glass is more structurally defined than the copper-containing glasses. Incorporation of the copper in the glass disrupts the glass network by increasing the number of non-bridging oxygens, which indicates that  $\text{CuO}$  acting as a network modifier in this glass system. Understanding the distribution of Q-species is essential because the formation of non-bridging oxygens will affect glass solubility, which plays a critical role in the dissolution of the particle surface that initiates the bioactive sequence.<sup>25</sup>

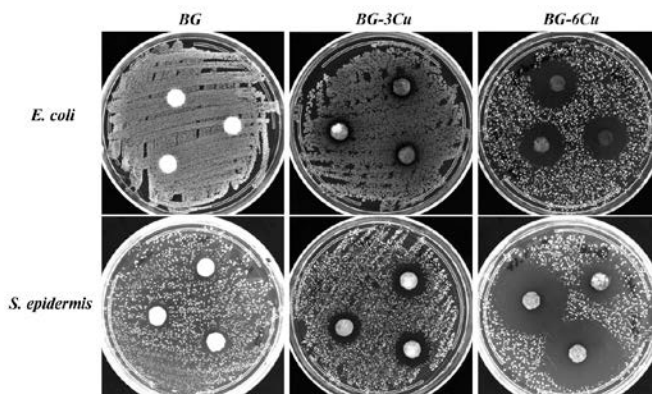


**Figure 6.** Antibacterial agar diffusion of BG, BG-3Cu, and BG-6Cu glasses against *E. coli* and *S. epidermidis*.

One of the primary advantages of bioactive glass compositions is the ability to incorporate therapeutic ions to improve the antibacterial efficacy of the glass and, therefore, to reduce the infection risk.<sup>16</sup> The antibacterial efficacy of the glass compositions was evaluated using agar diffusion testing method and against two common bacteria strains: aerobic Gram-positive coccus *S. epidermidis* and aerobic Gram-negative, *E. coli*. Glass disks were placed within inoculated plated, cultured for 24 h, and then tested for their inhibition zones.

The results from the agar diffusion test of the glass samples are presented in Figure 6. The copper-containing glasses are showing significantly higher antibacterial efficacy compared to control glass. No inhibition zone was detected for control glass against *E. coli*, however, for BG-3Cu, and BG-6Cu glasses, 3 and 9 mm of inhibition zone was observed. Glasses showed better antibacterial properties against *S. epidermidis* bacteria, with 2, 5 and 16 mm of inhibition zone for, respectively.

From Figure 6, it is evident that the BG, BG-3Cu, and BG-6Cu glasses inhibition zones associated with the copper glasses increase with the copper concentration in the glass. The antibacterial mechanism of copper can be complex. However, previous studies suggest that copper ions disrupt the function of microbes by binding to proteins and enzymes in the microbes and therefore impede their activity. Using copper in the composition of the bioactive glasses can provide an alternative to antibiotics loaded biomaterials.<sup>18, 26</sup>

## CONCLUSION

The substitution of CuO for SiO<sub>2</sub> was investigated to study the structural effects and antibacterial efficacy in the bioactive glass compositions. Results from DTA, XPS, and NMR indicated that the copper ions act as network modifiers in the glass structure. The addition of copper resulted in a higher number of non-bridging oxygens at the expense of bridging-oxygen. This resulted in a more disrupted network in copper-containing glasses, which in turn could increase the solubility and bioactivity of the glass in physiological solutions. The results from the agar diffusion antibacterial test indicated significantly higher efficacy of copper-containing glasses, as potential alternatives for antibiotics in the biomedical glasses.

## REFERENCES

- <sup>1</sup>Jones, J. R., Review of bioactive glass: from Hench to hybrids, *Acta Biomater.*, **2013**, *9*(1), 4457-86. <https://doi.org/10.1016/j.actbio.2012.08.023>
- <sup>2</sup>Baino, F., Hamzehlou, S., Kargozar, S., Bioactive Glasses: Where Are We and Where Are We Going? *J. Funct. Biomater.*, **2018**, *9* (1), 25. <https://doi.org/10.3390/jfb9010025>
- <sup>3</sup>Rahaman, M. N., Day, D. E., Bal, B. S., Fu, Q., Jung, S. B., Bonewald, L. F., Tomsia, A. P., Bioactive glass in tissue engineering, *Acta Biomater.*, **2011**, *7* (6), 2355-73. <https://doi.org/10.1016/j.actbio.2011.03.016>
- <sup>4</sup>Rabiee, S. M., Nazparvar, N., Azizian, M., Vashae, D., Tayebi, L., Effect of ion substitution on properties of bioactive glasses: A review, *Ceram. Int.*, **2015**, *41* (6), 7241-7251. <https://doi.org/10.1016/j.ceramint.2015.02.140>
- <sup>5</sup>Hoppe, A., Guldal, N. S., Boccaccini, A. R., A review of the biological response to ionic dissolution products from bioactive glasses and glass-ceramics, *Biomaterials*, **2011**, *32* (11), 2757-74, <https://doi.org/10.1016/j.biomaterials.2011.01.004>
- <sup>6</sup>Ribas, R. G., Schatkoski, V. M., do Amaral Montanheiro, T. L., de Menezes, B. R. C., Stegemann, C., Leite, D. M. G., Thim, G. P., Current advances in bone tissue engineering concerning ceramic and bioglass scaffolds: A review, *Ceram. Int.*, **2019**, *45*(17), 21051-21061. <https://doi.org/10.1016/j.ceramint.2019.07.096>
- <sup>7</sup>Chon, S. S., Piraino, L., Mokhtari, S., Krull, E. A., Coughlan, A., Gong, Y., Mellott, N. P., Keenan, T. J., Wren, A. W., Synthesis, characterization and solubility analysis of amorphous SiO<sub>2</sub>-CaO-Na<sub>2</sub>O-P<sub>2</sub>O<sub>5</sub> scaffolds for hard tissue repair, *J. Non-Cryst. Solids.*, **2018**, *490*, 1-12. <https://doi.org/10.1016/j.jnoncrysol.2018.03.006>
- <sup>8</sup>Balamurugan, A., Balossier, G., Laurent-Maquin, D., Pina, S., Rebelo, A. H. S., Faure, J., Ferreira, J. M. F., An in vitro biological and anti-bacterial study on a sol-gel derived silver-incorporated bioglass system, *Dent. Mater.*, **2008**, *24*(10), 1343-1351. <https://doi.org/10.1016/j.dental.2008.02.015>
- <sup>9</sup>Fiume, E., Barberi, J., Verne, E., Baino, F., Bioactive Glasses: From Parent 45S5 Composition to Scaffold-Assisted Tissue-Healing Therapies, *J. Funct. Biomater.*, **2018**, *9*(1), 24. <https://doi.org/10.3390/jfb9010024>
- <sup>10</sup>Sanz-Herrera, J. A., Boccaccini, A. R., Modelling bioactivity and degradation of bioactive glass based tissue engineering scaffolds, *Int. J. Solids Struct.*, **2011**, *48* (2), 257-268. <https://doi.org/10.1016/j.ijsolstr.2010.09.025>
- <sup>11</sup>Tilocca, A., Models of structure, dynamics and reactivity of bioglasses: a review, *Int. J. Mater. Chem.*, **2010**, *20* (33), 6848-6858. <https://doi.org/10.1039/C0JM01081B>
- <sup>12</sup>Wang, Z., Cheng, L., Effects of doping CeO<sub>2</sub>/TiO<sub>2</sub> on structure and properties of silicate glass, *J. Alloys Compd.*, **2014**, *597*, 167-174. <https://doi.org/10.1016/j.jallcom.2014.01.232>
- <sup>13</sup>Kaur, G., Pandey, O. P., Singh, K., Homa, D., Scott, B., Pickrell, G., A review of bioactive glasses, *J. Biomed. Mater. Res., Part A.*, **2014**, *102* (1), 254-274. <https://doi.org/10.1002/jbm.a.34690>
- <sup>14</sup>Lázaro, G. S., Santos, S. C., Resende, C. X., dos Santos, E. A., Individual and combined effects of the elements Zn, Mg and Sr on the surface reactivity of a SiO<sub>2</sub>-CaO-Na<sub>2</sub>O-P<sub>2</sub>O<sub>5</sub> bioglass system, *J. Non-Cryst. Solids.*, **2014**, *386*, 19-28. <https://doi.org/10.1016/j.jnoncrysol.2013.11.038>
- <sup>15</sup>Babu, M. M., Prasad, P. S., Rao, P. V., Govindan, N. P., Singh, R. K., Kim, H.-W., Veeraiah, N., Titanium incorporated Zinc-Phosphate bioactive glasses for bone tissue repair and regeneration: Impact of Ti<sup>4+</sup> on physico-mechanical and in vitro bioactivity, *Ceram. Int.*, **2019**, *45* (17), 23715-23727. <https://doi.org/10.1016/j.ceramint.2019.08.087>
- <sup>16</sup>Waltimo, T., Brunner, T. J., Vollenweider, M., Stark, W. J., Zehnder, M., Antimicrobial Effect of Nanometric Bioactive Glass 45S5, *J. Dent. Res.*, **2007**, *86* (8), 754-7. <https://doi.org/10.1177%2F154405910708600813>
- <sup>17</sup>Mokhtari, S., Skelly, K. D., Krull, E. A., Coughlan, A., Mellott, N. P., Gong, Y., Borges, R., Wren, A. W., Copper-containing glass polyalkenoate cements based on SiO<sub>2</sub>-ZnO-CaO-SrO-P<sub>2</sub>O<sub>5</sub> glasses: glass characterization, physical and antibacterial properties, *J. Mater. Sci.*, **2017**, *52* (15), 8886-8903. <https://doi.org/10.1007/s10853-017-0945-5>
- <sup>18</sup>Finney, L., Vogt, S., Fukai, T., Glesne, D., Copper and angiogenesis: Unravelling a relationship key to cancer progression, *Clin. Exp. Pharmacol. Physiol.*, **2009**, *36* (1), 88-94. <https://doi.org/10.1111/j.1440-1681.2008.04969.x>
- <sup>19</sup>Mokhtari, S., Wren, A. W., Investigating the effect of Copper Addition on SiO<sub>2</sub>-ZnO-CaO-SrO-P<sub>2</sub>O<sub>5</sub> Glass Polyalkenoate Cements: Physical, Mechanical and Biological Behavior, *Biomed. Glasses*, **2019**, *5* (1), 13-33. <https://doi.org/10.1515/bglass-2019-0002>
- <sup>20</sup>Li, Z., Khun, N. W., Tang, X.-Z., Liu, E., Khor, K. A., Mechanical, tribological and biological properties of novel 45S5 Bioglass® composites reinforced with in situ reduced graphene oxide, *J. Mech. Behav. Biomed. Mater.*, **2017**, *65*, 77-89. <https://doi.org/10.1016/j.jmbbm.2016.08.007>
- <sup>21</sup>Brückner, R., Chun, H.-U., Goretzki, H., Sammet, M., XPS measurements and structural aspects of silicate and phosphate glasses, *J. Non-Cryst. Solids.*, **1980**, *42* (1-3), 49-60. [https://doi.org/10.1016/0022-3093\(80\)90007-1](https://doi.org/10.1016/0022-3093(80)90007-1)
- <sup>22</sup>Maekawa, H.; Maekawa, T.; Kawamura, K.; Yokokawa, T., The structural groups of alkali silicate glasses determined from 29Si MAS-NMR, *J. Non-Cryst. Solids.*, **1991**, *127* (1), 53-64. [https://doi.org/10.1016/0022-3093\(91\)90400-Z](https://doi.org/10.1016/0022-3093(91)90400-Z)
- <sup>23</sup>Angeli, F., Gaillard, M., Jollivet, P., Charpentier, T., Influence of Glass Composition and Alteration Solution on Leached Silicate Glass Structure, *Geochim. Cosmochim. Acta.*, **2006**, *70* (10), 2577-2590. <https://doi.org/10.1016/j.gca.2006.02.023>
- <sup>24</sup>Stebbins, J. F., Identification of multiple structural species in silicate glasses by <sup>29</sup>Si NMR, *Nature*, **1987**, *330* (6147), 465. <https://doi.org/10.1038/330465a0>
- <sup>25</sup>Vuong, B. X., Hiệp, Đ. T., In vitro studies of bioglass material by X-ray diffraction and solid-state MAS-NMR, *Glass Phys. Chem.*, **2016**, *42* (2), 188-193. <https://doi.org/10.1134/S108765961602005X>
- <sup>26</sup>Gross, T. M., Lahiri, J., Golas, A., Luo, J., Verrier, F., Kurzejewski, J. L., Baker, D. E., Wang, J., Novak, P. F., Snyder, M. J., Copper-containing glass ceramic with high antimicrobial efficacy, *Nature Comm.*, **2019**, *10* (1), 1979. <https://doi.org/10.1038/s41467-019-09946-9>

Received: 08.11.2019.

Accepted: 02.12.2019.



# HEPES BUFFER MEDIATED SYNTHESIS OF 3,4-DIHYDRO-3,3-DIMETHYL-9-ARYLACRIDIN-1-ONES

Suchita S. Gadekar, <sup>[a]</sup> Suryakant B. Sapkal, <sup>[b]</sup> Balaji R. Madje <sup>[a]\*</sup>

**Keywords:** HEPES buffer; phenylacridin-1-ones; organocatalyst.

One-pot three-component synthesis of 3,4-dihydro-3,3-dimethyl-9-phenylacridin-1(2*H*,9*H*,10*H*)-one derivatives has been described by the cyclocondensation of aromatic aldehydes, aromatic amines and dimedone in the presence of 4-(2-hydroxyethyl)-1-piperazineethanesulfonic acid (HEPES) in ethanol at reflux condition. Besides buffering agent, HEPES as an organocatalyst has been used for the first time in multicomponent organic transformation and succeeded along with various merits of green chemistry practices. The reaction is mechanized by zwitterionic interactions between organocatalyst and reactants to form targeted molecules.

\* Corresponding Authors

E-Mail: drmadjebr@rediffmail.com

[a] Department of Chemistry Vasantrao Naik Mahavidyalaya, Aurangabad-431003, MS, India

[b] Department of Chemistry, Jawaharlal Nehru Engineering College, Aurangabad-431 004, India

## INTRODUCTION

Nowadays, the time has come to expand the horizon of our conscious foresight about environmental consequences and its inequality in the world that leads to natural disasters. It is expected from all the chemists and co-workers while performing any chemical transformations in the laboratory. Therefore, chemists have to modify the protocols or keep control of it so that the developed methodology can help to protect human health and maintains the environment unaffected. Keeping these factors in view, it was thought worthiness to synthesize 3,4-dihydro-3,3-dimethyl-9-phenylacridin-1-ones by means of buffer mediated organocatalyst with conventional techniques. In literature buffering activity of HEPES is widely utilized to maintain local pH of the biochemical, biological reactions and environmental studies, <sup>1-3</sup> for the synthesis of specific sized nanogold particles,<sup>4</sup> detection of ATP in clinical applications,<sup>5</sup> to study function characteristics of hemoglobin.<sup>6</sup>

Beside this other various organocatalysts have been extensively used for the synthesis of different heterocyclic organic compounds through C-C and C-heteroatom bond formation reactions.<sup>7,8</sup> The catalytic proficiency of an organocatalyst is quite significant and beneficent than biocatalysts and metal catalysts toward organic transformations. The mechanistic role of an organocatalyst for the initiation or the activation of the reactant molecule is either by providing or removing protons or electrons for the reacting species.<sup>9</sup>

Our targeted molecule based on the acridine nucleus is very versatile in pharmacological behavior such as a wide range of anesthetic activity *viz* surface anesthesia, infiltration anesthesia, peripheral and spinal anesthesia, etc., antimalarial agent, antiseptic and anticancer agents.<sup>10,11</sup> Other few literature reports revealed that acridine moiety shows antibacterial activity, antifungal activity,<sup>12</sup> antiproliferative activity<sup>13</sup> and antioxidant.<sup>14</sup> Because of the wide

spectrum of medicinal activity chemists have attempted to synthesize acridine derivatives by several ways that have been discussed in the reported review and multi-step synthetic routes under different reaction conditions and use of various reagents by conventional and non-conventional as well.<sup>15</sup> Some multicomponent methodologies have also been reported, like protic pyridinium ionic liquid,<sup>16</sup> L-proline,<sup>17</sup> nano ferrite<sup>18</sup>, etc. However, aspects of green chemistry need some more effort that could develop sustainable protocols.

Therefore, we used HEPES buffering agent preferentially as an organocatalyst, which found to be smart and compatible in various reaction conditions with a variety of substrates and contributes a part of green chemistry.

## EXPERIMENTAL

All the reagents and solvents were used for the reactions and column chromatography was purchased from HiMedia, Finechem, Spectrochem and Rankem chemical companies and used directly without further purification. The progress of the reactions was monitored by Thin Layer chromatography 60 F254 (TLC). <sup>1</sup>H NMR spectra were recorded on 300 MHz FT-NMR spectrometer in CDCl<sub>3</sub> as a solvent and chemical shifts were reported in parts per million (ppm) relative to tetramethylsilane (CH<sub>3</sub>)<sub>4</sub>Si.

### Experimental procedure for the preparation of 3,4-dihydro-3,3-dimethyl-9-phenylacridin-1(2*H*,9*H*,10*H*)-one derivatives

In the hard glass test tube benzaldehyde (0.221 g, 0.002 mol) and aniline (0.193 g, 0.002 mol) and HEPES (40 mg) in 25 mL ethyl alcohol were stirred at reflux temperature for 30-35 minutes. To this solution, dimedone (0.290g, 0.002 mol) was added portion wise with continued stirring at same temperature. The progress of the reaction was monitored after interval of each half hour by TLC. The reaction is completed after specified period of time. After completion the reaction mixture was poured on crushed ice. The obtained solid was filtered, dried and purified by recrystallization in ethanol to yield a pure product. Similar procedure was applied for the synthesis of other derivatives. All compounds were characterized by spectroscopic analysis.



**3,4-Dihydro-3,3-dimethyl-9-phenylacridin-1(2H,9H,10H)-one (4a)**

M. P. 170-172 °C; <sup>1</sup>H NMR (CDCl<sub>3</sub>) δ ppm; of 10.12 (s, 1H, N-H), 6.45 - 7.85 (m, 9H, Ar-H), 5.55 (s, 1H, C-H), 3.01 (q, 4H, CH<sub>2</sub>, J = 24.6), 1.75 (s, 6H, CH<sub>3</sub>); MS m/z = 303.14; IR (KBr); ν cm<sup>-1</sup> 3015 (N-H Str.), 2867 (CH<sub>3</sub> Str.), 1715 (C=O Str.), 1399 (C=C Str.).

**9-(4-Chlorophenyl)-3,4-dihydro-3,3-dimethylacridin-1(2H,9H,10H)-one (4b)**

M. P. 167-169 °C; <sup>1</sup>H NMR (CDCl<sub>3</sub>) δ ppm; of 9.98 (s, 1H, N-H), 7.12 (d, 2H, Ar-H, J = 1.4), 7.30 (d, 2H, Ar-H, J = 8.10), 6.45 - 6.99 (m, 4H, Ar-H), 4.75 (s, 1H, C-H), 2.67 (s, 4H, CH<sub>2</sub>), 1.15 (s, 6H, CH<sub>3</sub>); MS m/z = 337.17; IR (KBr); ν cm<sup>-1</sup> 3109 (N-H Str.), 3004 (CH<sub>3</sub> Str.), 1778 (C=O Str.), 1429 (C=C Str.), 760 (C-Cl Str.).

**7-Chloro-3,4-dihydro-3,3-dimethyl-9-phenylacridin-1(2H,9H,10H)-one (4c)**

M. P. 188-190 °C; <sup>1</sup>H NMR (CDCl<sub>3</sub>) δ ppm; of 10.02 (s, 1H, N-H), 7.82 (d, 2H, Ar-H, J = 1.9), 7.34 (s, 1H, Ar-H), 6.90 - 7.15 (m, 5H, Ar-H), 4.96 (s, 1H, C-H), 3.07 (s, 4H, CH<sub>2</sub>), 2.15 (s, 6H, CH<sub>3</sub>); MS m/z = 337.30; IR (KBr); ν cm<sup>-1</sup> 3120 (N-H Str.), 3024 (CH<sub>3</sub> Str.), 1790 (C=O Str.), 1429 (C=C Str.), 810 (C-Cl Str.).

**3,4-Dihydro-3,3-dimethyl-9-p-tolylacridin-1(2H,9H,10H)-one (4d)**

M. P. 199-201 °C; <sup>1</sup>H NMR (CDCl<sub>3</sub>) δ ppm; of 9.42 (s, 1H, N-H), 7.15 - 7.78 (m, 8H, Ar-H), 4.74 (s, 1H, C-H), 2.81 (q, 4H, CH<sub>2</sub>, J = 21.7), 1.75 (s, 6H, CH<sub>3</sub>), 2.25 (s, 3H, CH<sub>3</sub>); MS m/z = 317.20; IR (KBr); ν cm<sup>-1</sup> 2983 (N-H Str.), 2796 (CH<sub>3</sub> Str.), 1648 (C=O Str.), 1290 (C=C Str.).

**3,4-Dihydro-9-(4-hydroxy-3-methoxyphenyl)-3,3-dimethylacridin-1(2H,9H,10H)-one (4e)**

M. P. 145-147 °C; <sup>1</sup>H NMR (CDCl<sub>3</sub>) δ ppm; of 9.98 (s, 1H, N-H), 7.12 (d, 2H, Ar-H, J = 1.4), 7.30 (d, 2H, Ar-H, J = 8.10), 6.45 - 6.99 (m, 4H, Ar-H), 4.75 (s, 1H, C-H), 2.67 (s, 4H, CH<sub>2</sub>), 1.15 (s, 6H, CH<sub>3</sub>), 5.98 (s, 1H, O-H); MS m/z = 349.12; IR (KBr); ν cm<sup>-1</sup> 3109 (N-H Str.), 3004 (CH<sub>3</sub> Str.), 1778 (C=O Str.), 1429 (C=C Str.), 760 (C-Cl Str.), 3358 (OH Str.).

**3,4-Dihydro-3,3,7-trimethyl-9-phenylacridin-1(2H,9H,10H)-one (4f)**

M. P. 158-160 °C; <sup>1</sup>H NMR (CDCl<sub>3</sub>) δ ppm; of 9.42 (s, 1H, N-H), 7.15 - 7.78 (m, 8H, Ar-H), 4.74 (s, 1H, C-H), 2.81 (q, 4H, CH<sub>2</sub>, J = 21.7), 1.75 (s, 6H, CH<sub>3</sub>), 2.05 (s, 3H, CH<sub>3</sub>); MS m/z = 317.28; IR (KBr); ν cm<sup>-1</sup> 2983 (N-H Str.), 2796 (CH<sub>3</sub> Str.), 1648 (C=O Str.), 1290 (C=C Str.).

**3,4-Dihydro-3,3,7-trimethyl-9-(4-nitrophenyl)acridin-1(2H,9H,10H)-one (4g)**

M. P. 197-199 °C; <sup>1</sup>H NMR (CDCl<sub>3</sub>) δ ppm; of 10.95 (s, 1H, N-H), 8.02 (d, 2H, Ar-H, J = 1.3), 7.94 (s, 1H, Ar-H), 7.30 (d, 2H, Ar-

H, J = 9.75), 7.09 (s, 1H, Ar-H), 5.60 (s, 1H, C-H), 2.51 (q, 4H, CH<sub>2</sub>, J = 24.6), 2.02 (s, 3H, CH<sub>3</sub>), 1.20 (s, 6H, CH<sub>3</sub>); MS m/z = 364.4; IR (KBr); ν cm<sup>-1</sup> 3065 (N-H Str.), 2937 (CH<sub>3</sub> Str.), 1721 (C=O Str.), 1520 (NO<sub>2</sub> Str.), 1461 (C=C Str.).

**9-(4-(Dimethylamino)phenyl)-3,4-dihydro-3,3-dimethylacridin-1(2H,9H,10H)-one (4h)**

M. P. 160-162 °C; <sup>1</sup>H NMR (CDCl<sub>3</sub>) δ ppm; of 9.82 (s, 1H, N-H), 6.45 - 7.85 (m, 8H, Ar-H), 5.05 (s, 1H, C-H), 3.01 (q, 4H, CH<sub>2</sub>, J = 24.6), 1.75 (s, 6H, CH<sub>3</sub>), 3.25 (s, 6H, CH<sub>3</sub>); MS m/z = 346.14; IR (KBr); ν cm<sup>-1</sup> 3015 (N-H Str.), 2867 (CH<sub>3</sub> Str.), 1715 (C=O Str.), 1399 (C=C Str.), 1155 (C-N Str.).

**3,4-Dihydro-3,3,9-trimethylacridin-1(2H,9H,10H)-one (4i)**

M. P. 176-178 °C; <sup>1</sup>H NMR (CDCl<sub>3</sub>) δ ppm; of 8.62 (s, 1H, N-H), 6.45 - 7.85 (m, 4H, Ar-H), 3.95 (s, 1H, C-H), 2.71 (q, 4H, CH<sub>2</sub>, J = 24.6), 1.25 (s, 6H, CH<sub>3</sub>), 1.45 (s, 3H, CH<sub>3</sub>); MS m/z = 241.10; IR (KBr); ν cm<sup>-1</sup> 3015 (N-H Str.), 2867 (C-H Str.), 1715 (C=O Str.), 1399 (C=C Str.).

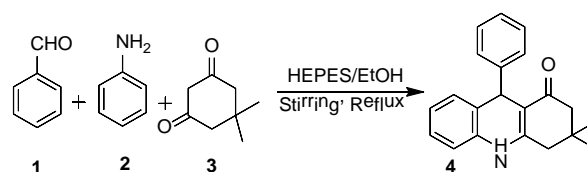
**9-(Furan-2-yl)-3,4-dihydro-3,3-dimethylacridin-1(2H,9H,10H)-one (4j)**

M. P. 120-122 °C; <sup>1</sup>H NMR (CDCl<sub>3</sub>) δ ppm; of 4.22 (s, 1H, N-H), 6.45 - 6.85 (m, 7H, Ar-H), 4.77 (s, 1H, C-H), 4.01 (q, 4H, CH<sub>2</sub>, J = 24.6), 1.11 (s, 6H, CH<sub>3</sub>); MS m/z = 293.14; IR (KBr); ν cm<sup>-1</sup> 3110 (N-H Str.), 2967 (C-H Str.), 1615 (C=O Str.), 1400 (C=C Str.).

**RESULTS AND DISCUSSION**

To take a broad view of an experimental procedure, we have optimized the reaction conditions by several methods, out of which few successful reports have been demonstrated here with this discussion. Previously, we fruitfully attempted to establish such conventional and non-conventional methods for the preparation of various heterocyclic compounds.<sup>19,20</sup>

For the synthesis of 3,4-dihydro-3,3-dimethyl-9-phenylacridin-1(2H,9H,10H)-one (**4**) initially, in the hard test tube we refluxed benzaldehyde (**1**), aniline (**2**) and dimedone (**3**) with constant stirring in the presence of HEPES as a organocatalyst in ethanol as a reaction medium (Scheme 1).



**Scheme 1.** Synthesis of 3,4-dihydro-3,3-dimethyl-9-phenylacridin-1(2H,9H,10H)-one.

But we observed that it took a prolonged time (18 hrs) with less product yield. Then, we decided to optimize the reaction concerning catalyst concentration, reaction time and percent yield.

After several experimental attempts, we came to know that reaction proceeds to completion by proper sequential addition of reactant and catalyst. Accordingly, benzaldehyde, aniline and HEPES were refluxed for 30-35 minutes yellow coloration is observed in the reaction vessel, which indicates the formation of Schiff's base as an intermediate. □

**Table 1.** Screening of solvents for model reaction (preparation of 1).

No.	Solvent	Time, h	Yield, %
1	Methanol	6.50	45
2	Ethanol	3.00	79
3	Isopropyl alcohol	5.50	60
4	Aqueous alcohol (1:1)	11.50	40
5	Acetone	5.50	60
6	DCM	7.20	45
7	Chloroform	6.00	50
8	Ethyl acetate	6.20	50

Later on, dimedone is added in that reaction vessel portion-wise under the same reaction condition that leads to the formation of the targeted product by cyclocondensation manner within the next couple of hours. To establish the optimized protocol, we examined different protic-non protic and polar-nonpolar solvents such as alcohols, aqueous alcohol, acetone, dichloromethane (DCM), chloroform, ethyl acetate, etc. (Table 1) and a stoichiometric study has also been completed (Table 2).

**Table 2.** Effect of catalyst concentration on model reaction.

Sr.	Catalyst, mg	Time, h	Yield, %
1	10	3	20
2	20	3	40
3	30	3	60
4	40	3	79
5	50	3	80

After the successful screening of suitable solvent and stoichiometry determination for catalyst, it has been reported that synthesis of 3,4-dihydro-3,3-dimethyl-9-phenylacridin-1(2H,9H,10H)-ones by the cyclocondensation of benzaldehyde, aniline and dimedone is in the presence of HEPES as an organocatalyst in ethanol as a reaction medium. □

To take a broad view, the set procedure has been implemented for various aldehydes and anilines to produce different derivatives of 3,4-dihydro-3,3-dimethyl-9-phenylacridin-1(2H,9H,10H)-one (Table 3).

**Table 3.** HEPES catalyzed synthesis of 3,4-dihydro-3,3-dimethyl-9-phenylacridin-1(2H,9H,10H)-one derivatives.

Entry	R/Aldehyde	R'/Amine	Time, h	Yield, %
4a	H	H	3	79
4b	4-Cl	H	3	76
4c	H	4-Cl	3	71
4d	4-CH <sub>3</sub>	H	3	78
4e	4-OH, 3-OCH <sub>3</sub>	H	3	70
4f	H	3-CH <sub>3</sub>	3	72
4g	3-NO <sub>2</sub>	4-CH <sub>3</sub>	3	69
4h	4-N(CH <sub>3</sub> ) <sub>2</sub>	H	3	80
4i	Acetaldehyde	H	3	64
4j	Furfuraldehyde	H	3	69

During derivatization, it has been noted that aromatic aldehydes and anilines with different substitutions at different positions have been reacted smoothly with appreciable product yield. In conjunction with an output of the reaction in our hand, heterocyclic reactants also give a compatible yield of the product, whereas aliphatic aldehyde resulted in comparatively less yield and took more time for transformation. The formation of products was confirmed by their physical constant and structures were elucidated by spectroscopic analysis. □

## CONCLUSIONS

We have developed a sustainable protocol, which will be the user-friendly synthetic route for pharmacodynamic 3,4-dihydro-3,3-dimethyl-9-phenylacridin-1(2H,9H,10H)-one derivatives favored by buffering agent HEPES as a catalyst in ethyl alcohol. HEPES have a zwitterionic structure that drives successful interaction between reactants at near-neutral pH. This synthetic strategy also covers the advantages of one-pot multicomponent transformations, which will make this research work practical and economically feasible and provides foresight for sustainability.

## ACKNOWLEDGMENTS

The authors are thankful to the Principal of Vasantrao Naik College, Aurangabad, for providing lab infrastructure and facilities for this research work. □

## REFERENCES

- <sup>1</sup>Dezfuli, S. N., Huan, Z., Mol, J. M. C., Leeflang, M. A., Chang, J., Zhou, J., Influence of HEPES buffer on the local pH and formation of surface layer during in vitro degradation tests of magnesium in DMEM. *Progr. Nat. Sci. Mater. Int.*, **2014**, *24*, 531–538. DOI: 10.1016/j.pnsc.2014.08.009.
- <sup>2</sup>Yamamoto, A., Hiromoto, S., Effect of inorganic salts, amino acids and proteins on the degradation of pure magnesium in vitro. *Mater. Sci. Eng. C.*, **2009**, *29*, 1559–1568. DOI: 10.1016/j.msec.2008.12.015.
- <sup>3</sup>Ferreira, C. M. H., Pinto, I. S. S., Soares, E. V., Soares, H. M. V. M., (Un)suitability of the use of pH buffers in biological, biochemical and environmental studies and their interaction with metal ions—a review. *RSC Adv.*, **2015**, *5*, 30989–31003. DOI: 10.1039/c4ra15453c.
- <sup>4</sup>Xie, J., Lee, J. Y., Wang, D. I. C., Seedless, Surfactantless, High-Yield Synthesis of Branched Gold Nanocrystals in HEPES Buffer Solution. *Chem. Mater.*, **2007**, *19*, 2823–2830. DOI: 10.1021/cm0700100.
- <sup>5</sup>Masson, J. F., Gauda, E., Mizaikoff, B., Kranz, C., The interference of HEPES buffer during amperometric detection of ATP in clinical applications. *Anal Bioanal Chem.*, **2008**, *390*, 2067–2071. doi: 10.1007/s00216-008-2015-y
- <sup>6</sup>Weber, R. E., Use of ionic and zwitterionic (TrisBisTris and HEPES) buffers in studies on hemoglobin function. *J. App. Phys.*, **1992**, *72*(4), 1611–5, DOI: 10.1152/jappl.1992.72.4.1611.
- <sup>7</sup>Evans, C. S., Davis, L. O., Recent Advances in Organocatalyzed Domino C–C Bond-Forming Reactions. *Molecules*, **2018**, *23*, 33–43. DOI: 10.3390/molecules23010033.
- <sup>8</sup>Bae, H. Y., Hofler, D., Kaib, P. S. J., Kasaplar, P., De, C. K., Dohring, A., Lee, S., Kaupmees, K., Leito, I., List, B. Approaching sub-ppm-level asymmetric organocatalysis of a



- highly challenging and scalable carbon-carbon bond forming reaction. *Nature Chem.*, **2018**, *10*, 888–894. DOI: 10.1038/s41557-018-0065-0.
- <sup>9</sup>List, B., Introduction: Organocatalysis. *Chem. Rev.*, **2007**, *107*(12), 5413–5415. DOI:10.1021/cr078412e□
- <sup>10</sup>Kumar, R., Kaur, M., Kumari, M., Acridine: a versatile heterocyclic nucleus. *Acta Polon. Pharm. Drug Res.*, **2012**, *69*(1), 3–9.
- <sup>11</sup>Chen, Y. L., Chen, I. L., Lu, C. M., Tzeng, C. C., Tsao, L. T., Wang, J. P., Synthesis and Anti-Inflammatory Evaluation of 9-Phenoxyacridine and 4-Phenoxyfuro[2,3-*b*]quinoline Derivatives. *Bioorg. Med. Chem.*, **2003**, *11*, 3921–2927. DOI: 10.1016/S0968-0896(03)00439-5.
- <sup>12</sup>Hangirgekar, S., Phulwal, S., Synthesis, Characterization and Biological Evaluation of Some New Acridine Derivatives. *Het Lett.* **2018** *8* 1, 95–104.
- <sup>13</sup>Ferreira, R., Avino, A., Mazzini, S., Eritja, R., Synthesis, DNA-Binding and Antiproliferative Properties of Acridine and 5-Methylacridine Derivatives. *Molecules*, **2012**, *17*, 7067. DOI: 10.3390/molecules17067067.
- <sup>14</sup>Kumar, L. J., Sarveswari, S., Vijayakumar, V., DMFDMA catalyzed synthesis of 2-((dimethylamino)methylene)-3,4-dihydro-9-arylacridin-1(2H)-ones and their derivatives: invitro antifungal, antibacterial and antioxidant evaluations. *Open Chem.*, **2018**, *16*, 1077–1088. DOI: 10.1515/chem-2018-0110.
- <sup>15</sup>Santos, C. M. M., Pinto, D. C. G. A., Silva, V. L. M., Silva, A. M. S., Arylxanthonones and arylacridones: a synthetic overview. *Pure Appl. Chem.*, **2016**, *88*(6), 579–594. DOI: 10.1515/pac-2016-0407.
- <sup>16</sup>Alinezhad, H., Tajbakhsh, M., Norouzi, M., Bagheri, S., Rakhtshah, J., Green and expeditious synthesis of 1,8-dioxodecahydroacridine derivatives catalyzed by protic pyridinium ionic liquid. *J. Chem. Sci.*, **2013**, *125*(6), 1517–1522. DOI: 10.1007/s12039-013-0517-4.
- <sup>17</sup>Wang, H., Li, L., Lin, W., Xu, P., Huang, Z., Shi, D., An Efficient Synthesis of Pyrrolo[2,3-*kl*]acridin-1-one Derivatives Catalyzed by l-Proline. *Org. Lett.*, **2012**, *14*(17), 4598–4601. DOI: 10.1021/ol302058g.
- <sup>18</sup>Sunkara, J. R., Rallabhandi, M., Prasangi, S., Palla, M., One-Pot Facile Synthesis of Acridinediones and their Derivatives by Nano Ferrite as a Catalyst. *Chem. Sci. Trans.*, **2016**, *5*(4), 1001–1007. DOI : 10.7598/cst2016.1269.
- <sup>19</sup>Gadekar, S. S., Sapkal, S. B., Shingare, R. M., Madje, B. R., Thiamine hydrochloride (vb ) catalyzed the synthesis of 3-amino alkylated indoles, *Bionano Frontier*, **2017**, *10*(2), 1–3.
- <sup>20</sup>Gadekar, S. S., Sapkal, S. B., Shingare, R. M., Madje, B. R., An organocatalyzed expeditious synthesis route to benzimidazoles under ultrasound technique, *Heterocycl. Lett.*, **2017**, *7*(2), 499–505, 2017.

This paper was presented at the “*International Symposium on Exploring New Horizons in Chemical Sciences*,” January 10–12, **2019**, Aurangabad, India (ENHCS–2019).

Received: 11.03.2019.

Accepted: 15.12.2019



# PYRIDINE AND BENZOISOTHIAZOLE BASED PYRAZOLINES: SYNTHESIS, CHARACTERIZATION, BIOLOGICAL ACTIVITY, MOLECULAR DOCKING AND ADMET STUDY

Pintu G. Pathare<sup>[a]</sup>, Sunil U. Tekale<sup>[a]</sup>, Manoj G. Damale<sup>[b]</sup>, Jaiprakash N. Sangshetti<sup>[c]</sup>, Rafique U. Shaikh<sup>[d]</sup>, László Kótai<sup>[e]</sup>, Rajendra P. Pawar<sup>[a]\*</sup>

**Keywords:** Pyrazolines; antioxidant; antimicrobial; molecular docking.

Synthesis, characterization, antioxidant and antimicrobial activities of novel pyrazolines and phenylpyrazoline containing substituted pyridine and piperazine benzoisothiazole moieties have been reported. When these synthesized compounds were exposed for antioxidant screening, some among them exhibited prominent DPPH radical scavenging activity and superoxide radical (SOR) scavenging activity where ascorbic acid used as standard. During the antimicrobial screening compounds, some derivatives were found to be very active against *Cryptococcus neoformans*, which was supported on the basis of higher free binding energies with methionyl-tRNA synthetase.

## \* Corresponding Authors

E-Mail: [rppawar@yahoo.com](mailto:rppawar@yahoo.com)

<sup>[a]</sup> Department of Chemistry, Deogiri College, Station Road, Aurangabad, MS 431 005, India

<sup>[b]</sup> Department of Pharmaceutical Chemistry, Shri. Bhagwan College of Pharmacy, Aurangabad, MS 431003, India.

<sup>[c]</sup> Y. B. Chavan College of Pharmacy, Dr. Rafiq Zakaria Campus, Aurangabad, MS 431001, India.

<sup>[d]</sup> Department of Botany, Poona College of Arts, Commerce, and Science, Pune, MS 411001, India.

<sup>[e]</sup> Research Centre for Natural Sciences, Budapest, H-1519 Hungary.

Thus, considering the biological significance of pyrazolines and in continuation of our efforts in the development of biologically active entities;<sup>15-17</sup> in the present work, we report the synthesis, characterization, antimicrobial and antioxidant activities of some novel pyrazolines bearing pyridine and benzoisothiazole containing piperazine moiety.

The results of biological activities were supported by molecular docking studies. ADMET study was performed to know the drug-likeness and toxicity profile of the synthesized compounds.

## INTRODUCTION

Pyrazolines, a class of five-membered heterocycles, is recognized for never-ending research and development in terms of therapeutic potential. As a result, pyrazolines have become an obvious core of numerous drugs having diverse activities.<sup>1</sup> The broad spectrum of activities shown by the pyrazolines encourages searchers to modify their structures by building with some biologically important heterocyclic compounds like alkyl, aromatic, heterocyclic rings and other groups at different positions on the ring which helps to create a novel class of desired compounds.

Pyrazoline and its analogs act as significant pharmacies and synthons in the field of organic chemistry and drug designing. They are well-acknowledged for pharmacologically interesting heterocyclic systems through recent literature survey.<sup>2</sup> Pyrazolines possess a wide range of biological properties such as anticancer,<sup>3-5</sup> anti-inflammatory,<sup>6</sup> antibacterial,<sup>7</sup> anti-depressive and anticonvulsant,<sup>8</sup> antimicrobial,<sup>9</sup> antinociceptives<sup>10</sup> and enzyme inhibitors.<sup>11</sup> Thus pyrazolines are well recognized for various biological activities.<sup>12,13</sup> Hence, synthesis of new heterocycles bearing pyrazolines remains the core area of research. Numerous methods were developed for the synthesis of pyrazoline and their synthetic counterparts, among which the classical method involves cyclization of the Michael acceptor unit (chalcone) with hydrazine hydrate or phenylhydrazine in the presence of cyclizing agents like acetic acid or simple heating procedure.<sup>14</sup>

## MATERIALS AND METHODS

Melting points were recorded in an electrothermal melting point apparatus and were uncorrected. The consumption of starting material and formation of the products was monitored on silica precoated thin layer chromatography plate using 40 % ethyl acetate : n-hexane as the mobile phase. FTIR spectra were recorded using KBr pellets (100 mg) on Shimadzu FT-IR spectrophotometer. <sup>1</sup>H and <sup>13</sup>C NMR spectra were recorded on Bruker 400 MHz spectrometer and chemical shifts were expressed in  $\delta$  ppm with reference to tetramethylsilane (TMS) as the internal standard.

In the antimicrobial activity, the zones of inhibition and the antioxidant activity performed spectrophotometrically were expressed as mean  $\pm$  SD of three replicates.

### General procedure for the synthesis of pyrazolines

A mixture of chalcone (0.7g, 0.16 mol) and hydrazine hydrate (1.0 mL) or phenylhydrazine in ethanol (1.0 mL) was stirred for 2 h at 25-35 °C. Sometimes heating at 45-50 °C was required for dehydration. The precipitated solid was filtered off to get a crude product which was crystallized with hot ethanol to get pure white color material.

**2-((4-(4,5-Dihydro-3-phenyl-1H-pyrazol-5-yl)-2-methoxyphenoxy)methyl)-3,4-dimethoxypyridine (1)**

<sup>1</sup>H NMR (400 MHz, DMSO-*d*<sub>6</sub>) δ ppm 2.89 (dd, *J* = 10.4 & 10.8 Hz, 1H), 3.39 (dd, *J* = 10.4 & 10.8 Hz, 1H), 3.72 (3H, s), 3.77 (3H, s), 3.90 (3H, s), 4.78 (t, 1H), 5.08 (s, 2H), 6.85 (d, *J* = 8.4 Hz, 1H), 7.00 (s, 1H), 7.04 (d, *J* = 8.4 Hz, 1H), 7.14 (d, *J* = 5.6 Hz, 1H), 7.31 (d, *J* = 6.8 Hz, 1H), 7.37 (t, *J* = 7.2 Hz, 2H), 7.50 (s, 1H, -NH), 7.61 (d, *J* = 7.6 Hz, 2H), 8.20 (d, *J* = 5.6 Hz, 1H); <sup>13</sup>C NMR (101.3 MHz, CDCl<sub>3</sub>) δ ppm 41.2, 54.9, 55.2, 61.42, 62.58, 68.11, 107.65, 109.61, 114.65, 116.4(2), 118.51, 118.94, 127.44, 130.21, 134.70, 144.66, 145.79, 148.07, 149.85, 149.95, 154.16, 157.61, 158.75; ESIMS *m/z* 420.4 [M + H]<sup>+</sup>.

**2-(5-(4-((3,4-Dimethoxypyridin-2-yl)methoxy)-3-methoxyphenyl)-4,5-dihydro-1H-pyrazol-3-yl)phenol (2)**

<sup>1</sup>H-NMR (400 MHz, DMSO-*d*<sub>6</sub>) δ ppm 3.07 (dd, *J* = 10.8 Hz & 11.2 Hz, 1H); 3.56 (dd, *J* = 10.4 Hz & 11.2 Hz, 1H); 3.72 (s, 3H); 3.77 (s, 3H); 3.90 (s, 3H); 4.8 (t, 1H); 5.03 (s, 2H); 6.87-6.91 (m, 2H); 7.03 (s, 1H); 7.07 (d, *J* = 8.4 Hz, 1H); 7.15 (d, *J* = 5.6 Hz, 1H); 7.22 (t, *J* = 8.0 Hz, 2H); 7.29 (d, *J* = 7.6 Hz, 1H); 8.21 (d, *J* = 5.6 Hz, 1H); 10.19 (s, 1H); 11.18 (s, 1H); <sup>13</sup>C NMR (101.3 MHz, CDCl<sub>3</sub>) δ ppm 41.51; 55.59; 55.7; 61.4; 62.5; 68.1; 107.6; 109.6; 114.6; 116.4(2); 118.5; 118.9; 127.4; 130.2; 134.7; 144.6; 145.7; 148.0; 149.8; 149.9; 154.1; 157.6; and 158.7; ); FT-IR (KBr) cm<sup>-1</sup> 761, 825, 1163, 1224, 1352, 1496, 1591 & 1516; ESIMS *m/z* 436.4 [M + H]<sup>+</sup>.

**2-(5-(4-((3,4-Dimethoxypyridin-2-yl)methoxy)-3-methoxyphenyl)-4,5-dihydro-1H-pyrazol-3-yl)-4-methylphenol (3)**

<sup>1</sup>H NMR (400 MHz, DMSO-*d*<sub>6</sub>) δ ppm 2.23 (s, 3H), 3.05 (dd, *J* = 10.8 & 11.2, 1H), 3.31 (dd, *J* = 10.4 & 10.6, 1H), 3.75 (s, 3H), 3.78 (s, 3H), 3.90 (s, 3H), 4.99 (t, 1H), 5.06 (s, 2H), 6.45 (bs, 2H), 6.77 (d, *J* = 8.4 Hz, 1H), 6.95 (d, *J* = 7.2 Hz, 1H), 7.07 (d, *J* = 7.6 Hz, 1H), 7.11-7.16 (m, 3H), 7.59 (s, 1H), 8.22 (d, *J* = 5.6 Hz, 1H); <sup>13</sup>C NMR (101.3 MHz, CDCl<sub>3</sub>) δ ppm 20.69, 31.19, 55.69, 55.91, 61.55, 68.19, 77.34, 107.74, 109.73, 113.95, 117.42, 118.54, 120.77, 123.64, 130.70, 131.03, 133.18, 142.67, 144.82, 145.89, 148.53, 149.87, 150.09, 154.14, 158.8; ESIMS *m/z* 450.4 [M+H]<sup>+</sup>.

**2-((4-(4,5-Dihydro-3-(2-methoxyphenyl)-1H-pyrazol-5-yl)-2-methoxyphenoxy)methyl)-3,4-dimethoxypyridine (4)**

<sup>1</sup>H NMR (400 MHz, DMSO-*d*<sub>6</sub>) δ ppm 2.91 (dd, *J* = 10.8 & 11.2 Hz, 1H), 3.38 (dd, *J* = 10.4 & 10.8 Hz, 1H), 3.71 (s, 3H), 3.74 (s, 3H), 3.75 (s, 3H), 3.87 (s, 3H), 4.69 (t, 1H), 5.00 (s, 2H), 6.85 (d, *J* = 7.2 Hz, 1H), 6.92 (t, 2H), 6.97 (s, 1H), 7.02 (dd, *J* = 5.2 & 4.4 Hz, 1H), 7.12 (d, *J* = 5.6 Hz, 1H), 7.27 (d, *J* = 7.6 Hz, 1H), 7.30 (d, *J* = 2.8 Hz, 1H), 7.62 (d, *J* = 7.6 Hz, 1H), 8.19 (d, *J* = 5.6 Hz, 1H); ESIMS *m/z* 450.4 [M + H]<sup>+</sup>.

**2-((4-(3-(4-Fluorophenyl)-4,5-dihydro-1H-pyrazol-5-yl)-2-methoxyphenoxy)methyl)-3,4-dimethoxy pyridine (5)**

<sup>1</sup>H NMR (400 MHz, DMSO-*d*<sub>6</sub>) δ ppm 2.84 (dd, *J* = 10.8 & 10.8 Hz, 1H), 3.39 (dd, *J* = 9.6.4 & 10.4 Hz, 1H), 3.71 (s, 3H), 3.74 (s, 3H), 3.77 (s, 3H), 3.90 (s, 3H), 4.66 (t, 1H), 5.08 (s, 2H), 6.88 (d, *J* = 7.2 Hz, 1H), 6.92 (t, 2H), 6.97 (s, 1H), 7.02 (dd, *J* = 5.2 & 4.4 Hz, 1H), 7.11 (t, *J* = 8.0 Hz, 2H), 7.15 (d, *J* = 5.6 Hz, 1H), 7.55 (dd, *J* = 5.6 & 4.8 Hz, 2H), 8.23 (d, *J* = 5.6 Hz, 1H); 41.32, 55.76, 59.64, 64.17, 71.99, 105.8, 109.51, 114.27, 115.29, 115.42, 118.44, 126.15, 126.54, (127.48, 127.58 F-C), 129.03, 129.06, 135.56, 147.51, 148.75, 149.86, 150.11, 154.18, 161.55 (F-C), 164.0 (F-C), 164.19; ESIMS *m/z* 438.3 [M + H]<sup>+</sup>.

**6-(5-(4-((3,4-Dimethoxypyridin-2-yl)methoxy)-3-methoxyphenyl)-4,5-dihydro-1H-pyrazol-3-yl)-2H-benzo[*b*][1,4]oxazin-3(4H)-one (6)**

<sup>1</sup>H NMR (400 MHz, DMSO-*d*<sub>6</sub>) δ ppm 2.79 (dd, *J* = 9.2 & 9.6 Hz, 1H), 3.71 (s, 3H), 3.76 (s, 3H), 3.79 (dd, *J* = 10.8 & 10.8 Hz, 1H), 3.90 (s, 3H), 4.59 (s, 2H), 4.75 (s, 2H) 5.02 (s, 2H), 6.85 (d, *J* = 7.2 Hz, 1H), 6.94 (d, *J* = 8.4 Hz, 1H), 6.95 (s, 1H), 7.05 (d, *J* = 8.4 Hz, 1H), 7.09 (d, *J* = 8.4 Hz, 1H), 7.14 (d, *J* = 5.6 Hz, 1H), 7.25 (s, 1H), 7.41 (s, 1H), 8.22 (d, *J* = 5.6 Hz, 1H), 10.21 (s, 1H), 10.77 (s, 1H), <sup>13</sup>C NMR (101.3 MHz, CDCl<sub>3</sub>) δ ppm 41.55, 55.65, 55.78, 61.48, 63.99, 67.16, 67.93, 107.70, 109.69, 113.04, 114.04, 116.57, 118.49, 122.17, 126.57, 127.60, 135.39, 144.18, 144.67, 145.77, 147.88, 149.79, 149.99, 150.73, 158.87, 165.57; FT-IR (KBr) cm<sup>-1</sup> 1597, 1521, 1498, 1354, 1228, 1166, 828, 767; ESIMS *m/z* 491.4 [M + H]<sup>+</sup>.

**2-((4-(4,5-Dihydro-3-phenyl-1H-pyrazol-5-yl)-2-methoxyphenoxy)methyl)-4-methoxy-3,5-dimethylpyridine (7)**

<sup>1</sup>H NMR (400 MHz, DMSO-*d*<sub>6</sub>) δ ppm 2.22 (s, 3H), 2.25 (s, 3H), 2.89 (dd, *J* = 10.4 & 10.8 Hz, 1H), 3.39 (dd, *J* = 10.4 & 10.8 Hz, 1H), 7.04 (d, *J* = 8.4 Hz, 1H), 3.73 (s, 6H), 4.78 (t, 1H), 5.08 (s, 2H), 6.85 (d, *J* = 8.4 Hz, 1H), 7.00 (s, 1H), 7.04 (d, 1H), 7.31 (d, *J* = 6.8 Hz, 1H), 7.37 (t, *J* = 7.2 Hz, 2H), 7.50 (s, 1H, -NH), 7.61 (d, *J* = 7.6 Hz, 2H), 8.20 (s, 1H); <sup>13</sup>C NMR 101.3 MHz, CDCl<sub>3</sub>) δ ppm 10.7, 13.2, 41.3, 55.8, 59.7, 64.1, 72.1, 109.3, 114.3, 118.5, 125.8(2), 126.2, 126.6, 128.4(2), 128.6, 132.7, 135.7, 147.6, 148.8, 149.9, 151.2, 154.2, 164.2; ESIMS *m/z* 418.3[M + H]<sup>+</sup>.

**2-(5-(4-((4-Methoxy-3,5-dimethyl pyridin-2-yl)methoxy)-3-methoxy phenyl)-4,5-dihydro-1H-pyrazol-3-yl)phenol (8)**

<sup>1</sup>H NMR (400 MHz, DMSO-*d*<sub>6</sub>) δ ppm 2.20 (s, 3H), 2.24 (s, 3H), 2.98 (dd, *J* = 12.8 & 11.2 Hz, 1H), 3.54 (dd, *J* = 10.4 & 10.4 Hz, 1H), 3.72 (s, 6H), 4.77(t, *J* = 10.0 Hz, 1H), 5.07(s, 2H), 6.85 - 6.89 (m, 3H), 7.02 (s, 1H), 7.05 (d, *J* = 8.0 Hz, 1H), 7.20 (t, *J* = 8.0 Hz, 1H), 7.27 (d, *J* = 8.0 Hz, 1H), 7.75 (s, 1H, -NH), 8.19 (s, 1H), 11.15 (s, 1H, -OH); <sup>13</sup>C NMR (101.3 MHz, CDCl<sub>3</sub>) δ ppm 10.7, 13.21, 41.4, 55.8, 59.7, 62.5, 71.9, 109.6, 114.3, 116.3(2), 118.5, 118.9, 126.2, 126.6, 127.4, 130.1, 134.8, 147.7, 148.7, 149.9, 154.0, 154.1, 157.5, 164.1; ESIMS *m/z* 434.3[M + H]<sup>+</sup>.

**2-(5-(4-((4-Methoxy-3,5-dimethylpyridin-2-yl)methoxy)-3-methoxyphenyl)-4,5-dihydro-1H-pyrazol-3-yl)-4-methylphenol (9)**

<sup>1</sup>H NMR (400 MHz, DMSO-d<sub>6</sub>) δ ppm 2.20 (s, 3H), 2.24 (s, 3H), 2.36 (s, 3H), 2.99 (dd, *J* = 12.8 & 11.2 Hz, 1H), 3.54 (dd, *J* = 10.4 & 10.4 Hz, 1H), 3.72 (s, 6H), 4.77 (t, 1H), 5.08 (s, 2H), 6.85-6.89 (m, 2H), 7.02 (s, 1H), 7.05 (d, *J* = 8.0 Hz, 1H), 7.20 (t, *J* = 7.6 Hz, 1H), 7.27 (d, *J* = 8.0 Hz, 1H), 7.75 (s, 1H, -NH), 8.19 (s, 1H), 11.15 (s, 1H, -OH); <sup>13</sup>C NMR (101.3 MHz, CDCl<sub>3</sub>) δ ppm 10.74, 13.21, 31.12, 41.49, 55.81, 59.72, 62.5, 71.9, 109.6, 114.3, 116.3, 118.5, 118.9, 126.2, 126.6, 127.4, 130.1(2), 134.8, 147.7, 148.7, 149.9, 154.0, 154.1, 157.5, 164.1; ESIMS *m/z* 448.4 [M + H]<sup>+</sup>.

**2-((4-(3-(4-Fluorophenyl)-4,5-dihydro-1H-pyrazol-5-yl)-2-methoxyphenoxy)methyl)-3,4-dimethoxypyridine (10)**

<sup>1</sup>H NMR (400 MHz, DMSO-d<sub>6</sub>) δ ppm 2.22 (3H, s), 2.25 (3H, s), 2.84 (1H, dd, *J* = 10.8 & 10.8 Hz), 3.37 (1H, dd, *J* = 10.8 & 10.8 Hz), 3.73 (6H, s), 4.78 (1H, t, *J* = 10.4 Hz), 5.08 (2H, s), 6.85 (1H, d, *J* = 8.4 Hz), 7.00 (1H, s), 7.05 (1H, d, *J* = 8.4 Hz), 7.22 (1H, t, *J* = 8.0 Hz), 7.49 (1H, s), 7.65 (1H, t, *J* = 6.8 Hz), 8.20 (1H, s); <sup>13</sup>C NMR (101.3 MHz) in CDCl<sub>3</sub> δ ppm 10.7, 13.1, 41.3, 55.7, 59.6, 64.1, 71.9, 109.5, 114.2, 115.2, 115.4, 118.4, 126.1, 126.5, (127.4, 127.5), (129.03, 129.06), 135.5, 147.5, 148.7, 149.8, 150.1, 154.1, 161.5 (F-C), 164.0 (F-C), 164.1; ESIMS *m/z* 436.3 [M + H]<sup>+</sup>.

**6-(5-(4-((4-Methoxy-3,5-dimethylpyridin-2-yl)methoxy)-3-methoxyphenyl)-4,5-dihydro-1H-pyrazol-3-yl)-2H-benzo[b][1,4]oxazin-3(4H)-one (11)**

<sup>1</sup>H NMR (400 MHz, DMSO-d<sub>6</sub>) δ ppm 2.22 (s, 3H), 2.25 (s, 3H), 2.78 (dd, *J* = 11.2 & 11.2 Hz, 1H), 3.34 (dd, *J* = 12.8 Hz & 12.8 Hz, 1H), 3.73 (s, 3H), 3.74 (s, 3H), 4.59 (s, 2H), 4.75 (t, *J* = 10.8 Hz, 1H), 5.08 (s, 2H), 6.85 (d, *J* = 8.0 Hz, 1H), 6.93 (d, *J* = 8.4 Hz, 1H), 7.0 (s, 1H), 7.05 (d, *J* = 8.0 Hz, 1H), 7.09 (d, *J* = 8.8 Hz, 1H), 7.25 (s, 1H), 7.40 (s, 1H, -NH), 8.2 (s, 1H), 10.79 (bs, 1H); <sup>13</sup>C NMR (101.3 MHz, CDCl<sub>3</sub>) δ ppm 10.7, 13.2, 41.5, 55.7, 59.7, 63.8, 67.0, 71.7, 109.7, 113.0, 114.2, 116.4, 118.5, 122.0, 126.2, 126.5, 126.6, 127.4, 135.5, 144.1, 147.5, 148.6, 149.8, 150.6, 154.0, 164.2, 165.6; ESIMS *m/z* 490.3 [M + H]<sup>+</sup>.

**3-(4-(4-(4,5-Dihydro-3-phenyl-1H-pyrazol-5-yl)-2-methoxyphenoxy)butyl)piperazin-1-yl)benzo[d]isothiazole (12)**

<sup>1</sup>H NMR (400 MHz, DMSO-d<sub>6</sub>) δ ppm 1.61 (m, 2H), 1.75 (m, 2H), 2.45 (t, 2H), 2.59 (bpeak, 4H), 2.98 (dd, *J* = 11.2 Hz & 11.2 Hz, 1H), 3.63 (dd, *J* = 10.4 Hz & 11.2 Hz, 1H), 3.43 (bpeak, 4H), 3.75 (s, 3H), 3.97 (t, 2H), 4.78 (t, 1H), 6.86 (d, *J* = 2.4 Hz, 1H), 6.93 (d, *J* = 8.4 Hz, 1H), 7.01 (t, *J* = 2.4 Hz, 1H), 7.31 (t, *J* = 7.2 Hz, 1H), 7.43 (t, *J* = 6.8 Hz, 2H), 7.52 (d, *J* = 3.6 Hz, 1H, -NH), 7.56 (t, *J* = 5.4 Hz, 1H), 7.62 (d, *J* = 7.2 Hz, 2H), 8.05 (d, *J* = 8 Hz, 2H); ESIMS *m/z* 542.4 [M + H]<sup>+</sup>.

**2-(5-(4-(4-(4-(Benzo[d]isothiazol-3-yl)piperazin-1-yl)butoxy)-3-methoxyphenyl)-4,5-dihydro-1H-pyrazol-3-yl)phenol (13)**

<sup>1</sup>H-NMR (400 MHz, CDCl<sub>3</sub>) δ ppm 1.61 (m, 2H), 1.75 (m, 2H), 2.42 (t, 2H), 2.59 (m, 4H), 2.98 (dd, *J* = 11.6 & 11.2 Hz, 1H), 3.43 (bpeak, 4H), 3.56 (dd, *J* = 10.4 & 10.4 Hz, 1H), 3.76 (s, 3H), 3.97 (t, 2H), 4.78 (t, 1H), 6.86-6.95 (m, 4H), 7.03 (d, *J* = 2.4 Hz, 1H), 7.23 (t, *J* = 8.0 Hz, 1H), 7.29 (dd, *J* = 1.2 & 8.4 Hz, 1H), 7.43 (t, *J* = 8.0 Hz, 1H), 7.56 (t, *J* = 8.0 Hz, 1H), 7.78 (d, *J* = 8.0 Hz, 1H), 8.04 (d, *J* = 8.4 Hz, 2H), 11.18 (s, 1H), 8.17 (d, *J* = 8.0 Hz, 2H); <sup>13</sup>C NMR (101.3 MHz, CDCl<sub>3</sub>) δ ppm 23.2, 27, 41.6, 49.9(2), 52.9(2), 55.9, 58.1, 62.6, 68.7, 109.7, 113.0, 116.4, 118.6, 118.9, 120.4, 127.37, 127.60, 123.7, 123.8, 127.4, 127.4, 127.9, 130.2, 134.3, 148.1, 149.6, 152.6, 154.2, 157.6, 163.8; FT-IR (KBr) cm<sup>-1</sup> 758, 838, 1137, 1236, 1253, 1375, 1484, 1592 & 1514; ESIMS *m/z* 558.4 [M + H]<sup>+</sup>.

**3-(4-(4-(4-(3-(4-Fluorophenyl)-4,5-dihydro-1H-pyrazol-5-yl)-2-methoxyphenoxy)butyl)piperazin-1-yl)benzo[d]isothiazole (14)**

<sup>1</sup>H NMR (400 MHz, DMSO-d<sub>6</sub>) δ ppm 1.74 (m, 2H), 1.90 (m, 2H), 2.51 (t, 2H), 2.66 (m, 4H), 3.00 (dd, *J* = 9.2 Hz & 9.2 Hz, 1H), 3.42 (dd, *J* = 10.8 Hz & 10.8 Hz, 1H), 3.56 (t, 4H), 3.85 (s, 3H), 4.06 (t, 1H), 4.88 (t, 2H), 6.87 (d, *J* = 8.0 Hz, 1H), 6.93 (d, *J* = 8.4 Hz, 1H), 6.99 (d, *J* = 2.4 Hz, 1H), 7.21 (t, 1H), 7.43 (t, 1H), 7.51 (d, *J* = 3.6 Hz, 2H), 7.65 (dd, *J* = 5.2 Hz & 5.6 Hz, 2H), 8.05 (d, *J* = 8.4 Hz, 2H); <sup>13</sup>C NMR (101.3 MHz, CDCl<sub>3</sub>) δ ppm 23.2, 27.0, 41.5, 49.95(2), 52.9(2), 55.9, 58.1, 64.2, 68.7, 109.7, 112.7, 115.3, 115.5, 118.5, 120.4, 123.8(2), 127.4, 127.6, 127.7, 127.9, 129.1, 135.0, 148.0, 149.6, 150.4, 152.6, 162.0 (F-C), 163.8, 164.0 (F-C); ESIMS *m/z* 560.4 [M + H]<sup>+</sup>.

**6-((R)-5-(4-(4-(4-(Benzo[d]isothiazol-3-yl)piperazin-1-yl)butoxy)-3-methoxyphenyl)-4,5-dihydro-1H-pyrazol-3-yl)-2H-benzo[b][1,4]oxazin-3(4H)-one (15)**

<sup>1</sup>H NMR (400 MHz, DMSO-d<sub>6</sub>) δ ppm 1.61 (m, 2H), 1.74 (m, 2H), 2.42 (t, 2H), 2.59 (bpeak, 4H), 2.77 (dd, *J* = 10.8 Hz & 10.8 Hz, 1H), 3.31 (dd, *J* = 10.4 & 10.2 Hz, 1H), 3.33 (bpeak, 4H), 3.75 (t, 3H), 3.96 (t, 2H), 4.59 (s, 2H), 4.69 (t, 1H), 6.84 (d, *J* = 8.4 Hz, 2H), 6.926 (d, *J* = 7.6 Hz, 2H), 6.98 (d, *J* = 1.2 Hz, 1H), 7.08 (d, *J* = 8.0 Hz, 1H), 7.263 (d, *J* = 1.6 Hz, 1H), 7.41-7.45 (m, 2H), 7.55 (t, 1H), 8.05 (d, *J* = 8.0 Hz, 2H), <sup>13</sup>C NMR (101.3 MHz, CDCl<sub>3</sub>) δ ppm 23.2, 27.0, 41.6, 49.9(2), 52.9(2), 55.9, 58.1, 63.9, 67.1, 68.7, 109.8, 112.9, 116.5, 118.5, 120.4(2), 122.2, 123.7, 123.8, 126.5, 127.4, 127.5, 127.9, 134.9, 144.2, 147.9, 149.5, 150.7, 152.6, 163.8, 165.6; ESIMS *m/z* 613.4 [M + H]<sup>+</sup>.

**3-(4-(4-(4-(3-(3-(4-Fluorophenyl)-1-isopropyl-1H-indol-6-yl)-4,5-dihydro-1H-pyrazol-5-yl)-2-methoxyphenoxy)butyl)piperazine-1-yl)benzo[d]isothiazole (16)**

<sup>1</sup>H NMR (400 MHz, DMSO-d<sub>6</sub>) δ ppm 1.51 (d, 6H), 1.62 (m, 2H), 1.74 (m, 2H), 2.42 (m, 2H), 2.59 (bpeak, 4H), 2.95 (dd, *J* = 11.2 Hz & 10.8 Hz, 1H), 3.43 (bpeak, 4H), 3.50 (dd, *J* = 10.4 & 10.4 Hz, 1H), 3.76 (s, 3H), 3.97 (d, 2H), 4.78 (t, 1H), 4.81 (m, 1H), 6.89 (m, 3H), 7.03 (s, 1H), 7.24-7.32 (m, 3H), 7.43 (t, 1H), 7.56 (t, 1H), 7.62 (t, 2H), 7.71 (dd, *J* = 5.6 Hz & 5.6 Hz, 2H), 7.85 (s, 1H), 7.95 (s, 1H), 8.05 (d, *J* = 7.2 Hz, 2H); <sup>13</sup>C NMR (101.3 MHz, CDCl<sub>3</sub>) δ ppm 22.7,



23.2, 27.1, 42.0, 47.3, 49.9(2), 52.9(2), 55.9, 58.2, 63.9, 68.8, 109.7, 110.0, 112.9, 115.4, 115.6, 116.6, 117.9, 118.1, 118.6, 120.1, 120.4, 121.8, 123.7, 123.8, 125.1, 126.0, 127.4, 127.9(2), 128.7, 128.8, 131.4, 135.6, 136.3, 147.9, 149.6, 152.6, 152.9, 163.8; ESIMS  $m/z$  717.6  $[M + H]^+$ .

**3-(4-(4-(4,5-Dihydro-1,3-diphenyl-1H-pyrazol-5-yl)-2-methoxyphenoxy)butyl)piperazin-1-yl)benzo[d]isothiazole (17)**

$^1H$  NMR (400 MHz,  $CDCl_3$ )  $\delta$  ppm 1.72 (m, 2H), 1.88 (m, 2H), 2.47 (t, d,  $J = 7.2$  Hz, 2H), 2.67 (bpeak, 4H), 3.14 (dd,  $J = 7.6$  Hz & 7.6 Hz, 1H), 3.56 (bpeak, 4H), 3.77-3.84 (m, 4H), 4.04 (t,  $J = 6.8$  Hz, 2H), 5.18 (dd,  $J = 8.0$  Hz & 8.0 Hz, 1H), 6.78 (t,  $J = 7.6$  Hz, 1H), 6.82-6.87 (m, 3H), 7.09 (d,  $J = 8.0$  Hz, 2H), 7.17 (t,  $J = 8.0$  Hz, 2H), 7.32-7.40 (m, 4H), 7.46 (t,  $J = 7.6$  Hz, 1H), 7.73 (d,  $J = 7.2$  Hz, 2H), 7.80 (d,  $J = 8.0$  Hz, 1H), 7.90 (d,  $J = 8.0$  Hz, 1H);  $^{13}C$  NMR ( $CDCl_3$ )  $\delta$  ppm 23.3, 27.1, 43.6, 50.0(2), 52.9(2), 55.9, 58.2, 64.6, 68.7, 109.0, 113.1, 113.4(2), 118.0, 119.1, 120.5, 123.7, 123.8, 125.6(2), 127.4, 127.9, 128.4(2), 128.7(2), 132.7, 135.2, 145.1, 146.8, 147.7, 149.9, 152.6, 163.8; ESIMS  $m/z$  618.5  $[M + H]^+$ .

**3-(4-(4-(3-(4-Fluorophenyl)-4,5-dihydro-1-phenyl-1H-pyrazol-5-yl)-2-methoxyphenoxy) butyl)piperazin-1-yl)benzo[d]isothiazole (18)**

$^1H$  NMR (400 MHz,  $DMSO-d_6$ )  $\delta$  ppm 1.73 (m, 2H), 1.89 (m, 2H), 2.50 (t, 2H), 2.69 (bpeak, 4H), 3.11 (dd,  $J = 7.6$  Hz & 7.2 Hz, 1H), 3.56 (bpeak, 4H), 3.75-3.88 (m, 4H), 4.04 (t,  $J = 7.2$  Hz, 2H), 5.19 (dd,  $J = 8.0$  Hz, 8.0 Hz, 1H), 6.73 (t,  $J = 7.6$  Hz, 1H), 6.84 (d,  $J = 8.8$  Hz, 2H), 7.08 (d,  $J = 4.4$  Hz, 2H), 7.32-7.36 (m, 2H), 7.42-7.47 (m, 2H), 7.55-7.58 (m, 2H), 7.80 (d,  $J = 8.0$  Hz, 1H), 7.18 (t,  $J = 7.6$  Hz, 2H), 7.36 (t,  $J = 7.2$  Hz, 2H), 7.47 (t,  $J = 7.6$  Hz, 1H), 7.71 (t,  $J = 7.6$  Hz, 2H), 7.81 (d,  $J = 8.4$  Hz, 1H), 7.90 (d,  $J = 8.0$  Hz, 1H); ESIMS  $m/z$  636.5  $[M + H]^+$ .

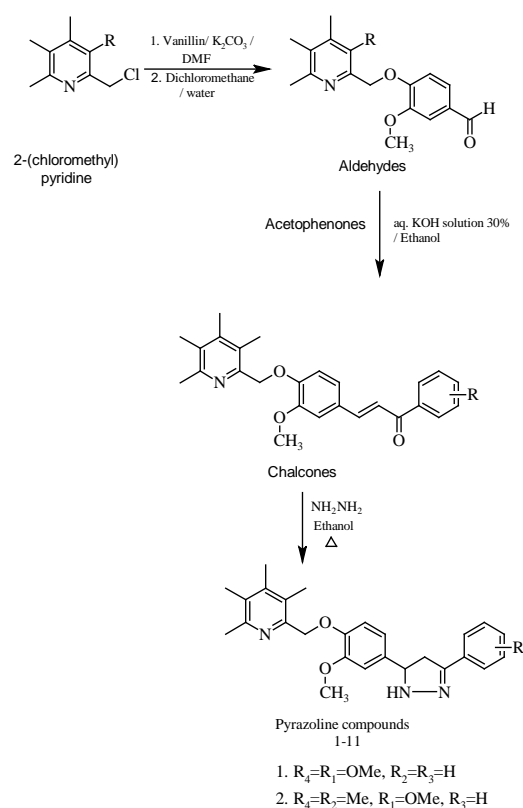
**3-(4-(4-(3-(3-(4-Fluorophenyl)-1-isopropyl-1H-indol-6-yl)-4,5-dihydro-1-phenyl-1H-pyrazol-5-yl)-2-methoxyphenoxy)-butyl)piperazin-1-yl)benzo[d]isothiazole (19)**

$^1H$  NMR (400 MHz,  $DMSO-d_6$ )  $\delta$  ppm 1.58 (m, 6H), 1.72 (m, 2H), 1.89 (m, 2H), 2.49 (t, 2H), 2.67 (bpeak, 4H), 3.23 (dd,  $J = 10.8$  Hz & 11.2 Hz, 1H), 3.56 (bpeak, 4H), 3.79 (s, 3H), 3.90 (dd,  $J = 10.2$  Hz & 10.8 Hz, 1H), 4.03 (t, 2H), 4.73 (m, 1H), 5.15 (dd,  $J = 9.6$  Hz & 9.6 Hz, 1H), 6.74-6.90 (m, 5H), 7.09-7.20 (m, 5H), 7.32-7.36 (m, 2H), 7.42-7.47 (m, 2H), 7.55-7.58 (m, 2H), 7.80 (d,  $J = 8.0$  Hz, 1H), 7.91 (dd,  $J = 8.4$  Hz & 5.6 Hz, 2H), 7.94 (s, 1H);  $^{13}C$  NMR (101.3 MHz,  $CDCl_3$ )  $\delta$  ppm 22.8(2), 27.1, 44.2, 47.3, 50.0(2), 52.9(2), 55.98, 58.2, 64.6, 68.7, 109.1, 110.1, 113.1, 113.3(2), 115.5, 115.7, 116.7, 117.6, 118.0, 118.7, 120.0, 120.5(2), 121.8, 123.8, 123.8, 125.0, 126.0, 127.4(2), 128.0, 128.7, 128.8, 131.4, 131.4, 135.7, 136.3, 145.6, 147.7, 148.4, 150.0, 152.7, 160.1, 162.6, 163.9; ESIMS  $m/z$  793.7  $[M+H]^+$ .

## RESULT AND DISCUSSIONS

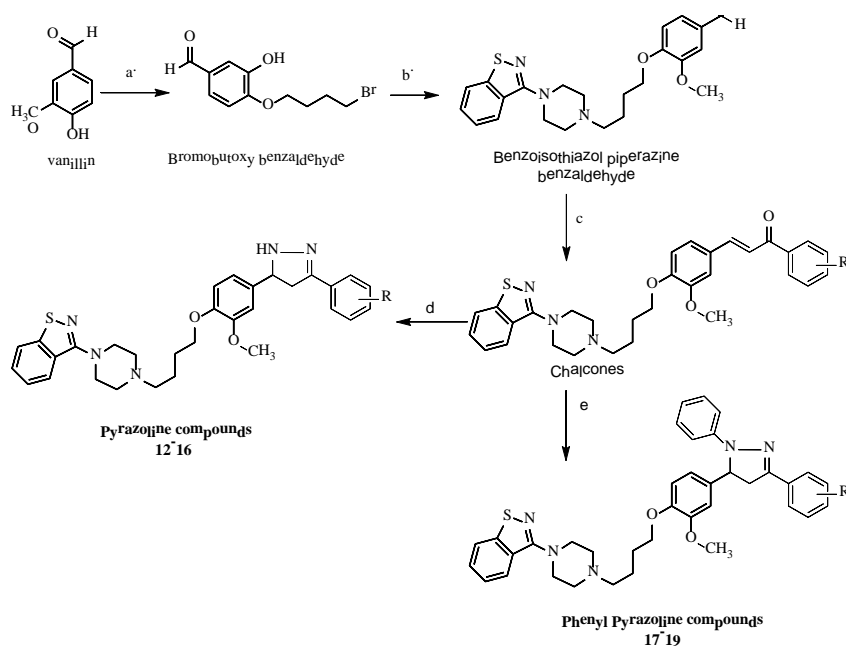
In this communication, two new series of pyrazoline containing substituted chloromethyl pyridine and alkoxy linkage side chain containing benzoisothiazole represented as in Schemes 1 and 2. The essentials of synthesized compounds were confirmed by their physical properties and spectroscopic techniques like  $^1H$  NMR,  $^{13}C$  NMR, Mass spectroscopy and FT-IR.

Substituted chloromethylpyridines were treated with vanillin at room temperature in the presence of potassium carbonate and DMF used as a solvent to get aldehydes. These aldehydes were reacted further with different acetophenones, as shown in Table 1, in the presence of 30 % aq. KOH solution where ethanol used as a solvent in the reaction to form the respective chalcones. Pyrazolines were synthesized by refluxing chalcones with hydrazine hydrate in the presence of ethanol as the solvent.



**Scheme 1.** Synthesis of pyrazoline compounds (1-11).

Spectroscopic data confirmed the assigned structure for 1-19, where its  $^1H$  NMR,  $^{13}C$  NMR and mass spectroscopy where disappearance of the  $C=C$  bond two trans proton coupling having  $J$  value  $\sim 16.0$  Hz of chalcones and formation of three peaks displayed in pyrazoline ( $\delta \sim 2.8$ , 3.4 and a triplet at  $\sim 4.7$  ppm ( $D_2O$ -exchangeable, 1H, NH)).  $^{13}C$ -NMR shows signals corresponding to respective types of carbon in different chemical shifts of pyrazoline compounds details of the chemical shift were captured in the characterization part.



**Scheme 2.** Synthesis of pyrazoline and phenyl pyrazoline compounds (**12-19**): Reaction conditions a)  $K_2CO_3$ /DMF/1,4-dibromobutane, dichloromethane and water. b)  $K_2CO_3$ /DMF/3-(piperazin-1-yl)benzo[d]isothiazole, isopropyl alcohol. c) 30% aq. solution of KOH. d)  $NH_2NH_2$ /ethanol/  $\Delta$  e)  $PhNHNH_2$ , EtOH,  $\Delta$

Mass spectroscopy gives corresponding  $[M+1]$  molecular ion peak at their corresponding molecular weight, as shown in Table 1. The IR spectrum of compounds showed a broad band at  $\sim 3446\text{ cm}^{-1}$  recognized for -OH group and the characteristic N=N band was assigned at  $1591\text{ cm}^{-1}$  two strong bands at  $\sim 1650\text{ cm}^{-1}$  and  $\sim 1607\text{ cm}^{-1}$  referring to carbonyl and carbon-carbon double bond disappearance confirmed the formation of pyrazolines compounds.

The synthesized compounds were assigned on the basis of  $^1H$  NMR,  $^{13}C$  NMR, mass and IR spectral analytical studies to confirm the proposed structures. Physical constant data were tabulated in Table 1.

### Molecular docking

To study binding conformations of the synthesized compounds, the Autodock Vina program was used for docking pyrazoline derivatives into the active sites of methionyl-tRNA synthetase. The AutoDock Tools 1.5.4 (ADT) was used to prepare the input files for docking.<sup>18</sup> The crystal structure of *Thermus thermophilus* methionyl-tRNA synthetase reveals two RNA-binding modules. All water molecules and ions were removed from the protein crystallographic structures; polar hydrogens were added and partial atomic charges were assigned by Kollman united charges method.<sup>19-21</sup>

Sidechains of lysine, arginine, and histidine residues were protonated while the carboxylic groups of glutamic and aspartic acid were deprotonated. For each ligand, nonpolar hydrogens were merged, Gasteiger charges were assigned and rotatable bonds were set up. The structures were then saved in the corresponding pdbqt file required for the Autodock.

### Antioxidant activity

Antioxidant potential of the synthesized compounds was measured in terms of DPPH, OH and superoxide radical (SOR) scavenging activity carried out using reported methods,<sup>22</sup> following the procedure as discussed in our previous publications.<sup>16</sup> The results of antioxidant activity are summarized in Table 2. The detailed procedure for the antioxidant activity is provided in the supplementary material.

### Antimicrobial screening

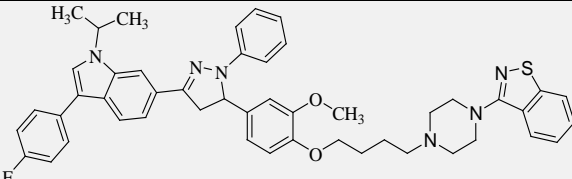
To confirm the inhibitory activity, the hit compounds were re-tested against the strains in a dose-response assay to determine the minimum inhibitory concentration (MIC) of the compounds. Samples were prepared in DMSO and water to a final testing concentration of  $32\text{ }\mu\text{g mL}^{-1}$  or  $20\text{ }\mu\text{M}$  in 384-well, non-binding surface plate (NBS) for each bacterial/fungal strain, in duplicate ( $n=2$ ), and keeping the final DMSO concentration to a maximum of 1 % DMSO. All the sample-preparation was done using liquid handling robots. All bacteria were cultured in cation-adjusted Mueller Hinton broth (CAMHB) at  $37\text{ }^\circ\text{C}$  overnight. A sample of each culture was then diluted 40-fold in fresh broth and incubated at  $37\text{ }^\circ\text{C}$  for 1.5-3 h. The resultant mid-log phase cultures were diluted ( $\text{CFU mL}^{-1}$  measured by OD600), added to each well of the compound containing plates giving a cell density of  $5 \times 10^5\text{ CFU mL}^{-1}$  and a total volume of  $50\text{ }\mu\text{L}$ . All the plates were covered and incubated at  $37\text{ }^\circ\text{C}$  for 18 h without shaking.

**Table 1.** Physical constant of the synthesized compounds.

Code	Structure of compounds	Molecular formula	Molecular wt.	M. P., °C	Yield, %
1		C <sub>24</sub> H <sub>25</sub> N <sub>3</sub> O <sub>4</sub>	419.47	171	92
2		C <sub>24</sub> H <sub>25</sub> N <sub>3</sub> O <sub>5</sub>	435.47	176	87
3		C <sub>25</sub> H <sub>27</sub> N <sub>3</sub> O <sub>5</sub>	449.5	175	83
4		C <sub>25</sub> H <sub>27</sub> N <sub>3</sub> O <sub>5</sub>	449.5	173	85
5		C <sub>24</sub> H <sub>24</sub> FN <sub>3</sub> O <sub>4</sub>	437.46	169	88
6		C <sub>26</sub> H <sub>26</sub> N <sub>4</sub> O <sub>6</sub>	490.51	207	93
7		C <sub>25</sub> H <sub>27</sub> N <sub>3</sub> O <sub>3</sub>	417.5	161	70
8		C <sub>25</sub> H <sub>27</sub> N <sub>3</sub> O <sub>4</sub>	433.5	163	68
9		C <sub>26</sub> H <sub>29</sub> N <sub>3</sub> O <sub>4</sub>	447.53	165	69

10		<chem>C25H26FN3O3</chem>	435.49	166	70
11		<chem>C27H28N4O5</chem>	488.54	225	72
12		<chem>C31H35N5O2S</chem>	541.71	163	69.8
13		<chem>C31H35N5O3S</chem>	557.71	171	78
14		<chem>C31H34FN5O2S</chem>	559.7	160	79
15		<chem>C33H36N6O4S</chem>	612.74	171	78
16		<chem>C42H45FN6O2S</chem>	716.91	172	80
17		<chem>C37H39N5O2S</chem>	617.8	168	71
18		<chem>C37H38FN5O2S</chem>	635.79	164	69



19		C <sub>48</sub> H <sub>49</sub> FN <sub>6</sub> O <sub>2</sub> S	793.01	174	70
----	---	--	--------	-----	----

**Table 2.** Radical scavenging profile of the synthesized compounds

Compound	% Radical scavenging activity		
	DPPH	OH	SOR
1	NR	44.76 ± 1.03	32.74 ± 1.27
2	40.76 ± 1.76	26.01 ± 1.09	60.52 ± 1.03
3	20.76 ± 1.63	11.59 ± 1.36	32.41 ± 0.89
4	23.62 ± 1.61	11.99 ± 0.72	41.36 ± 0.56
5	78.52 ± 1.51	07.82 ± 0.64	52.16 ± 2.14
6	37.09 ± 1.49	31.95 ± 0.76	53.14 ± 1.29
7	39.16 ± 0.13	27.03 ± 0.14	32.63 ± 1.34
8	56.93 ± 1.93	12.04 ± 1.20	21.52 ± 1.87
9	41.15 ± 2.14	12.70 ± 1.91	43.87 ± 1.64
10	52.71 ± 1.02	12.48 ± 1.85	36.46 ± 1.35
11	20.28 ± 0.21	34.61 ± 1.43	35.82 ± 0.87
12	33.11 ± 0.52	10.49 ± 1.84	37.42 ± 1.49
13	47.53 ± 0.63	31.95 ± 0.12	53.45 ± 1.26
14	64.02 ± 0.84	15.43 ± 0.46	45.61 ± 1.47
15	59.88 ± 2.14	17.31 ± 1.74	37.46 ± 1.67
16	37.81 ± 1.84	21.22 ± 1.61	44.21 ± 1.34
17	68.88 ± 0.83	07.82 ± 1.76	55.41 ± 0.57
18	78.88 ± 0.73	31.95 ± 0.73	65.43 ± 0.39
19	75.02 ± 2.59	31.98 ± 2.46	37.63 ± 0.16
*AA	91.25 ± 1.91	89.11 ± 1.67	79.86 ± 1.24

\*AA: ascorbic acid. Results represented here are the mean of  $n=3 \pm SD$ . NR: No reaction under the experimental conditions.

Fungi strains were cultured for 3 days on yeast extract-peptone dextrose (YPD) agar at 30 °C. A yeast suspension of  $1 \times 10^6$  to  $5 \times 10^6$  CFU mL<sup>-1</sup> (as determined by OD530) was prepared from five colonies. The suspension was subsequently diluted and added to each well of the compound containing plates giving a final cell density of fungi suspension of  $2.5 \times 10^3$  CFU mL<sup>-1</sup> and a total volume of 50 µL. All plates were covered and incubated at 35 °C for 24 h without shaking.

Colistin and Vancomycin were used as positive bacterial inhibitor standard for gram-negative and gram-positive bacteria, respectively. Fluconazole was used as a positive fungal inhibitor standard for *C. Albicans* and *C. neoformans*. The antibiotics were provided in 4 concentrations, with 2 above and 2 below its MIC value, and plated into the first 8 wells of column 23 of the 384-well NBS plates. The quality control (QC) of the assays was determined by the antimicrobial controls and the Z'-factor (using positive and negative controls). Each plate was deemed to fulfill the quality criteria (pass QC) if the Z'-factor was above 0.4, and the antimicrobial standards showed the full range of activity, with full growth inhibition at their highest concentration, and no growth inhibition at their lowest concentration.

The inhibition of bacterial growth was determined by measuring absorbance at 600 nm (OD600) using a Tecan

M1000 Pro monochromator plate reader. The percentage of growth inhibition was calculated for each well using the negative control (media only) and positive control (bacteria without inhibitors) on the same plate as references. The significance of the inhibition values was determined by modifying Z-scores, calculated using the median of the samples (no controls) on the same plate. Samples with inhibition values above 80 % and Z-score above 2.5 for either replicate ( $n=2$  on different plates) were classed as actives, whereas samples with inhibition values between 50 – 80 % and Z-score below 2.5 for either replicate ( $n=2$  on different plates) were classed as partially active.

**Table 3.** Material assays for antimicrobial activity

Material	Code	Brand	Catalogue No.
Compound preparation	Plate PP	Corning	3364
Assay plates	NBS 384w	Corning	3640
Growth media-bacteria	CAMHB	Bacto Laboratories	212322
Culture agar-fungi	YPD	Becton Dickinson	242720
Growth media-fungi	YNB	Becton Dickinson	233520
Resazurin		Sigma-Aldrich	R7017

Percentage growth inhibition of individual samples was calculated based on negative controls (media only) and positive controls (bacterial media without inhibitors). The percentage of growth inhibition was calculated for each well using the negative control (media only) and positive control (without inhibitors) on the same plate. The growth rates for all bacteria and fungi have a variation of  $\pm 10$  %, which lies within the expected normal distribution of microbial growth. □

### Molecular docking

The synthesized compounds were docked against the active site of *Thermus thermophilus* methionyl-tRNA synthetase using Autodock vina docking tool whose results were expressed in terms of docking scores (Table 8). Analysis of docking interaction reveals that the pyrazoles bearing benzisothiazole ring (**12**, **13** and **15**) were the most active compounds against methionyl-tRNA synthetase. Results of observed antimicrobial activities are in good agreement for these tilted compounds in terms of higher negative values of Z-scores.

The benzisothiazole linked pyrazolines **12**, **13** and **15** bind efficiently into the active site residues like TYR13, GLU54, ARG132, ASP50, ASP260, GLY21, HIS22, LEU290, ILE261, VAL226, and LYS297.

**Table 4.** Standards for antimicrobial activity

Sample	Sample ID	Full MW	Stock conc. µg mL <sup>-1</sup>	Solvent	Source
Colistin	Sulfate MCC_000094:02	1400.63	10.0	DMSO	Sigma; C4461
Vancomycin	HCL MCC_000095:02	1485.71	10.0	DMSO	Sigma; 861987
Fluconazole	MCC_008383:01	306.27	2.56	DMSO	Sigma; F8929

**Table 5.** Bacterial and fungal species used along with abbreviations

ID	Batch	Microbe	Strain	Description
GN_001	02	<i>Escherichia coli</i>	ATCC 25922	FDA control strain
GN_003	02	<i>Klebsiella pneumoniae</i>	ATCC 700603	MDR
GN_034	02	<i>Acinetobacter baumannii</i>	ATCC 19606	Type strain
GN_042	02	<i>Pseudomonas aeruginosa</i>	ATCC 27853	Quality control strain
GP_020	02	<i>Staphylococcus aureus</i>	ATCC 43300	MRSA
FG_001	01	<i>Candida albicans</i>	ATCC 90028	CLSI reference
FG_002	01	<i>Cryptococcus neoformans</i>	ATCC 208821	Type strain

All antibiotic controls displayed inhibitory values within the expected range.

**Table 6.** Brief results of antimicrobial activity

Strain ID	Microbe	Antibiotic	Pass / Fail
GN_001:02	<i>E. coli</i>	Colistin	Pass
GN_003:02	<i>K. pneumoniae</i>	Colistin	Pass
GN_034:02	<i>A. baumannii</i>	Colistin	Pass
GN_042:02	<i>P. aeruginosa</i>	Colistin	Pass
GP_020:02	<i>S. aureus (MRSA)</i>	Vancomycin	Pass
FG_001:01	<i>C. albicans</i>	Fluconazole	Pass
FG_002:01	<i>C. neoformans (H99)</i>	Fluconazole	Pass

**Table 7.** Different bacteria, fungi and abbreviations used for antimicrobial activity

Abbreviation	Name	Description	Strain	Organism	Type
Sa	<i>Staphylococcus aureus</i>	MRSA	ATCC 43300	Bacteria	G+ve
Ec	<i>Escherichia coli</i>	FDA control	ATCC 25922	Bacteria	G-ve
Kp	<i>Klebsiella pneumoniae</i>	MDR	ATCC 700603	Bacteria	G-ve
Ab	<i>Acinetobacter baumannii</i>	Type strain	ATCC 19606	Bacteria	G-ve
Pa	<i>Pseudomonas aeruginosa</i>	Type strain	ATCC 27853	Bacteria	G-ve
Ca	<i>Candida albicans</i>	CLSI reference	ATCC 90028	Fungi	Yeast
Cn	<i>Cryptococcus neoformans</i> var. <i>grubii</i>	Type strain	H99; ATCC 208821	Fungi	Yeast

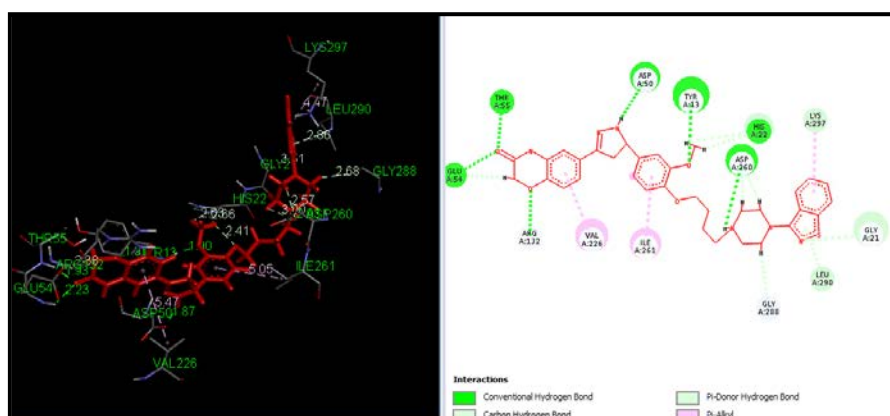
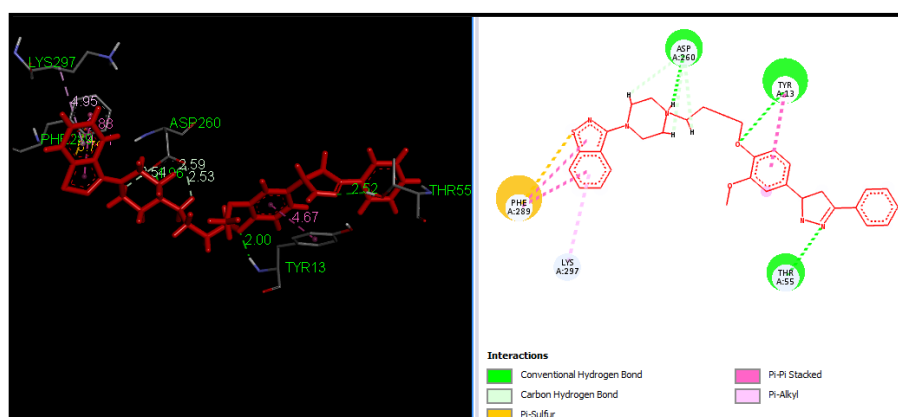
The 2*H*-1,4-benzoxazin-3(4*H*)-one derivatives **15** (-8.5243) interacts with the polar and charged amino acid residues THR55 and GLU54 with a carbonyl oxygen atom and an oxygen atom of oxazine at the distance of 1.90, 1.93 and 1.93 Å to form conventional hydrogen bond interactions. The charged amino acid ASP50 and hydrophobic amino acid TYR13 form conventional hydrogen bond interactions with pyrazole nitrogen and methoxyl oxygen atom with a distance of 1.87 and 1.90 Å, respectively. The polar amino acid HIS22 and ASP260 amino acid interact with a methoxyl hydrogen atom and the hydrogen atom of the piperazine ring to form a C-H bond and conventional hydrogen bond interactions.

The aliphatic amino acids VAL226, ILE261, GLY288, LEU290, and charged amino acid LYS297 interact with  $\pi$  electron cloud to form  $\pi$ -donor hydrogen and  $\pi$ -alkyl interactions (Figure 1).

The benzoisothiazole derivative **12** (-7.9567) interacts with the polar and charged amino acid of the active site. The charged amino acid ASP260 interacts with hydrogens of the piperazine ring to form conventional hydrogen bond interactions and C-H bond at a distance of 1.96, 2.53, 2.59 and 2.54 Å, respectively.

**Table 8.** In vitro activity and molecular docking of synthesized compounds

Compound code	Z-Score							Free binding energy, kcal mol <sup>-1</sup>
	Sa	Ec	Kp	Pa	Ab	Ca	Cn	
1	1.76	1.29	0.73	0.6	1.12	-4.54	1.95	-6.4069
2	0.96	-0.13	-1.09	1.33	-0.42	-2.63	1.52	-5.6208
3	1.31	-0.52	0.96	-1.56	0.14	0.05	-0.21	-6.9635
4	1.13	1.24	0.97	-1.04	0.21	0.49	0.05	-6.0319
5	0.29	-0.2	0.73	-0.6	0.34	-2.25	-0.13	-7.2436
6	0.13	0	0.7	-1.23	0.08	0.1	2.19	-6.584
7	0.99	-1.17	83	-0.62	0.32	0.55	-0.12	-4.5155
8	0.95	1	1.39	0.2	1.24	0.63	0.74	-6.3774
9	1.4	-1.66	0.7	-1.53	0.54	-0.83	-0.13	-5.5377
10	-0.11	0.04	-0.57	-1.35	-0.86	-0.89	0.22	-5.2221
11	-0.74	-1.24	-0.72	-0.8	-1.16	-0.48	2.11	-6.1736
12	0.72	1.38	0.26	0.65	1	0.47	-2.78	-7.9567
13	0.49	-0.49	0.52	-1.46	-0.19	-0.11	-2.77	-7.6732
14	0.24	0.83	0.44	-1.64	0.2	0.55	-0.81	-6.6984
15	0.39	-0.08	0.28	0.76	-0.04	0.67	-2.97	-8.5248
16	1.34	1.13	1.76	1.19	-1.62	-1.11	-0.41	-6.9736
17	3.31	3.77	3.9	0.9	2.53	-5.85	2.49	-6.351
18	0.42	0.52	0.78	-0.43	0.24	0.12	1.17	-5.5277
19	2.38	1.94	3.41	-0.23	3.39	-0.2	1.91	-5.112

**Figure 2.** Binding pose and molecular interactions of **15** in the active site of methionyl-tRNA synthetase.**Figure 3.** Binding pose and molecular interactions of **12** in the active site of methionyl-tRNA synthetase.

The polar amino acid THR55 and hydrophobic amino acid TYR13 interacts with pyrazole nitrogen atoms and phenoxy oxygen atom to form conventional hydrogen bond interaction with a distance of 2.00 and 2.52 Å respectively. The  $\pi$ -electron clouds of benzothiazole and phenoxy rings create  $\pi$ -sulfur,  $\pi$ - $\pi$  stacked and  $\pi$ -alkyl interactions with various distances (Figure 2).

## CONCLUSION

In summary, the present article reports a novel series of pyrazolines from chalcones and hydrazine hydrate or phenylhydrazine in the presence of ethanol as the alcoholic solvent. All structures of the newly synthesized molecules were characterized by spectroscopic data -  $^1\text{H}$  NMR,  $^{13}\text{C}$  NMR, Mass, and IR. Further, these newly synthesized compounds were evaluated for antioxidant and antimicrobial activity. Compounds **5**, **18** and **19** were found to be potentially active antioxidants in terms of the DPPH radical scavenging assay, whereas **2** and **18** compounds showed better activity by superoxide radical (SOR) scavenging assay method in but less as compared with the standard ascorbic acid. Compounds **12**, **13** and **15** were partially active against *Cryptococcus neoformans* var. *grubii* fungi. The molecular docking study and *in-vitro* antibacterial and antifungal activity suggested that **12**, **13** and **15** are the most active among all synthesized derivatives and will serve as excellent leads in the antimicrobial and antioxidant drug discovery process.

## ACKNOWLEDGMENTS

The authors are thankful to "Antimicrobial screening was performed by The Community for Antimicrobial Drug Discovery, funded by the Wellcome Trust, UK and the University of Queensland, Australia, for providing the results of antimicrobial activities.

## REFERENCES

- Varghese, B., Al-Busafi, S. N., Suliman, F. E. O., Al-Kindy, S. M. Z. Unveiling a versatile heterocycle: pyrazoline - A review, *RSC Adv.*, **2017**, 7, 46999-47016. DOI: [10.1039/C7RA08939B](https://doi.org/10.1039/C7RA08939B).
- Singh, P., Singh, J., Pant, G. J., Rawat, M. S. M., 2-Pyrazolines as biologically active and fluorescent agents: An Overview. *Anti-cancer Agents Med. Chem.*, **2018**, 18(10), 1366-1385. DOI: [10.2174/1871520618666180313153407](https://doi.org/10.2174/1871520618666180313153407)
- George, R. F., Fouad, M. A. and Gomaa, I. E. O., Synthesis and cytotoxic activities of some pyrazoline derivatives bearing phenyl pyridazine core as new apoptosis inducers. *Eur. J. Med. Chem.*, **2016**, 112, 48-59. DOI: [10.1016/j.ejmech.2016.01.048](https://doi.org/10.1016/j.ejmech.2016.01.048)
- Johnson, M., Younglove, B., Lee, L., LeBlanc, R., Holt, H., Hills, P., Mackay, H. N., Brown, T., Susan, L. M., Moses, L. Design, synthesis, and biological testing of pyrazoline derivatives of combretastatin-A4. *Bioorg. Med. Chem. Lett.*, **2007**, 17(21), 5897-5901 DOI: [10.1016/j.bmcl.2007.07.105](https://doi.org/10.1016/j.bmcl.2007.07.105).
- Insuausti, B., Tigreros, A., Orozco, F., Quiroga, J., Abonia, R., Nogueras, M., Sanchez, A. and Cobo, J., Synthesis of novel pyrazolic analogs of chalcones and their 3-aryl-4-(3-aryl-4,5-dihydro-1H-pyrazol-5-yl)-1-phenyl-1H-pyrazole derivatives as potential antitumor agents. *Bioorg. Med. Chem.*, **2010**, 18, 4965-4974. DOI: [10.1016/j.bmc.2010.06.013](https://doi.org/10.1016/j.bmc.2010.06.013)
- Suresh, K., Bawa, S., Drabu, S., Kumar, R., Gupta, H., Biological activities of pyrazoline derivatives: A recent development. *Recent Patent Anti-infect. Drug Discov.*, **2009**, 4, 154-163.
- Sasikala, R., Thirumurthy, K., Mayavel, P., Thirunarayanan, G., Eco-friendly synthesis and antimicrobial activities of some 1-phenyl-3(5-bromothiophen-2-yl)-5-(substituted phenyl)-2-pyrazolines, *Org. Med. Chem. Lett.*, **2012**, 2, article No. 20, DOI: [10.1186/2191-2858-2-20](https://doi.org/10.1186/2191-2858-2-20)
- Ruhoglu, O., Özdemir, Z., Çalis, U., Gümüşel, B., Bilgin, A. A. Synthesis of and pharmacological studies on the antidepressant and anticonvulsant activities of some 1,3,5-trisubstituted pyrazolines. *Arzneim-Forsch./Drug Res.*, **2005**, 55(8), 431-436.
- Govindaraju, M., Mylarappa, B. N., Ajaykumar, K., Synthesis of novel pyrazole derivatives and their efficacy as antimicrobial agents. *Int. J. Pharm. Pharm. Sci.*, **2013**, 5(4), 734-737.
- Tabarelli, Z., Rubin, M. A., Berlese, D. B., Sauzem, P. D., Missio, T. P., Teixeira, M. V., Sinhorin, A. P., Martins, M. A. P., Zanatta, N., Bonacorso, H. G. and Mello, C. F., Antinociceptive effect of novel pyrazolines in mice, *Braz. J. Med. Biol. Res.*, **2004**, 37, 1531-1540. DOI: [10.1590/S0100-879X2004001000013](https://doi.org/10.1590/S0100-879X2004001000013)
- Carrion, M. D., Lopez Cara, L. C., Encarnacion, M. C., Victor, T., Germaine, E., Dario, A. C., Espinosa, A., Gallo, M. A., Entrena, A., Pyrazoles and pyrazolines as neural and inducible nitric oxide synthase (nNOS and iNOS) potential inhibitors (III), *Eur. J. Med. Chem.* **2008**, 43, 2579-2591. DOI: [10.1016/j.ejmech.2008.01.014](https://doi.org/10.1016/j.ejmech.2008.01.014)
- Akranth, M., Rahmat A., Tauquir, A., Rikta, S., Tanwar, O., Mymona, A., Shaquizzaman, M., Mumtaz, A., Pyrazolines: A biological review. *Mini-Rev. Med. Chem.*, **2013**, 13(6), 921-931. DOI: [10.2174/1389557511313060012](https://doi.org/10.2174/1389557511313060012)
- Shaharyar, M., Siddiqui, A. A., Ali, M. A., Sriram, D. and Yogeewari, P., Synthesis and in vitro antimycobacterial activity of N1-nicotinoyl-3-(4'-hydroxy-3'-methyl phenyl)-5-[(sub)phenyl]-2-pyrazolines. *Bioorg. Med. Chem. Lett.*, **2006**, 16(15), 3947-3949 DOI: [10.1016/j.bmcl.2006.05.024](https://doi.org/10.1016/j.bmcl.2006.05.024)
- Rahman, M. A., Chalcone: A valuable insight into the recent advances and potential pharmacological activities. *Chem. Sci. J.*, **2011**, 29, 1-16.
- Kauthale, S., Tekale, S., Damale, M., Sangshetti, J., Pawar, R., Synthesis, biological evaluation, molecular docking, and ADMET studies of some isoxazole-based amides. *Med. Chem. Res.*, **2018**, 27(2), 429-441. DOI: [10.1007/s00044-017-2070-z](https://doi.org/10.1007/s00044-017-2070-z)
- Kauthale, S., Tekale, S., Damale, M., Sangshetti, J., Pawar, R., Synthesis, antioxidant, antifungal, molecular docking and ADMET studies of some thiazolyl hydrazones. *Bioorg. Med. Chem. Lett.*, **2017**, 27(16), 3891-3896. DOI: [10.1016/j.bmcl.2017.06.043](https://doi.org/10.1016/j.bmcl.2017.06.043)
- Deshmukh, S. U., Kharat, K. R., Yadav, A. R., Shisodia, S. U., Damale, M. G., Sangshetti, J. N., Pawar, R. P. Synthesis of novel  $\alpha$ -aminophosphonate derivatives, biological evaluation as potent antiproliferative agents and molecular docking. *Chem. Select*, **2018**, 3(20), 5552-5558 DOI: [10.1002/slct.201800798](https://doi.org/10.1002/slct.201800798)
- Trott, O., Olson, A. J., AutoDock Vina: Improving the speed and accuracy of docking with a new scoring function, efficient optimization and multithreading. *J. Comput. Chem.*, **2010**, 31(2), 455-461. DOI: [10.1002/jcc.21334](https://doi.org/10.1002/jcc.21334)
- Morris, G. M., Huey, R., Lindstrom, W., Sanner, M. F., Belew, R. K., Goodsell, D. S., Olson, A. J., AutoDock4 and Auto DockTools4: Automated docking with selective receptor flexibility. *Comput. Chem.*, **2009**, 30, 2785-2791. DOI: [10.1002/jcc.21256](https://doi.org/10.1002/jcc.21256)
- Sanner M. F. Python: A programming language for software integration and development, *J. Mol. Graph. Model.*, **1999**, 17, 57-61.



- <sup>21</sup>Bas, D. C., Rogers, D. M., Jensen, J. H., Very fast prediction and rationalization of pKa values for protein-ligand complexes, *Proteins*, **2008**, 73, 765-783. DOI: [10.1002/prot.22102](https://doi.org/10.1002/prot.22102)
- <sup>22</sup>Roberta, R., Luciana, G. M., Luciana, C. C., Glaucia, P., Evaluation of the antioxidant properties of the brazilian cerrado fruit annona crassiflora (araticum). *J. Food Sci.*, **2006**, 71, 102. DOI: [10.1111/j.1365-2621.2006.tb08882.x](https://doi.org/10.1111/j.1365-2621.2006.tb08882.x)

Received: 13.10.2019.

Accepted: 16.12.2019.



# SILVER ATOMS ENCAPSULATED IN G4 PAMAM (POLYAMIDOAMINE) DENDRIMERS AS A MODEL FOR THEIR USE IN NANOMEDICINE FOR PHOTOTHERAPY

**Tamar G. Giorgadze <sup>[a]\*</sup>, Irine G. Khutsishvili <sup>[a,b]</sup>, Zaza G. Melikishvili <sup>[c]</sup> and  
Vasil G. Bregadze <sup>[a]</sup>**

**Keywords:** G4 PAMAM (polyamidoamine) dendrimers, DNA, silver ions, nanomedicine; phototherapy.

The main goals of the research are to study the drug delivery nanoparticle, G4 PAMAM (polyamidoamine) dendrimer, using spectroscopic and thermodynamic methods and, based on the unique properties of G4 PAMAM dendrimer, create new, stable nano-sized (~5 nm) metalorganic nanocomplexes with silver atoms, which have a strong absorption in visible area and it can be used as a phototherapeutic agent for the treatment of cancer cells.

## \*Corresponding Authors

Fax: (+995 32) 239 14 94

E-Mail: tamari.giorgadze@tsu.ge

- [a] Andronikashvili Institute of Physics,  
Ivane Javakishvili Tbilisi State University,  
6 Tamarashvili Str., 0186 Tbilisi, Georgia  
[b] Institute of Biophysics, Ilia State University, 3/5 K.  
Cholokashvili Ave., 0162 Tbilisi, Georgia  
[c] Vladimir Chavchanidze Institute of Cybernetics of the  
Georgian Technical University, 5 S. Euli Str., 0186 Tbilisi,  
Georgia

## INTRODUCTION

In recent times, a major challenge in nanomedicine is to deliver medication in the local area of the disease or tumor. This can be achieved by using different nanosystems for drug delivery, which allows one to maximize clinical benefits and reduce the side effects of the drug.<sup>1-11</sup> The organic nanoparticles must be non-toxicity. Further, the structure of the drug delivery complex should be maintained as much as possible before the delivery to the damaged tissue. In addition, after the complex is injected into the diseased cell, the drug must be released with the help of enzymes located in the cell.<sup>12-15</sup> For the efficiency of drug delivery complex, the size of complex size is also important; due to clear reasons, it should be significantly smaller (at least by one order) than the size of the cell and at the same time, the amount of medicine located in the nanoparticles should be enough for cell treatment.<sup>16-20</sup>

The main goals of nanomedicine is targeted delivery of therapeutic and diagnostic agents, their proper operation, and minimization of potential negative effects. Upon reaching the required places (perhaps using different mechanisms), therapeutic agents should selectively destroy or restore damaged cells, however, they should have little to no effect on the healthy tissue. Therefore, it should take into account the finest mechanisms to control the exact delivery of the agent. In oncology, nanomaterials are used for targeted delivery of therapeutic and diagnostic agents to tumor cells. Trapped in the bloodstream, specially treated nanomaterial accumulates in the tumor area, which is

facilitated by the high permeability of tumor tissue (pore size of tumor tissue about 200 nm). It should be noted that the loading of tumor tissue with nanodrugs is much more effective than the loading of the same drugs with conventional diffusion.<sup>21,22</sup> Some of them remain in the tumor tissue for quite a long time, which significantly increases the anti-neoplastic effect of these substances. On the other hand, the wide surface of nanomaterial facilitates the better treatment of the targeted structures by the therapeutic agents.

In the case of organic nanoparticles, a single hollow nanoparticle can contain hundreds of drug molecules, the extraction and function of which is strictly purposeful. Extraction of nanoagents in tumor tissue often occurs as a result of the degradation of nanocarriers, although there are other mechanisms of actions of anticancer nanodrugs. This requires strict control over the degradation of nanoparticles, the degree of degradation of nanoparticles depends on the composition of its polymer coating. The polymer coating of medical therapeutic and diagnostic nanocarriers are necessary for the facilitation of their movement in the body, "clearing the way" and protecting the therapeutic/diagnostic agents.

Medical nanostructures, dendrimers, are synthetic branched polymers. Dendrimers have one starting atom, for example nitrogen, and as a result of a number of chemical reactions, it is linked to carbon and other elements. Each ending of the dendrimer contains reactive functional groups, so it easily attaches additional monomers, resulting in a dendrimer size increase. The dendrimer function is significantly related to its size, shape, and polarity.<sup>23,24</sup> Specifically, the hollow and branch structure of dendrimer is well-suited to the targeted delivery of the drug, and in some cases the same dendrimer can find the damaged cells and influence them.<sup>25-27</sup> For example, in the tumor, one branch of the dendrimer may be treated with tumor detection molecules (for example folic acid, as many receptors for folic acid are on tumor cells) and the neighboring branch with anti-tumor drug. Dendrimer may also have an effect on specific receptors of specific sites.<sup>28-30</sup> As a consequence of their unique structural topology and chemical versatility,

dendrimers have found (or are likely to find) applications that include catalysis,<sup>31-33</sup> drug delivery,<sup>34,35</sup> energy transfer,<sup>36-38</sup> and molecular recognition.<sup>39,40</sup>

In modern research, dendrimers are also used for synthesis of various metal nanoparticles. This means that the metal ions enter the existing hollow space in the structure of the dendrimer, and when the reductant ( $\text{NaBH}_4$ ) is added, they reduce to atoms and form a nanoparticle. In this case, the distribution of nanoparticle sizes is narrow.<sup>41</sup>

Dendrimer types and their functional and synthesis conditions determine nanoparticle size, morphology and suspension stability.<sup>42</sup> It should be noted that the reduction of some metal ions, for example silver, gold, platinum, palladium, is a complex process. At first, the copper ions are reduced and replaced with ions of other metals. With partial replacement, bimetallic nanoparticles can be formed.<sup>43</sup> Dendrimers encapsulated with metal nanoparticles are used as catalysts in some reactions: hydrogenations, hydroformylation, olefin metathesis, Heck reactions, Suzuki coupling, alkylation and oxidations.

As one of the prospective delivery agent, we consider G4 PAMAM (polyamidoamine) dendrimer (see Figure 1). Since the G4 PAMAM dendrimers satisfy all of the aforementioned qualities, they will satisfy the classification for drug delivery systems.<sup>9,10</sup> In particular, dendrimers have advantages over other delivery agents. The unique and most important characteristics are chemical content, huge surface, spherical form, "pockets" full of water between the branches, which represent a kind of trap for the drug. In addition, they have certain molecular size and shape, they have a large number of functional groups on the surface and are characterized by high penetration in the cell.<sup>25,26,27,44</sup>

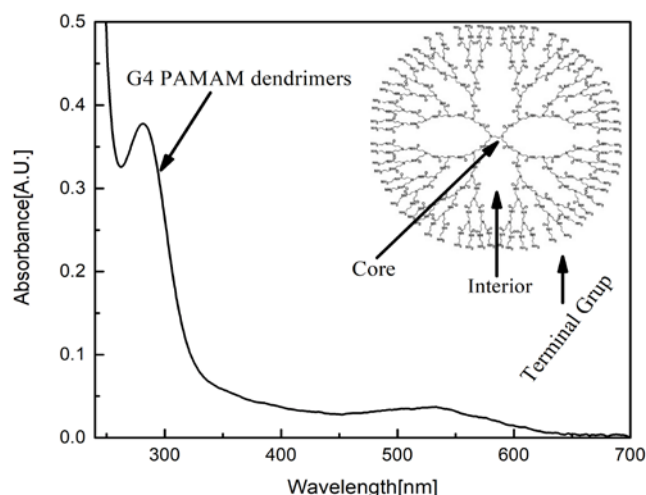


**Figure 1.** Absorption spectrum and structure of  $\text{G4}(\text{NH}_2)_{64}$  PAMAM dendrimer.

These characteristics of G4 PAMAM dendrimers gives us the opportunity to prepare new stable nanocomplexes (metal encapsulated G4 PAMAM dendrimers) with high absorption properties in visible and near infrared areas of the spectrum, which makes it possible to use them in nanomedicine.

## EXPERIMENTAL

In our tests, we have used the Calf thymus DNA (40 % GC) obtained from Sigma. The concentration of nucleic acids was determined by UV absorption using molar extinction coefficients ( $\epsilon=6600 \text{ cm}^{-1} \text{ M}^{-1}$  at  $\lambda=260 \text{ nm}$ ). The double helix structure of the polymers was proved by their hyperchromicity ( $>30 \%$ ) and their typical thermal denaturation transition (measured in  $0.01 \text{ M NaNO}_3$ ,  $\text{pH} \cong 6.0$ ). The pH was checked by a pH-meter HANNA Instruments pH213. The  $\text{G4}(\text{NH}_2)_{64}$  PAMAM dendrimer, with molecular sizes  $4.5 \text{ nm}$ , molecular weight  $14215$ , was also purchased from Sigma ( $\lambda = 280 \text{ nm}$ ). G4 PAMAM dendrimers were dissolved in a citrate buffer.

Double-distilled water served as a solvent. In tests with  $\text{Ag}^+$  ions, chemically pure  $\text{AgNO}_3$  was used and Tris buffer or  $\text{NaNO}_3$  served as background electrolyte. For the reduction of silver ions, ascorbic acid (AA) was used. We have used molar extinction coefficient for silver atom  $\epsilon=7160 \text{ cm}^{-1} \text{ M}^{-1}$  at  $\lambda = 430 \text{ nm}$ .

The measurement of absorption spectra was carried out by compact, precessive, mobile, small-power consuming optical fiber spectrometer AvaSpec ULS 2048-USB2. As a source of light we used a deuterium lamp in the ultraviolet region and quartz halogen incandescent lamp in the visible region.

Data collection, processing and visualization were carried out by CCD, connected to a personal computer and special computer programs, experimental results were processed by Origin software.

## RESULTS AND DISCUSSION

The  $\text{Ag}^+$  ions reduction process in drug delivery nanoparticles, G4 PAMAM dendrimers, was studied. Figure 2 depicts absorption spectra of the silver atoms obtained from the reduction of silver ions in G4 PAMAM dendrimers, induced by ascorbic acid (AA).

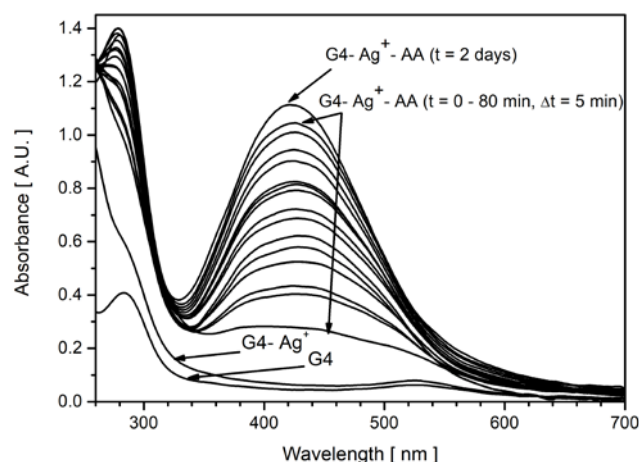


**Figure 2.** Time dependent absorption spectra of  $\text{Ag}^+$  reduction in  $\text{G4-Ag}^+-\text{AA}$  complex.  $[\text{G4}] = 1.4 \times 10^{-4} \text{ M}$ ,  $[\text{AgNO}_3] = 1.2 \times 10^{-4} \text{ M}$ ,  $[\text{AA}] = 2.4 \times 10^{-4} \text{ M}$ .

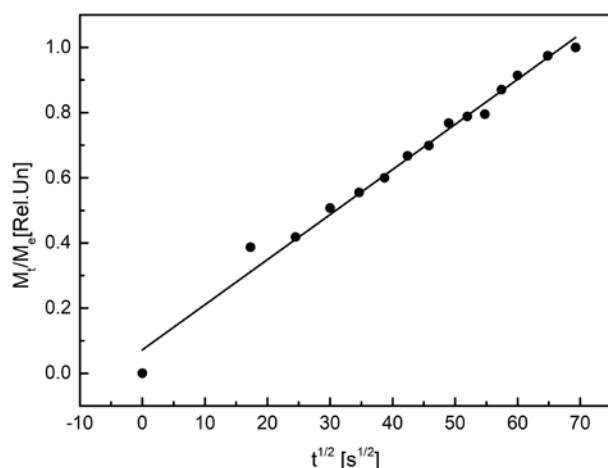
Therefore, using the unique features of G4 PAMAM dendrimers, new, stable, nanosized (~5 nm) complexes with 9-10 silver atoms, which have strong absorption in the visible area that make them eligible for use in nanomedicine, were created.

Figure 3 represents the kinetic curve of the reduction process of silver ions in G4 PAMAM dendrimers. The linear relationship shows that simple diffusion takes place (eqn. 1).

$$M_t/M_e = 2(Dt/\pi)^{1/2} [\text{cm/s}^{1/2}] \quad (1)$$

where  $M_t$  = the number of ions have been absorbed at  $t$ ,  $M_e$  = the number of ions in equilibrium (saturation in optical absorption).

It also shows that G4 PAMAM dendrimer does not change conformation during the formation of a nanocomplex with silver atoms.



**Figure 3.** Kinetic curve of  $\text{Ag}^+$  ions reduction in G4 dendrimers.

Figure 4 is a schematic representation of the model of the formation of the nanocomplex of G4  $(\text{NH}_2)_{64}$  PAMAM dendrimers with a silver atoms. The creation of nanocomplexes is a process consisting of two simple processes.

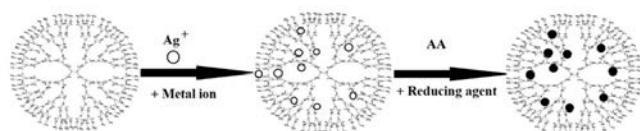


**Figure 4.** Model of creation of metal encapsulated G4 PAMAM dendrimers: reduction of silver ions to an atomic state in G4 PAMAM dendrimers.

It should be noted that the results presented in Figure 2 and 3 are of great spectroscopic interest. We have one G4 PAMAM dendrimer per 9-10 reduced silver atoms, and the absorption spectra show that the silver atom inside the dendrimer cavity is in the hydrated state. It should be noted that  $\text{Ag}^+$  ions in solutions are in an octahedral complex.

**Table 1.** Wavelengths of the maximum and full width at half maximum of the of the absorption spectra of silver atoms in different conditions.

Material	$\lambda_{\text{max}}$ , nm	Full width at half maximum, nm
AgNPs	431	140
AgNPs - DNA	425	133
$\text{Ag}^+$ -DNA-AA after 10	462	294
G4- $\text{Ag}^+$ -AA after 2 days	425	146

The location of the absorption maximum of silver atom ( $\lambda = 425$  nm) indicates that the silver atom  $\text{Ag}^0$  in G4 PAMAM dendrimer is in aqueous environment, i.e., that it is not connected to the polymer with a chemical or coordinate bond. This is the absorption maximum for the silver atom in a water environment with the shortest wavelength (Table 1). The diffusion of ascorbic acid molecule in G4 PAMAM dendrimer has a linear characteristic that indicates that the polymer molecule does not undergo the conformational changes.

Table 1 presents the wavelength of the maximum and full width at half maximum of the of the absorption spectra of silver atoms in AgNPs, AgNPs-DNA complex,  $\text{Ag}^+$ -DNA complex after the reduction of  $\text{Ag}^+$  by AA, and  $\text{Ag}^+$ -G4 PAMAM dendrimer complex after the reduction of  $\text{Ag}^+$  by AA. From the data presented in the table, it is clear that the shortest wavelength of absorption has the silver atoms incorporated into the G4 PAMAM dendrimer. The stronger the chromophore interacts with neighboring groups, the stronger the bathochromic shift.<sup>45</sup> Thus it may be concluded that the strongest interaction the silver atoms undergo are connected with the linear coordination between the DNA chains (inter strand croslink). It should be noted that linear coordination is characteristic of soft acids, namely  $\text{Ag}^+$ ,  $\text{Ag}^0$ ,  $\text{Cu}^+$ ,  $\text{Pt}^{2+}$ ,  $\text{Hg}^{2+}$ . In an earlier work,<sup>46</sup> it was shown that the interaction of AgNPs with DNA leads to wetting of small-sized AgNPs with hydrated surface of DNA.

Figure 5 shows the scheme of irradiation of silver atoms encapsulated in dendrimers ( $\lambda = 425$  nm) which will lead to excitation of silver atoms and the dissipation of energy on water molecules that will cause electrolytic dissociation of water molecules on  $\text{H}^+$  and  $\text{OH}^-$ , which is the necessary condition for hydrolysis of amide groups (HNCO) of G4 PAMAM dendrimer.

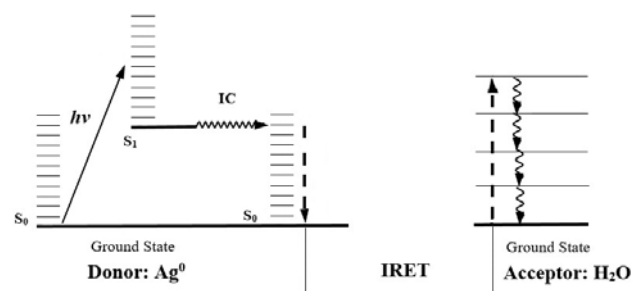


**Figure 5.** Scheme of energy levels corresponding to silver atom encapsulated in the G4 PAMAM dendrimer and high frequency vibration of water molecules (singlet-singlet energy transfer from donor to acceptor).



It should be noted that the excited silver atom does not have fluorescence in aqueous solutions, and therefore the complete dissipation of excited energy takes place on the water molecules.

Since the high-frequency vibration spectrum of the overtones of XH groups, including the OH groups of water molecules, can be easily observed in the near infrared and visible region,<sup>47</sup> the resonant interaction between the radiating oscillator (for example  $\text{Ag}^0$ ) and the high-frequency overtones oscillator in the region of  $\Delta E \gg h\nu_{\text{osc}}$  ( $2.9 \text{ eV} \gg 0.364 \text{ eV}$ ) is present.  $\Delta E$  is excitation energy of  $\text{Ag}^0$  and  $h\nu_{\text{osc}}$  is quantum of vibrational energy for normal oscillation of valence bond of water molecule.

Figure 6 schematically represents the hydrolysis of amide groups near the silver atom as a result of irradiation of silver atom encapsulated in G4 PAMAM dendrimer.

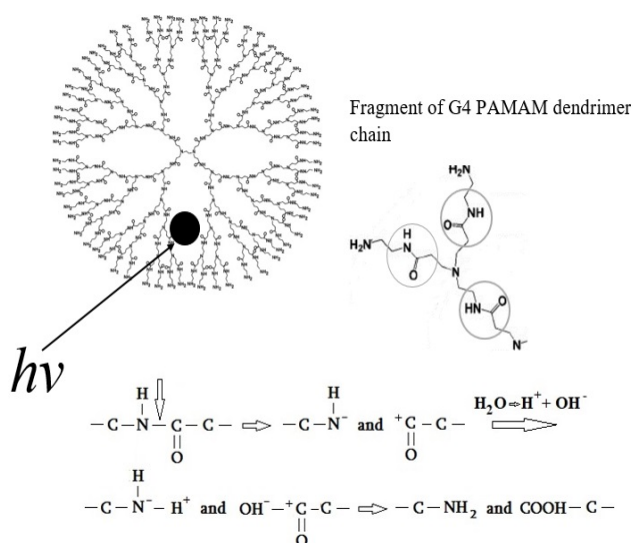


**Figure 6.** Hydrolysis of amide group in G4 PAMAM dendrimer due caused by the irradiation of  $\text{Ag}^0$  atom encapsulated in dendrimer.

The absorption spectra of the reduction of silver ions in the complex with the DNA, induced by the reductant AA is presented in figure 7. We added AA to the DNA- $\text{Ag}^+$  complex to reduce the silver ions to atoms ( $\text{Ag}^+ \rightarrow \text{Ag}^0$ ). Silver ions ( $\text{Ag}^+$ ) do not absorb in near ultraviolet or visible area, while the silver atoms ( $\text{Ag}^0$ ) absorb in visible area, so we have the possibility to observe the reduction process. The reduction of silver ions is a long process and, in about 160 min, we can clearly observe the appearance of absorption spectrum at  $\lambda = 464 \text{ nm}$ , and in 24 h absorption spectra specific for silver atoms can be observed.

We can see that the absorption spectra have a complex form. They resemble the absorption spectra of substances that have specific resonance interactions. Resonance interactions are specific for structures that have identical chromophore and hard structure,<sup>48</sup> for example, a similar structure of absorption spectra is characteristic for polypeptide in  $\alpha$ -helix state, where the chromophore is the peptide group.<sup>49</sup> Also the reason for the complicated

absorption spectra is the interaction of silver ions, which is characterized by inter-cross type of links with DNA, which reduces dynamic characteristics of double helix and makes it harder.

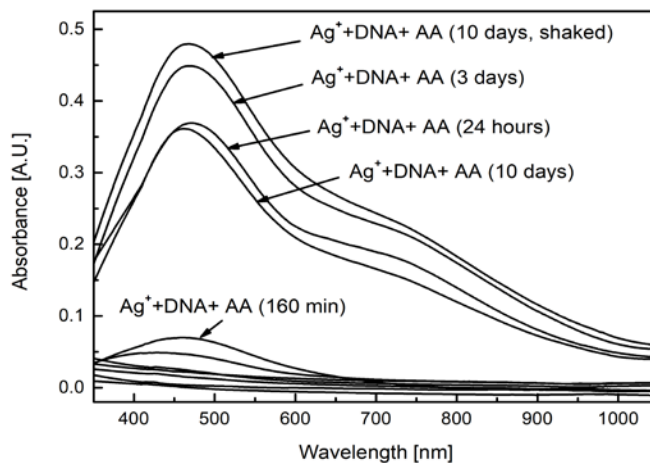


**Figure 7.** Time dependent absorption spectra of reduction of  $\text{Ag}^+$  ion  $\text{Ag}^0$  atom in DNA- $\text{Ag}^+$ -AA complex.  $[\text{DNA}] = 5.9 \times 10^{-4} \text{ M(P)}$ ,  $[\text{AgNO}_3] = 1.2 \times 10^{-4} \text{ M}$ ,  $[\text{AA}] = 2.4 \times 10^{-4} \text{ M}$ ,  $[\text{NaNO}_3] = 10^{-2} \text{ M}$ .

Figure 8 represents kinetics curve of  $\text{Ag}^+$  ions reduction on DNA, it shows, that curve is sigmoidal, which means that, unlike G4 PAMAM dendrimers (Figure 3), DNA changes conformation during the reduction of silver ions.

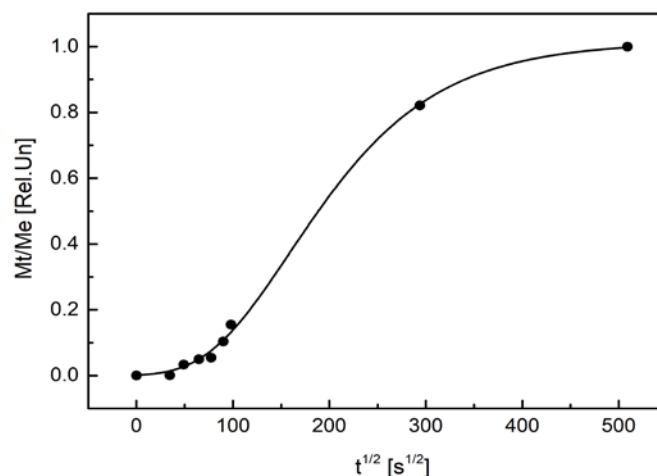


**Figure 8.** Kinetic curve of reduction of  $\text{Ag}^+$  ions on DNA.  $M_t$  = the number of ions have been absorbed at  $t$  time,  $M_e$  = the number of ions at saturation.

For phototherapy, we suggest the nanocomplex of silver atoms encapsulated in the G4 PAMAM dendrimer, which should be able to penetrate cell membrane and more importantly cell nucleus, the size of pores in nucleus membrane is 8-9 nm. The created complexes have absorption in visible area  $\lambda = 425 \text{ nm}$ . Irradiation at the frequency of their absorption will lead to excitation of silver atoms and the dissipation of energy on water molecules that will cause electrolytic dissociation of water molecules on  $\text{H}^+$  and  $\text{OH}^-$ , which is the necessary condition for hydrolysis of amide groups of G4 PAMAM dendrimer. Finally, the silver atoms released from G4 PAMAM dendrimer interact with DNA, which is a powerful toxic method for the destruction

of cells and in case of cancer cells it can be a potential medication for photo chemotherapy (see Figure 9).

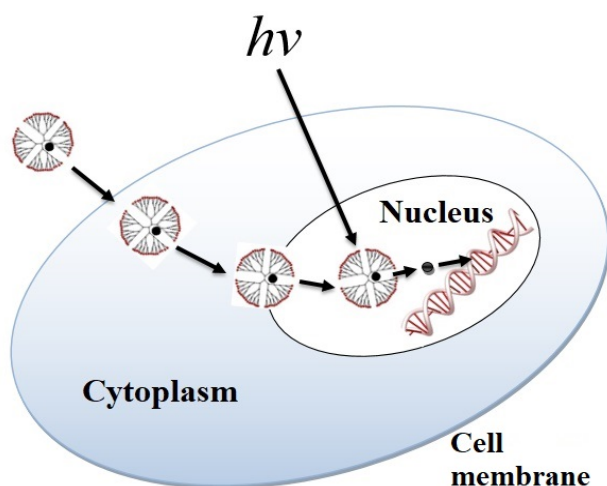


**Figure 9.** A schematic presentation of nanocomplex (silver atom encapsulated in G4 PAMAM dendrimer) entry in cell membrane through endocytosis, entry in nucleus from cytoplasm, irradiation of complex ( $\lambda=425$  nm) and interaction of released silver atom with DNA.

It should be noted that the new potential medication proposed by us (silver atom encapsulated in G4 PAMAM dendrimer) has low toxicity to life, since the free silver atom is oxidized to a silver ion and silver ions form insoluble salts with chloride ions, the number of which is high in the body, and finally, the removal from the body occurs by fecal masses.<sup>50</sup> The irradiation of silver atom encapsulated in G4 PAMAM dendrimer and the influence of released silver atom on DNA will be studied experimentally in the future.

## CONCLUSIONS

Silver ions reduction process in drug delivery nanoparticles, G4 PAMAM dendrimers, has been studied. Using the unique features of PAMAM dendrimers, new, stable, nanosized (~5 nm) complexes with 9-10 silver atoms in each dendrimer are created. Silver ions reduction process on DNA has been studied, and it has been shown that interaction of DNA with Ag<sup>0</sup> atoms cause conformational changes, which in the living organism is the precondition for cell damage. For phototherapy, we suggest the nanocomplex of silver atoms encapsulated in the G4 PAMAM dendrimer, which should be able to overcome the cell membrane and cell nucleus, the size of pores in nucleus membrane is 8-9 nm.

## ACKNOWLEDGEMENTS

The authors thank Dr. Sopio Melikishvili, Department of Nuclear Physics and Biophysics at the Comenius University for helpful advices and discussions during the research.

The work was partly supported by the grants of Shota Rustaveli National Science Foundation: GNSF/ST09\_508\_2-230, GNSF41/14 and GNSF 12/24.

## REFERENCES

- <sup>1</sup>Thrall, J. H., Nanotechnology and medicine, *Radiology*, **2004**, 230, 315–318. DOI: 10.1148/radiol.2302031698
- <sup>2</sup>Freitas, R. A., What is nanomedicine? *Nanomedicine*, **2005**, 1(1), 2-9. DOI: 10.1016/j.nano.2004.11.003
- <sup>3</sup>Parveen, S., Misra, R., Sahoo, S. K., Nanoparticles: a boon to drug delivery, therapeutics, diagnostics and imaging, *Nanomedicine*, **2012**, 8(2), 147-66. DOI: 10.1016/j.nano.2011.05.016
- <sup>4</sup>Jain, V., Jain, S., and Mahajan, S. C., Nanomedicines based drug delivery systems for anti-cancer targeting and treatment, *Curr. Drug Deliv.*, **2015**, 12 (2), 177-91. DOI: 10.2174/1567201811666140822112516
- <sup>5</sup>Mendes, L. P., Pan, J., Torchilin, V. P., Dendrimers as nanocarriers for nucleic acid and drug delivery in cancer therapy, *Molecules*, **2017**, 22(9), 1401. DOI: 10.3390/molecules22091401
- <sup>6</sup>Castro, E., Kumar, A., Nanomedicine in drug delivery systems, in *Nanomedicine in Drug Delivery*, edited by Kumar, A., Mansour, H. M., Friedman, A., Blough, E. R., **2013**, CRC Press, p. 1-22.
- <sup>7</sup>Wu, L. P., Ficker, M., Christensen, J. B., Trohopoulos, P. N., Moghimi, S. M., Dendrimers in medicine: therapeutic concepts and pharmaceutical challenges, *Bioconj. Chem.*, **2015**, 26(7), 1198-121. DOI: 10.1021/acs.bioconjchem.5b00031
- <sup>8</sup>Wolinsky, J. B., Grinstaff, M. W., Therapeutic and diagnostic applications of dendrimers for cancer treatment, *Adv. Drug Deliv. Rev.*, **2008**, 60(9), 1037-55. DOI: 10.1016/j.addr.2008.02.012
- <sup>9</sup>Kumar, P. S., Datta, M. Sh., Kumar, D. M., Kumar, T. V., Kumar, V. K., Ram C. D., Multivalent protein polymers with controlled chemical and physical properties, *J. Drug Deliv. Ther.*, **2016**, 6(1):67-92. DOI: 10.1016/j.addr.2010.05.002
- <sup>10</sup>Kumar, D. D., Singh A. K., Dendrimers: a novel carrier system for drug delivery, *J. Drug Deliv. Ther.*, **2014**, 4(5), 1-6. <https://doi.org/10.22270/jddt.v4i5.968>
- <sup>11</sup>Dixit, N., Glaum, M., Kumar, A., Cameron, D. F., Biological systems for the delivery of nanoparticles, in *Nanomedicine in Drug Delivery*, Edited by Arun Kumar, Heidi M. Mansour, Adam Friedman, Eric R. Blough, **2013**, CRC Press, 75-89.
- <sup>12</sup>Hasadsri, L., Kreuter, J., Hattori, H., et al. Functional protein delivery into neurons using polymeric nanoparticles, *J. Biol. Chem.*, **2009**, 284, 6972–81. DOI: 10.1074/jbc.M805956200
- <sup>13</sup>Kamps, J. A., Scherphof, G. L., Biodistribution and uptake of liposomes in vivo, *Methods Enzymol.*, **2004**, 387, 257–66. DOI: 10.1016/S0076-6879(04)87016-2
- <sup>14</sup>Kreuter, L., Tauber, U., Illi, V., Distribution and elimination of poly(methyl-2-<sup>14</sup>C-methacrylate) nanoparticle radioactivity after injection in rats and mice, *J. Pharm. Sci.*, **1979**, 68,1443–9. DOI: 10.1002/jps.2600681129
- <sup>15</sup>Li, S., Huang, L., Nonviral gene therapy: promises and challenges, *Gene Ther.*, **2000**, 7, 31-34. DOI: 10.1038/sj.gt.3301110
- <sup>16</sup>Moghimi, S. M., Hunter, A. C., Murray, J. C., Long-circulating and target-specific nanoparticles: theory to practice, *Pharmacol. Rev.*, **2001**, 53, 283–318.

- <sup>17</sup>Nishikawa, M., Huang, L., Nonviral vectors in the new millennium: delivery barriers in gene transfer, *Human Gene Ther.*, **2001**, *12*(8), 861–70. DOI: 10.1089/104303401750195836
- <sup>18</sup>Panyam, J., Labhasetwar, V., Biodegradable nanoparticles for drug and gene delivery to cells and tissue, *Adv. Drug Deliv. Rev.*, **2003**, *55*, 329–47. DOI: 10.1016/S0169-409X(02)00228-4
- <sup>19</sup>Patil, Y., Toti, U. Khadair, A. et al., Single-step surface functionalization of polymeric nanoparticles for targeted drug delivery, *Biomaterials*, **2009**, *30*, 859–66. DOI: 10.1016/j.biomaterials.2008.09.056
- <sup>20</sup>Ghaffarian, R., Muro, S., Models and methods to evaluate transport of drug delivery systems across cellular barriers, *J. Vis. Exp.*, **2013**, *80*, 50638. DOI: 10.3791/50638
- <sup>21</sup>Dibirdik, I., Yiv, S., Qazi, S., Uckun, F. M., In vivo anti-cancer activity of a liposomal nanoparticle construct of multifunctional tyrosine kinase inhibitor 4-(4'-Hydroxyphenyl)-Amino-6,7-Dimethoxyquinazoline, *J. Nanomedic. Nanotechnol.*, **2010**, *1*, 101. DOI: 10.4172/2157-7439.1000101
- <sup>22</sup>Nguyen, K. T., Targeted nanoparticles for cancer therapy: promises and challenges, *J. Nanomedic. Nanotechnol.*, **2011**, *2*, 103e. DOI: 10.4172/2157-7439.1000103e
- <sup>23</sup>Stangenberg, R., Saeed, I., Kuan, S. L., Baumgarten, M., Weil, T., Klapper, M., Müllen, K., Tuning polarity of polyphenylene dendrimers by patched surface amphiphilicity—precise control over size, shape, and polarity, *Macromol. Rapid Commun.*, **2014**, *35*(2), 152–60. DOI: 10.1002/marc.201300671
- <sup>24</sup>Ziraksaz, Z., Nomani, A., Soleimani, M., Bakhshandeh, B., Arefian, E., Haririan, I., Tabbakhian, M., Evaluation of cationic dendrimer and lipid as transfection reagents of short RNAs for stem cell modification, *Int. J. Pharm.*, **2013**, *448*(1), 231–8. DOI: 10.1016/j.ijpharm.2013.03.035
- <sup>25</sup>Kesharwani, P., Jain, K., Jain, N. K., Dendrimer as nanocarrier for drug delivery, *Prog. Polym. Sci.*, **2014**, *39*(2), 268–307. DOI: 10.1016/j.progpolymsci.2013.07.005
- <sup>26</sup>Pourianazar, T., Mutlu, P. K., Gunduz, U., Bioapplications of poly(amidoamine) (PAMAM) dendrimers in nanomedicine, *J. Nanoparticle Res.*, **2014**, *16*(4), 2342. DOI: 10.1007/s11051-014-2342-1
- <sup>27</sup>Lee, I., Athey, B. D., Wetzal, A. W., Meixner, W., Baker, J. R., Jr., Structural molecular dynamics studies on polyamidoamine dendrimers for a therapeutic application: effects of pH and generation, *Macromolecules*, **2002**, *35*, 4510–4520. DOI: 10.1021/ma010354q
- <sup>28</sup>Helms, B., Meijer, E.W., Dendrimers at work, *Science* **2006**, *313*, 929–930. DOI: 10.1126/science.1130639
- <sup>29</sup>Kadam U. S., Schulz B., Irudayaraj J., Detection and quantification of alternative splice sites in Arabidopsis genes AtDCL2 and AtPTB2 with highly sensitive surface enhanced Raman spectroscopy (SERS) and gold nanoprobe, *FEBS Lett.*, **2014**, *588*(9), 1637–43. DOI: 10.1016/j.febslet.2014.02.061
- <sup>30</sup>Karamchand, L., Kim, G., Wang, S., Hah, H. J., Ray, A., Jiddou, R., Lee, Y. K., Philbert, M., Kopelman, R., Modulation of hydrogel nanoparticle intracellular trafficking by multivalent surface engineering with tumor targeting peptide, *Nanoscale*, **2013**, *5*(21), 0327–44. DOI: 10.1039/c3nr00908d
- <sup>31</sup>Astruc, D., Chardac, F., Dendritic catalysts and dendrimers in catalysis, *Chem. Rev.*, **2001**, *101*, 2991. DOI: 10.1021/cr010323t
- <sup>32</sup>Crooks, R. M., Zhao, M., Sun, L., Chechik, V., Yeung, L. K., Dendrimer-encapsulated metal nanoparticles: synthesis, characterization, and applications to catalysis, *Acc. Chem. Res.*, **2001**, *34*, 181. DOI: 10.1021/ar000110a
- <sup>33</sup>van Heerbeek, R., Kamer, P. C. J., van Leeuwen, P. W. N. M., Reek, J. N. H., Dendrimers as support for recoverable catalysts and reagents, *Chem. Rev.*, **2002**, *102*, 3717. DOI: 10.1021/cr0103874
- <sup>34</sup>Patri, A. K., Majoros, I. J., Baker, J. R., Dendritic polymer macromolecular carriers for drug delivery, *Curr. Opin. Chem. Biol.*, **2002**, *6*, 466. DOI: 10.1016/S1367-5931(02)00347-2
- <sup>35</sup>Kojima, C., Kono, K., Maruyama, K., Takagishi, T., Synthesis of polyamidoamine dendrimers having poly(ethylene glycol) grafts and their ability to encapsulate anticancer drugs, *Bioconjugate Chem.*, **2000**, *11*, 910. DOI: 10.1021/bc0000583
- <sup>36</sup>Adronov, A., Fréchet, J. M. J., Light-harvesting dendrimers, *Chem. Commun.*, **2000**, *18*, 1701. DOI: 10.1039/B005993P
- <sup>37</sup>Adronov, A., S.L.Gilat, S. L., Fréchet, J. M. J., Ohta, K., Neuwahl, F. V. R., Fleming, G. R., light harvesting and energy transfer in laser-dye-labeled poly(aryl ether) dendrimers, *J. Am. Chem. Soc.*, **2000**, *122*, 1175. DOI: 10.1021/ja993272e
- <sup>38</sup>Swallen, S. F., Zhu, Z. G., Moore, J. S., Kopelman, R., Correlated excimer formation and molecular rotational dynamics in phenylacetylene dendrimers, *J. Phys. Chem. B*, **2000**, *104*, 3988. DOI: 10.1021/jp994284p
- <sup>39</sup>Fréchet, J. M. J., Dendrimers and supramolecular chemistry, *Proc. Natl. Acad. Sci. USA* **2002**, *99*(8), 4782–4787. DOI: 10.1073/pnas.082013899
- <sup>40</sup>Mayer, A. B. R., Colloidal metal nanoparticles dispersed in amphiphilic polymers, *Polym. Adv. Technol.*, **2001**, *12*, 96. DOI: 10.1002/1099-1581(200101/02)12:1/2<96::AID-PAT943>3.0.CO;2-G
- <sup>41</sup>Niu, Y., Crooks, R. M., Dendrimer-encapsulated metal nanoparticles and their applications to catalysis, *C. R. Chimie*, **2003**, *6*, 1049–1059. DOI: 10.1016/j.crci.2003.08.001
- <sup>42</sup>Camarada, M. B., Comer, J., Poblete, H., Azhagiya Singam, E. R., Marquez-Miranda, V., Morales-Verdejo, C., Gonzalez-Nilo, F. D., Experimental and computational characterization of the interaction between gold nanoparticles and polyamidoamine dendrimers, *Langmuir*, **2018**, *34*(34), 10063–10072. DOI: 10.1021/acs.langmuir.8b01809
- <sup>43</sup>Crooks, R. M., Zhao, M., Sun, L., Chechik, V., Yeung, L. K., Dendrimer-encapsulated metal nanoparticles: synthesis, characterization, and applications to catalysis, *Acc. Chem. Res.*, **2001**, *34*(3), 181–190. DOI: 10.1021/ar000110a
- <sup>44</sup>Medina, S. H., El-Sayed, M. E. H., Dendrimers as carriers for delivery of chemotherapeutic agents, *Chem. Rev.*, **2009**, *109*(7), 3141–3157. DOI: 10.1021/cr900174j
- <sup>45</sup>Liptay, W., in *Modern Quantum Chemistry*, Vol. 2, edited by Oktay Sinanoglu **1965**, Academic Press, New York, London, Ch. II-5.
- <sup>46</sup>Bregadze, V. G., Melikishvili, Z. G., Giorgadze, T. G., Photo-induced DNA-dependent conformational changes in silver nanoparticles, *Adv. Nanopart.*, **2013**, *2*, 176–181. DOI: 10.4236/anp.2013.22026
- <sup>47</sup>Hayward, R. J., Henry, B. R., Anharmonicity in polyatomic molecules: A local-mode analysis of the XH-stretching overtone spectra of ammonia and methane, *J. Mol. Spectr.*, **1974**, *50*, 58–67. DOI: 10.1016/0022-2852(74)90217-3
- <sup>48</sup>Davidov, A. S., *Theory of Molecular Excitons*, McGraw-Hill Book Company, New York, **1962**.
- <sup>49</sup>Tinoco, J., Halpern, A., W. Impson, W., The relation between conformation and light absorption in polypeptides and proteins in *Polyamino Acids, Polypeptides and Proteins*, University of Wisconsin Press, **1962**, 147–160.
- <sup>50</sup>Moskalev, Yu. I., *Mineral Metabolism*, Meditsina, Moscow, **1985**, 33.

Received: 29.10.2019.

Accepted: 26.01.2020.





# NUCLEOPHILIC SUBSTITUTION IN *N*-ALKOXY-*N'*-CHLOROCARBAMATES AS A WAY TO *N*-ALKOXY-*N'*,*N'*,*N'*-TRIMETHYLHYDRAZINIUM CHLORIDES

Vasiliy G. Shtamburg<sup>[a]\*</sup>, Victor V. Shtamburg<sup>[a]</sup>, Evgeniy A. Klots<sup>[b]</sup>, Andrey A. Anishchenko<sup>[c]</sup>, Alexander V. Mazepa<sup>[d]</sup> and Svetlana V. Kravchenko<sup>[e]</sup>

**Keywords:** *N*-Alkoxy-*N*-chlorocarbamates, *N*-alkoxyhydrazines, *N*-alkoxy-*N'*,*N'*,*N'*-trimethylhydrazinium chlorides, synthesis, O-*N*-*N* geminal systems, nucleophilic substitution at nitrogen.

A series of *N*-alkoxy-*N'*,*N'*,*N'*-trimethylhydrazinium chlorides by interaction of *N*-alkoxy-*N*-chlorocarbamates with trimethylamine could be prepared.

## \* Corresponding Authors

Phone: +380-97-651-61-72

E-Mail: stamburg@gmail.com

- [a] 49005 Ukraine, Dnepr, Gagarina st., 8. Ukrainian State University of Chemical Technology.
- [b] 25006 Ukraine, Kropyvnytskyi, Shevchenko st., 1. Volodymyr Vinnichenko Central Ukrainian State Pedagogical University.
- [c] 49050 Ukraine, Dnepr, Nauchnaya st. 25. O. Gonchar Dnepropetrovsk National University.
- [d] 65080 Odessa, Luystdorskaya Doroga st., 86. A.V. Bogatsky Physico-Chemical Institute of NAS of Ukraine.
- [e] 49600 Ukraine, Dnepr, Efremova st., 25. Dnipro State Agrarian and Economic University.

## INTRODUCTION

*N*-Alkoxy-*N'*,*N'*,*N'*-trimethylhydrazinium salts (**1**) are stable<sup>1,2</sup> derivatives of unstable *N*-alkoxyhydrazines<sup>3-10</sup> and they have a unique structure. *N*-Methoxy-*N'*,*N'*,*N'*-trimethylhydrazinium perchlorate has the longest N-N<sup>+</sup> bond [1.483(30 Å)]<sup>2</sup> and a very short N-OMe bond [1.391(3) Å].<sup>2</sup>

Normally, some types of *N*-alkoxyhydrazines such as *N*-alkoxy-*N*-alkylamines<sup>3,5</sup> and *N*-alkoxy-*N*-aminoamides<sup>4,6-10</sup> are destabilized by the  $n_{N'} \rightarrow \sigma^*_{N-O(R)}$  orbital interaction ("anomeric effect").<sup>6-10</sup> Usually, the *N*-alkoxy-*N*-chloro-*N*-*t*-alkylamines interaction with amines gives unstable *N*-alkoxyhydrazines which eliminate a molecule of alcohol yielding the proper diazenes<sup>3</sup> (Scheme 1). Only one single relatively stable *N*-alkoxyhydrazine (**2**) has been obtained but it is converted into diazene (**3**) by an action of methanol.<sup>3</sup>

*N*-Alkoxy-*N*-chloro derivatives of amines<sup>3,5</sup> and amides<sup>1-4,11-15</sup> selectively give stable *N*-alkoxyamino-pyridinium salts (**4**) by interacting with pyridines (Scheme 2).<sup>3,5,11-17</sup>

However the *N*-alkoxy-*N'*,*N'*,*N'*-trialkylhydrazinium salts (**1,5**)<sup>1,2</sup> are formed only during the reaction of *N*-alkoxy-*N*-chloroureas with trimethylamine and 1,4-diazabicyclo[2.2.2]octane (Scheme 3). The stability of the *N*-alkoxy-*N'*,*N'*,*N'*-trialkylhydrazinium salts (**1,5**)<sup>1,2</sup> as well as the 1-*N*-alkoxyamino-pyridinium salts (**4**)<sup>3,5,11-17</sup> is based

on the inability of  $n_{N'} \rightarrow \sigma^*_{N-O(R)}$  anomeric effect due to the absence of the lone electron pair in *N'* nitrogen atom. The mechanism of generation of *N*-alkoxy-*N'*,*N'*,*N'*-trialkylhydrazinium salts (**1,5**) is unknown but it may be presumed that at the first stage the labile product of nucleophilic substitution at the nitrogen atom (**6,7**) is formed. Then, the intermediates **6,7** are decarbamoylated by the action of excess amine. In a similar way the decarbamoylation in the presence of bases of the *N*-alkoxyaminopyridinium salts (**4b**) (or *N*-alkoxy-*N*-(4-dimethylaminopyridin-1-ium-yl)urea chlorides) produces 1-alkoxyaminopyridinium chlorides.<sup>14,17</sup>

The aim of our investigation is to study the possibility of synthesis of *N*-alkoxy-*N'*,*N'*,*N'*-trimethylhydrazinium chlorides (**1**) from methyl *N*-alkoxy-*N*-chlorocarbamates (**8a-f**) and ethyl *N*-chloro-*N*-methoxycarbamate (**9**).

## EXPERIMENTAL

<sup>1</sup>H NMR spectra were recorded on the 300 MHz VARIAN VXR-300 and the 400 MHz VARIAN JEMINI 400 spectrometers. <sup>13</sup>C NMR spectra were recorded on a Varian VXP-300 spectrometer (75 MHz). <sup>1</sup>H NMR chemical shifts were reported relative to the residual solvent protons as an internal standard ((CD<sub>3</sub>)<sub>2</sub>SO: 2.50 ppm) or with Me<sub>4</sub>Si as an internal standard (in CDCl<sub>3</sub>). Solvent carbon atoms served as an internal standard for <sup>13</sup>C NMR spectra ((CD<sub>3</sub>)<sub>2</sub>SO: 39.52 ppm). Mass spectrum was recorded on VG 770-70EQ spectrometer in FAB regime. The solvents were purified and dried according to the standard procedures.

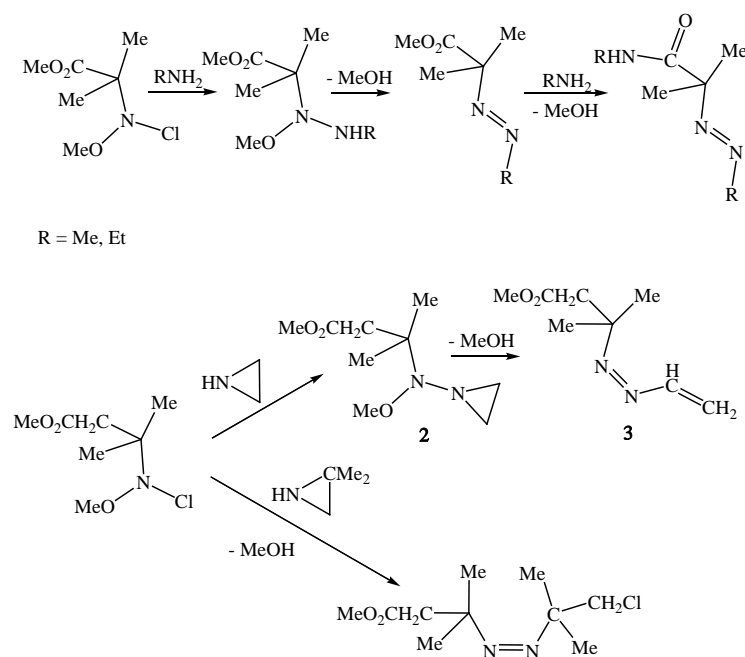
### *N*-Methoxy-*N'*,*N'*,*N'*-trimethylhydrazinium chloride (**1a**)

**Method A:** A solution of trimethylamine (3.735 mmol, 221 mg) in MeCN (3 mL) was added to a solution of methyl *N*-chloro-*N*-methoxycarbamate<sup>18</sup> (**8a**, 3.216 mmol, 449 mg) in MeCN (7 mL) at -29 °C, the reaction mixture was heated to 14 °C during 21 h, then the negligible precipitate formed was filtered off, the MeCN-filtrate was evaporated under vacuum (25 mm Hg), benzene (10 mL) was added, the mixture was kept at 5 °C for 4 days, then the benzene phase

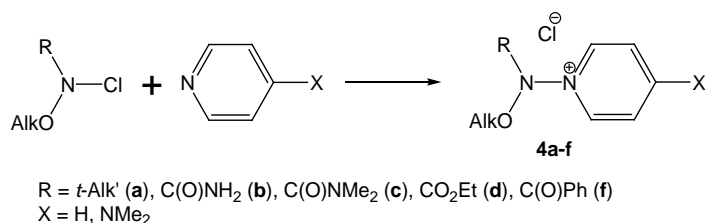


was decanted from obtained solid residue. The solid residue was washed by benzene (3mL), dried under vacuum 2 mm Hg, dissolved in MeCN and precipitated by EtOAc (2:1), dried under vacuum (2 mmHg), giving *N*-methoxy-*N'*,*N'*,*N'*-trimethylhydrazinium chloride (**1a**) as colorless hygroscopic

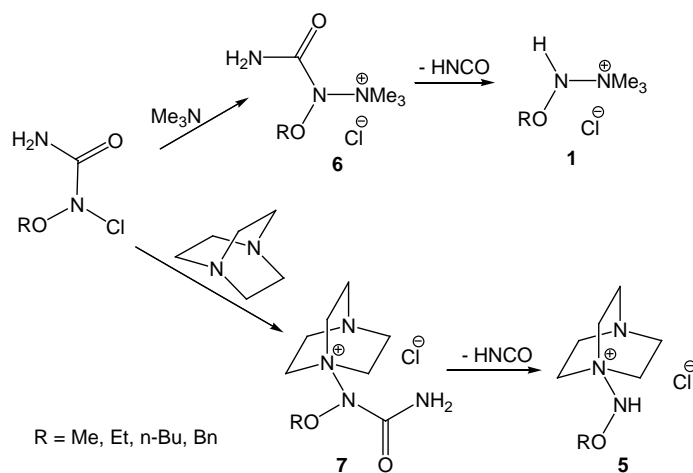
crystals (49 mg, 11 %).  $^1\text{H}$  NMR (300 MHz,  $(\text{CD}_3)_2\text{SO}$ )  $\delta$  = 3.239 (9H, s,  $\text{Me}_3\text{N}^+$ ), 3.740 (3H, s, NOME), 10.404 (1H, s, NH).  $^{13}\text{C}$  NMR (75 MHz,  $(\text{CD}_3)_2\text{SO}$ )  $\delta$  = 50.39 ( $\text{Me}_3\text{N}^+$ ), 64.71 (NOME). MS (FAB,  $m/z$ ,  $I_{\text{rel}}$ , (%)): 105  $\text{M}^+$  (65), 74 (100).



**Scheme 1.** The formation of diazenes as the result of *N*-alkoxy-*N*-chloro-*N*-tert.-alkylamines interaction with amines.



**Scheme 2.** The formation of *N*-alkoxyaminopyridinium salts (**4a-f**) from *N*-alkoxy-*N*-chloro compounds by an interaction with the pyridines.



**Scheme 3.** The earlier reported synthesis of the *N*-alkoxy-*N'*,*N'*,*N'*-trialkylhydrazinium salts (**1,5**).

From MeCN–EtOAc phase after evaporation under vacuum and crystallization compound (**1a**) (199 mg, 44 %) was obtained additionally.

The benzene extract was evaporated under vacuum (20 mm Hg), the residue was maintained at 4 mm Hg giving *N,N'*-dimethoxy-*N,N'*-di(methoxycarbonyl)hydrazine (**10a**) as white crystals (51 mg, 15 %), mp 52–53 °C (hexane), which was identified by <sup>1</sup>H NMR spectra and mass spectrum.<sup>2,18</sup> <sup>1</sup>H NMR (300 MHz, CDCl<sub>3</sub>) δ = 3.891 (12H, s, NOME, CO<sub>2</sub>Me). <sup>1</sup>H NMR (400 MHz, CDCl<sub>3</sub>) δ = 3.902 (6H, s, NOME), 3.916 (6H, s, CO<sub>2</sub>Me). MS (FAB, KI, *m/z*, *I*<sub>rel</sub>, (%)): 247 [M+K]<sup>+</sup> (100).

**Method B:** A solution of trimethylamine (4.284 mmol, 253 mg) in MeCN (5 mL) was added to a solution of ethyl *N*-chloro-*N*-methoxycarbamate<sup>19</sup> (**9**) (2.108 mmol, 324 mg) in MeCN (5 mL) at -30 °C, the reaction mixture was heated to 18 °C for 22 h, then the negligible precipitate formed was filtered off, the MeCN-filtrate was evaporated under vacuum (20 mm Hg), the residue was washed by Et<sub>2</sub>O (10 mL), the residue was dissolved in MeCN (4 mL) and benzene (8 mL) was added. The precipitated viscous oil was separated from PhH–MeCN phase, dried under vacuum (2 mm Hg), giving *N*-methoxy-*N',N',N'*-trimethylhydrazinium chloride (**1a**) as colorless hygroscopic crystals (143 mg, 48 %) which was identified by <sup>1</sup>H and <sup>13</sup>C MR spectra, and MS spectrum.

The Et<sub>2</sub>O-extract was evaporated under vacuum (20 mm Hg), the residue was washed by CCl<sub>4</sub> (5 mL) for 40 h, then it was separated and dried under vacuum (2 mm Hg), giving **1a** (125 mg, 42 %) additionally.

#### 1-*N*-Ethoxy-*N',N',N'*-trimethylhydrazinium chloride (**1b**)

A solution of trimethylamine (2.487 mmol, 147 mg) in MeCN (2 mL) was added to a solution of methyl *N*-chloro-*N*-ethoxycarbamate<sup>20</sup> (**8b**) (1.370 mmol, 210 mg) in MeCN (5 mL) at -15 °C, the reaction mixture was kept at -15 °C for 2 h and at 5 °C for 20 h. The negligible precipitate was then filtered off, the MeCN-filtrate was evaporated under vacuum (15 mm Hg), the residue was washed by Et<sub>2</sub>O (5 mL) and dried at 2 mm Hg, giving *N*-ethoxy-*N',N',N'*-trimethylhydrazinium chloride (**1b**) as white hygroscopic solid (209 mg, 98 %). <sup>1</sup>H NMR (300 MHz, (CD<sub>3</sub>)<sub>2</sub>SO) δ = 1.192 (3H, t, <sup>3</sup>*J*=6.9 Hz, NOCH<sub>2</sub>Me), 3.253 (9H, s, Me<sub>3</sub>N<sup>+</sup>), 3.900–4.050 (2H, m, NOCH<sub>2</sub>Me), 10.334 (1H, s, NHO). <sup>13</sup>C NMR (75 MHz, (CD<sub>3</sub>)<sub>2</sub>SO) δ = 13.76 (Me), 50.27 (Me<sub>3</sub>N<sup>+</sup>), 72.24 (OCH<sub>2</sub>). MS (FAB, *m/z*, *I*<sub>rel</sub>, (%)): 275 [2M•Cl]<sup>+</sup>(6), 273 [2M•Cl]<sup>+</sup>(18), 119 M<sup>+</sup> (100), 73(73).

#### *N*-*n*-Propyloxy-*N',N',N'*-trimethylhydrazinium chloride (**1c**)

A solution of trimethylamine (2.739 mmol, 162 mg) in MeCN (2 mL) was added to a solution of methyl *N*-chloro-*N*-*n*-propyloxycarbamate (**8c**) (1.996 mmol, 336 mg) in MeCN (5 mL) at -25 °C, the reaction mixture was heated to -14 °C for 1 h, then it was maintained at 15 °C for 24 h and the negligible precipitate was filtered off. The MeCN-solution was evaporated under vacuum (20 mm Hg), the residue was dried at 2 mm Hg, washed by benzene (10 mL), dried under vacuum (2 mm Hg) and giving *N*-*n*-propyloxy-*N',N',N'*-trimethylhydrazinium chloride (**1c**) as white

hygroscopic solid (178 mg, 53 %). <sup>1</sup>H NMR (400 MHz, (CD<sub>3</sub>)<sub>2</sub>SO) δ = 0.895 (3H, t, *J*=7.2 Hz, NO(CH<sub>2</sub>)<sub>2</sub>Me), 1.499–1.613 (2H, m, NOCH<sub>2</sub>CH<sub>2</sub>Me), 3.252 (9H, s, Me<sub>3</sub>N<sup>+</sup>), 3.788–3.865 (1H, m, NOCH<sub>2</sub>), 3.886–3.958 (1H, m, NOCH<sub>2</sub>), 10.438 (1H, s, NHO). <sup>13</sup>C NMR (100 MHz, (CD<sub>3</sub>)<sub>2</sub>SO) δ=10.14 (NO(CH<sub>2</sub>)<sub>2</sub>Me), 21.46 (NOCH<sub>2</sub>CH<sub>2</sub>Me), 50.31 (Me<sub>3</sub>N<sup>+</sup>), 78.12 (NOCH<sub>2</sub>). MS (FAB, *m/z*, *I*<sub>rel</sub>, (%)): 303 [2M<sup>+</sup>•Cl<sup>-</sup>] (4), 301 [2M<sup>+</sup>•Cl<sup>-</sup>] (13), 133 M<sup>+</sup> (100), 73(35), 56(37).

#### *N*-*n*-Butyloxy-*N',N',N'*-trimethylhydrazinium chloride (**1d**)

A solution of trimethylamine (2.490 mmol, 147 mg) in MeCN (3 mL) was added to a solution of methyl *N*-*n*-butyloxy-*N*-chlorocarbamate<sup>20,21</sup> (**8c**) (1.663 mmol, 302 mg) in MeCN (4 mL) at -30 °C, the reaction mixture was heated to 15 °C for 18 h and the negligible precipitate was filtered off. The MeCN-filtrate was evaporated under vacuum (20 mm Hg), the residue was washed by benzene (10 mL), dried under vacuum (4 mm Hg) and extracted by CH<sub>2</sub>Cl<sub>2</sub> (10 mL). The CH<sub>2</sub>Cl<sub>2</sub>-extract was evaporated under vacuum (20 mm Hg), the residue was extracted by acetone (3 mL), Me<sub>2</sub>C(O)-extract was evaporated under vacuum and dried at 4 mm Hg, giving *N*-*n*-butyloxy-*N',N',N'*-trimethylhydrazinium chloride (**1d**) as viscous yellowish oil (151 mg, 50 %). <sup>1</sup>H NMR (400 MHz, (CD<sub>3</sub>)<sub>2</sub>SO) δ = 0.899 (3H, t, <sup>3</sup>*J*=7.2 Hz, OCH<sub>2</sub>CH<sub>2</sub>CH<sub>2</sub>Me), 1.357 (2H, sex, <sup>3</sup>*J*=7.2 Hz, OCH<sub>2</sub>CH<sub>2</sub>CH<sub>2</sub>Me), 1.545 (2H, quint, <sup>3</sup>*J*=7.2 Hz, OCH<sub>2</sub>CH<sub>2</sub>CH<sub>2</sub>Me), 3.217 (9H, s, Me<sub>3</sub>N<sup>+</sup>), 3.781–3.913 (1H, m, NOCH<sub>2</sub>), 3.950–4.035 (1H, m, NOCH<sub>2</sub>), 10.129 (1H, s, NHO). <sup>13</sup>C NMR (75 MHz, (CD<sub>3</sub>)<sub>2</sub>SO) δ = 13.75 (Me), 18.48, 30.19 (CH<sub>2</sub>), 50.41 (Me<sub>3</sub>N<sup>+</sup>), 76.53 (NOCH<sub>2</sub>). MS (FAB, *m/z*, *I*<sub>rel</sub>, (%)): 331 [2M•Cl]<sup>+</sup>(1.5), 329 [2M•Cl]<sup>+</sup>(5), 147 M<sup>+</sup> (100), 57 Bu<sup>+</sup> (48).

#### *N*-Benzyloxy-*N',N',N'*-trimethylhydrazinium chloride (**1e**)

A solution of trimethylamine (2.856 mmol, 169 mg) in MeCN (2 mL) was added to a solution of methyl *N*-benzyloxy-*N*-chlorocarbamate<sup>18</sup> (**8e**) (1.454 mmol, 314 mg) in MeCN (5 mL) at -15 °C, the reaction mixture was heated to 5 °C for 2 h, was kept at 5 °C for 20 h, then it was evaporated under vacuum (15 mm Hg), the residue washed by Et<sub>2</sub>O (7 mL), dried at 2 mm Hg, giving *N*-benzyloxy-*N',N',N'*-trimethylhydrazinium chloride (**1e**) as hygroscopic white solid (256 mg, 86 %). <sup>1</sup>H NMR (300 MHz, (CDCl<sub>3</sub>) δ=3.409 (9H, s, Me<sub>3</sub>N<sup>+</sup>), 4.880 (1H, d, <sup>2</sup>*J*=10.5 Hz, NOCH<sub>2</sub>Ph), 4.943 (1H, d, <sup>2</sup>*J*=10.5 Hz, NOCH<sub>2</sub>Ph), 7.342 (5H, s, Ph); 10.963 (1H, s, NHO). <sup>1</sup>H NMR (300 MHz, (CD<sub>3</sub>)<sub>2</sub>SO) δ = 3.314 (9H, s, Me<sub>3</sub>N<sup>+</sup>), 4.86–5.14 (2H, m, NOCH<sub>2</sub>Ph), 7.31–7.45 (5H, m, Ph), 10.629 (1H, s, NHO). <sup>13</sup>C NMR (75 MHz, (CD<sub>3</sub>)<sub>2</sub>SO) δ = 50.52 (Me<sub>3</sub>N<sup>+</sup>), 78.34 (NOCH<sub>2</sub>), 128.31 [C(4) Ph], 128.39, 128.41 [C(2,4) and C(3,5) Ph], 135.92 [C(1) Ph]. MS (FAB, *m/z*, *I*<sub>rel</sub>, (%)): 181 M<sup>+</sup> (100), 91(55), 74 (53).

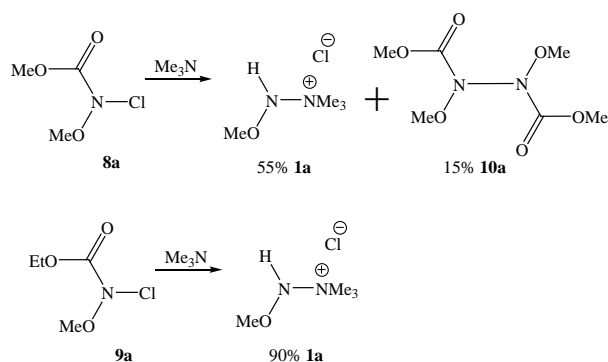
#### *N*-*n*-Octyloxy-*N',N',N'*-trimethylhydrazinium chloride (**1f**)

A solution of trimethylamine (2.988 mmol, 177 mg) in MeCN (2 mL) was added to a solution of methyl *N*-chloro-*N*-*n*-octyloxycarbamate<sup>19</sup> (**8f**) (0.979 mmol, 233 mg) in MeCN (5 mL) at -17 °C, the reaction mixture was heated to 11 °C for 21 h, then it was evaporated under vacuum (15 Hg), the residue was extracted by CH<sub>2</sub>Cl<sub>2</sub> (8 mL), the

negligible solid was filtered off. The CH<sub>2</sub>Cl<sub>2</sub>-extract was evaporated under vacuum (20 mm Hg), the residue was dissolved in benzene (6 mL), and hexane (12 mL) was added. The precipitated liquid phase was separated, washed by hexane (4 mL), dried under vacuum (2 mm Hg) giving *N*-*n*-octyloxy-*N*',*N*',*N*'-trimethylhydrazinium chloride (**1f**) as colorless hygroscopic solid (89 mg, 38 %). <sup>1</sup>H NMR (300 MHz, CDCl<sub>3</sub>) δ = 0.855 (3H, t, *J*=6.9 Hz, NO(CH<sub>2</sub>)<sub>7</sub>Me), 1.159–1.368 (10H, m, NOCH<sub>2</sub>CH<sub>2</sub>(CH<sub>2</sub>)<sub>5</sub>Me), 1.553–1.664 (2H, m, NOCH<sub>2</sub>CH<sub>2</sub>(CH<sub>2</sub>)<sub>5</sub>Me), 3.494 (9H, s, Me<sub>3</sub>N<sup>+</sup>), 3.911 (2H, t, *J*=6.3 Hz, NOCH<sub>2</sub>), 10.721 (1H, s, NHO). <sup>1</sup>H NMR (300 MHz, (CD<sub>3</sub>)<sub>2</sub>SO) δ = 0.850 (3H, t, *J*=6.3 Hz, NO(CH<sub>2</sub>)<sub>7</sub>Me), 1.204–1.344 (10H, m, NOCH<sub>2</sub>CH<sub>2</sub>(CH<sub>2</sub>)<sub>5</sub>Me), 1.489–1.604 (2H, m, NOCH<sub>2</sub>CH<sub>2</sub>(CH<sub>2</sub>)<sub>5</sub>Me), 3.248 (9H, s, Me<sub>3</sub>N<sup>+</sup>), 3.816–3.911 (1H, m, NOCH<sub>2</sub>), 3.952–4.029 (1H, m, NOCH<sub>2</sub>), 10.413 (1H, s, NHO). <sup>13</sup>C NMR (75 MHz, (CD<sub>3</sub>)<sub>2</sub>SO) δ = 13.90 (Me), 22.04, 25.17, 28.08, 28.58, 28.75, 31.19 (CH<sub>2</sub>), 50.37 (Me<sub>3</sub>N<sup>+</sup>), 76.78 (NOCH<sub>2</sub>). MS (FAB, *m/z*, I<sub>rel</sub>, (%)): 443 [2M<sup>+</sup>•Cl]<sup>+</sup> (2), 441 [2M<sup>+</sup>•Cl]<sup>+</sup> (6), 203 M<sup>+</sup> (100).

## RESULTS AND DISCUSSION

It has been found that methyl *N*-chloro-*N*-methoxycarbamate (**8a**) interacts with an excess of trimethylamine in MeCN forming of *N*-methoxy-*N*',*N*'-trimethylhydrazinium chloride (**1a**) as the main product (Scheme 4). Also, *N*,*N*'-dimethoxy-*N*,*N*'-di(methoxycarbonyl)hydrazine (**10a**) has been obtained as by-product in a relatively small yield. Ethyl *N*-chloro-*N*-methoxycarbamate (**9**) reacts with trimethylamine in MeCN producing *N*-methoxy-*N*',*N*'-trimethylhydrazinium chloride (**1a**) (Scheme 4).

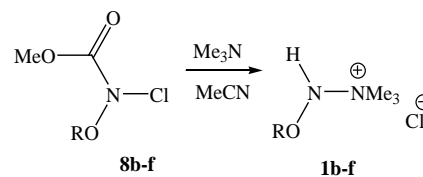


**Scheme 4.** Synthesis of *N*-methoxy-*N*',*N*'-trimethylhydrazinium chloride **1a** from methyl (**8a**) and ethyl (**9**) *N*-chloro-*N*-methoxycarbamates.

In a similar manner methyl *N*-alkoxy-*N*-chlorocarbamates (**8b-f**) react with trimethylamine yielding *N*-alkoxy-*N*',*N*'-trimethylhydrazinium chlorides (**1b-f**) (Scheme 5). The structure of the synthesized *N*-alkoxy-*N*',*N*'-trimethylhydrazinium chlorides (**1a-f**) has been confirmed by data of <sup>1</sup>H and <sup>13</sup>C NMR spectra and mass spectra.

In <sup>1</sup>H NMR spectra of compounds **1a-f** the characteristic chemical shifts of hydrogen atoms of Me<sub>3</sub>N<sup>+</sup> group are

observed at 3.2 – 3.3 ppm, and protons of NHO group in a low field are observed at 10.1 – 10.6 ppm (Table 1).



R = Et (**b**), *n*-Pr (**c**), *n*-Bu (**d**), Bn (**e**), *n*-C<sub>8</sub>H<sub>17</sub> (**f**)

**Scheme 5.** Synthesis of *N*-alkoxy-*N*',*N*'-trimethylhydrazinium chlorides **1b-f**.

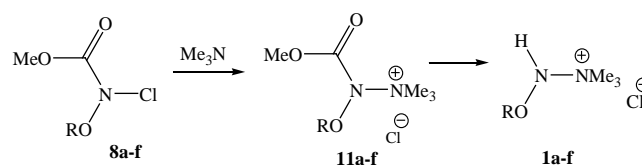
**Table 1.** The characteristic <sup>1</sup>H NMR chemical shifts of *N*-alkoxy-*N*',*N*'-trimethylhydrazinium chlorides (**1a-f**) in (CD<sub>3</sub>)<sub>2</sub>SO.

R	Resonance, σ, ppm	
	Me <sub>3</sub> N <sup>+</sup>	NHO
Me ( <b>1a</b> )	3.239	10.404
Et ( <b>1b</b> )	3.253	10.334
Pr ( <b>1c</b> )	3.252	10.438
<i>n</i> -Bu ( <b>1d</b> )	3.217	10.129
PhCH <sub>2</sub> ( <b>1e</b> )	3.314	10.629
<i>n</i> -C <sub>8</sub> H <sub>17</sub> ( <b>1f</b> )	3.248	10.413

**Table 2.** The characteristic <sup>13</sup>C NMR chemical shifts of *N*-alkoxy-*N*',*N*'-trimethylhydrazinium chlorides (**1a-f**) in (CD<sub>3</sub>)<sub>2</sub>SO

R	Resonance, σ, ppm	
	Me <sub>3</sub> N <sup>+</sup>	NOCH <sub>2</sub>
Me ( <b>1a</b> )	50.39	64.71 (Me)
Et ( <b>1b</b> )	50.27	72.24
Pr ( <b>1c</b> )	50.31	78.12
<i>n</i> -Bu ( <b>1d</b> )	50.41	76.53
PhCH <sub>2</sub> ( <b>1e</b> )	50.52	78.34
<i>n</i> -C <sub>8</sub> H <sub>17</sub> ( <b>1f</b> )	50.37	76.78

In <sup>13</sup>C NMR spectra of compounds **1a-f** the characteristic chemical shifts of carbon atoms of Me<sub>3</sub>N<sup>+</sup> group are observed at 50.3 – 50.5 ppm and NOCH<sub>2</sub> group at 72.2 – 78.3 ppm (Table 2). In the mass spectra the signals of M<sup>+</sup> ion are present. The signals of [2M•Cl]<sup>+</sup> ions are often observed as well. As the mechanism of compounds **1a-f** formation remains unclear, one may assume that it occurs in two stages (Scheme 6). At the first stage the unstable intermediates (**11a-f**) are formed by nucleophilic substitution at the nitrogen atom in *N*-alkoxy-*N*-chlorocarbamates **8,9** (Scheme 6). Then the intermediates **11a-f** produce *N*-alkoxy-*N*',*N*'-trimethylhydrazinium chlorides (**1a-f**) by the methoxycarbonyl group elimination.



R = Me (**a**), Et (**b**), *n*-Pr (**c**), *n*-Bu (**d**), Bn (**e**), *n*-C<sub>8</sub>H<sub>17</sub> (**f**)

**Scheme 6.** The possible route of *N*-alkoxy-*N*',*N*'-trimethylhydrazinium chlorides **1a-f** formation

This reaction is a new kind of the synthesis of *N*-alkoxy-*N'*,*N'*,*N'*-trimethylhydrazinium chlorides (**1a-f**), which confirms that this type of reactions can be performed.

## CONCLUSIONS

It has been found that the synthesis of *N*-alkoxy-*N'*,*N'*,*N'*-trimethylhydrazinium chlorides by the *N*-alkoxy-*N*-chlorocarbamates interaction with trimethylamine is possible.

## REFERENCES

- Shtamburg, V. G., Tsygankov, A. V., Shishkin, O. V., Zubatyuk, R. I., Shtamburg, V. V., Gerasimenko, M. V., Mazepa, A. V., Kostyanovsky, R. G., 1-Alkoxyamino-4-dimethylaminopyridinium derivatives as new representatives of O-N-N<sup>+</sup> geminal systems and their structure, *Mendeleev Commun.*, **2012**, 22(2), 92–94. <https://doi.org/10.1016/j.men.com.2012.02.014>
- Shtamburg, V. G., Shishkin, O. V., Zubatyuk, R. I., Shtamburg, V. V., Tsygankov, A. V., Mazepa, A. V., Kadorkina, G. K., Kostyanovsky, R. G., Synthesis and structure of *N*-alkoxyhydrazines and *N*-alkoxy-*N'*,*N'*,*N'*-trialkylhydrazinium salts, *Mendeleev Commun.*, **2013**, 23(5), 289–291. <https://doi.org/10.1016/j.men.com.2013.09.018>
- Shtamburg, V. G., Rudchenko, V. F., Nasibov, Sh. S., Chervin, I. I., Pleshkova, A. P., Kostyanovsky, R. G., Geminal Systems. Communication 16. Reactions of *N*-Chloro-*N*-alkoxyamines with Amines, *Bull. Acad. Sci. USSR. Div. Chem. Sci.*, **1981**, 30(10), 1914–1920. <https://doi.org/10.1007/BF00963422>
- Rudchenko, V. F., Shevchenko, V. I., Kostyanovsky, R. G., Geminal systems. Communication 29. Reaction of *N*-Chloro-*N*-methoxy-*N'*,*N'*-dimethylurea with *N*-Nucleophiles, *Bull. Acad. Sci. USSR. Div. Chem. Sci.*, **1986**, 35(3), 551–554. <https://doi.org/10.1007/BF00953223>
- Rudchenko, V. F., Kostyanovsky, R. G., Geminal oxygen-nitrogen-halogen systems. *N*-Halohydroxylamine derivatives, *Russ. Chem. Rev.*, **1998**, 67(3), 179–192. <https://doi.org/10.1070/RC1998v067n03ABEH000351>
- Glover, S. A., Anomeric Amides – Structure, Properties and Reactivity, *Tetrahedron*, **1998**, 54(26), 7229–7271. [https://doi.org/10.1016/S0040-4020\(98\)00197-5](https://doi.org/10.1016/S0040-4020(98)00197-5)
- Glover, S. A., Rauk, A., Conformational Stereochemistry of the HERON Amide, *N*-Methoxy-*N*-dimethylaminoformamide: A Theoretical Study, *J. Org. Chem.*, **1999**, 64(7), 2340–2345. <https://doi.org/10.1021/jo982048p>
- Glover, S. A., Chapter 18. *N*-Heteroatom-substituted hydroxamic esters, in *The Chemistry of Hydroxylamines, Oximes and Hydroxamic Acids*, Eds Rappoport, Z., Liebman, J. F., John Wiley and Sons, New York, **2009**, 839–923. <https://doi.org/10.1002/9780470741962.ch18>
- Glover, S. A., White, J. M., Rosser, A. A., Digianantonio, K. M. Structure of *N,N*-Dialkoxyamides: Pyramidal Anomeric Amides with Low Amidity, *J. Org. Chem.*, **2011**, 76, 9757–9763. <https://doi.org/10.1021/jo201856u>
- Glover, S. A., Rosser, A. A., Heteroatom Substitution at Amide Nitrogen – Resonance Reduction and HERON Reactions of Anomeric Amides, *Molecules*, **2018**, 23(11), 2834. <https://doi.org/10.3390/molecules23112834>
- Shtamburg, V. G., Shishkin, O. V., Zubatyuk, R. I., Kravchenko, S. V., Shtamburg, V. V., Distanov, V. B., Tsygankov, A. V., Kostyanovsky, R. G., Synthesis, structure and properties of *N*-alkoxy-*N*-(1-pyridinium)urea salts, *N*-alkoxy-*N*-acyloxyureas and *N,N*-dialkoxyureas, *Mendeleev Commun.*, **2007**, 17(3), 178–180. <https://doi.org/10.1016/j.men.com.2007.05.016>
- Shtamburg, V. G., Shtamburg, V. V., Tsygankov, A. V., Anishchenko, A. A., Zubatyuk, R. I., Shishkina, S. V., Mazepa, A. V., Klots, E. A., Synthesis and Structure of New *N*-Alkoxy-*N*-(1-pyridinium)urea Chlorides, *Eur. Chem. Bull.*, **2016**, 5(4), 142–146. <https://doi.org/10.17628/ECB.2016.5.142>
- Shtamburg, V. G., Shishkina, S. V., Shtamburg, V. V., Mazepa, A. V., Kadorkina, G. K., Kostyanovsky, R. G., 1-Alkoxyamino-4-dimethylaminopyridinium Salts: Synthesis and Structure, *Mendeleev Commun.*, **2016**, 26(2), 169–171. <https://doi.org/10.1016/j.men.com.2016.03.030>
- Shtamburg, V. G., Shtamburg, V. V., Kravchenko, S. V., Mazepa, A. V., Anishchenko, A. A., Posokhov, E. A., A New Synthesis of *N*-Alkoxyaminopyridinium Salts, *Bulletin of National University “KhPI”. Series: New solutions in modern technology*, **2017**(7), 211–218. <https://doi.org/10.20998/2413-4295.2017.07.30>
- Shtamburg, V. G., Anishchenko, A. A., Shishkina, S. V., Konovalova, I. S., Shtamburg, V. V., Mazepa, A. V., Kravchenko, S. V., 1-(*N*-Ethoxycarbonyl-*N*-isopropoxy)amino-dimethylaminopyridinium Chloride. Synthesis and Structure, *Eur. Chem. Bull.*, **2017**, 6(10), 470–474. <https://doi.org/10.17628/ecb.2017.6.470-474>
- Shtamburg, V. G., Tsygankov, A. V., Klots, E. A., Fedyanin, I. V., Lyssenko, K. A., Kostyanovsky, R. G., *N,N*-Dimethoxy-*N*-tert.-alkylamines: New Synthesis Methods and Crystal Structure of Precursor, *Mendeleev Commun.*, **2006**, 16(2), 84–85. <https://doi.org/10.1070/MC2006v016n02ABEH002222>
- Shtamburg, V. G., Shtamburg, V. V., Anishchenko, A. A., Kravchenko, S. V., Mazepa, A. V., Klots, E. A., Decarbamylation of *N*-Alkoxy-*N*-(4-dimethylaminopyridin-1-ium-1-yl)urea Chlorides in Dimethylsulfoxide as A Route to 1-Alkoxyamino-4-dimethylaminopyridinium Chlorides, *Eur. Chem. Bull.*, **2018**, 7(9), 267–271. <https://doi.org/10.17628/ecb.2018.7.267-271>
- Shtamburg, V. G., Rudchenko, V. F., Nasibov, Sh. S., Chervin I. I., Kostyanovsky, R. G., *N*-Chloro-*N*-methoxyuretilane, *Russ. Chem. Bull., Int. Ed.*, **1981**, 30(2), 423–426. <https://doi.org/10.1070/RC1981v030n02ABEH000423>
- Shtamburg, V. G., Klots, E. A., Pleshkova, A. P., Avramenko, V. I., Ivonin, S. P., Tsygankov, A. V., Kostyanovsky, R. G., Geminal systems. 50. Synthesis and alcoholysis on *N*-acyloxy-*N*-alkoxy derivatives of ureas, carbamates and benzamide, *Russ. Chem. Bull., Int. Ed.*, **2003**, 52(10), 2251–2260. <https://doi.org/10.1023/B:RUCB.0000011887.405.29.b0>
- Shtamburg, V. G., Kostyanovsky, R. G., Tsygankov, A. V., Shtamburg, V. V., Shishkin, O. V., Zubatyuk, R. I., Mazepa, A. V., Kravchenko, S. V., Geminal Systems. Communication 64. *N*-Alkoxy-*N*-chloroureas and *N,N*-Dialkoxyureas, *Russ. Chem. Bulletin. Intern. Ed.*, **2015**, 64(1), 62–75. <https://doi.org/10.1007/s11172-015-0822-9>
- Shtamburg, V. G., Anishchenko, A. A., Shtamburg, V. V., Tsygankov, A. V., Kostyanovsky, R. G., Alcoholysis of *N*-Acetoxy-*N*-alkoxycarbamates. Synthesis of *NH,N,N*-Dialkoxyamines from *N,N*-Dialkoxyureas, *Eur. Chem. Bull.*, **2014**, 3(12), 1119–1125. <https://doi.org/10.17628/ecb.2014.3.1119-1125>

Received: 30.10.2019.

Accepted: 26.01.2020.





# GREEN SYNTHESIS OF QUINOXALINE DERIVATIVES AT ROOM TEMPERATURE IN ETHYLENE GLYCOL WITH H<sub>2</sub>SO<sub>4</sub>/SiO<sub>2</sub> CATALYST

Mozhgan Bashirzadeh<sup>[a]</sup> and Farahnaz K. Behbahani<sup>[a]\*</sup>

**Keywords:** Quinoxalines, sulfuric acid/SiO<sub>2</sub> catalyst, diketones, phenylene diamine, green synthesis

In this study, the preparation of quinoxaline derivatives using  $\alpha$ -diketones, 1,2-phenylene diamines in the presence of H<sub>2</sub>SO<sub>4</sub>/SiO<sub>2</sub> catalyst in ethylene glycol and at room temperature is reported. The advantages of this method are high yields of the products, utilizing of reusable catalyst, easy separation and mild reaction conditions. Also, reusability of the catalyst was investigated and found that catalytic activity of the catalyst did not decreased after 4th times.

\* Corresponding Authors

E-Mail: Farahnazkargar@yahoo.com

[a] Department of Chemistry, Karaj Branch, Islamic Azad University, Karaj, Iran. P.O.Box: 314/85313

## INTRODUCTION

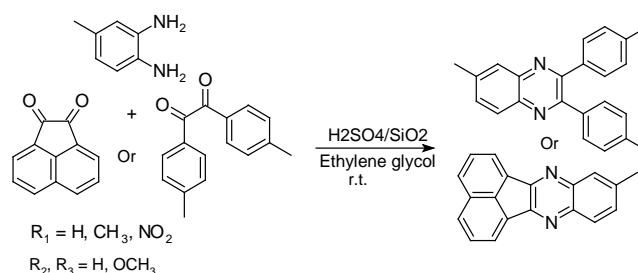
Quinoxaline derivatives are well known in the pharmaceutical industry and have been shown to have a broad spectrum of biological activities including antibacterial, antiviral, anti-inflammatory, anticancer, and kinase inhibitory activities.<sup>1,2</sup> In addition, quinoxaline derivatives have been evaluated as semiconductors, dyes, and biocides.<sup>3</sup> In this regards, a very procedures have respectively been developed for the preparation of substituted quinoxalines.<sup>4,5</sup>

In these methods the condensation reaction between an aryl 1,2-diamine with a 1,2-dicarbonyl compound have been reported<sup>4</sup>. The others synthetic routes towards quinoxalines, including oxidative coupling of epoxides with ene-1,2-diamines using Bi-catalyst, heteroannulation of nitroketene and N,S-aryliminoacetals with POCl<sub>3</sub>, cyclization of  $\alpha$ -arylimino oximes of  $\alpha$ -dicarbonyl compounds and from  $\alpha$ -hydroxy ketones via a tandem oxidation process using Pd(OAc)<sub>2</sub> or RuCl<sub>2</sub>-(PPh<sub>3</sub>)<sub>3</sub>-TEMPO as well as MnO<sub>2</sub>.<sup>5</sup>

Most of the existing methodologies suffer from disadvantages such as the use of volatile organic solvents, unsatisfactory product yields, critical product isolation procedures, expensive and detrimental metal precursors and harsh reaction conditions, which limit their use under the aspect of environmentally benign processes. Also silica-supported reagent, H<sub>2</sub>SO<sub>4</sub>/SiO<sub>2</sub> for its ease of preparation, low cost, high efficiency and environmental benignness,<sup>6</sup> has already been used in cycloadditions,<sup>7</sup> Beckmann rearrangements,<sup>8</sup> glycosylations,<sup>9</sup> condensations,<sup>10</sup> esterification,<sup>11</sup> acetylation of (+)cedrol compound,<sup>12</sup> synthesis of 2,4,5-triaryl-1H-imidazoles,<sup>13</sup> and as catalyst in organic transformations: a comprehensive review.<sup>14</sup>

On the other hand, during our continuing efforts to develop convenient approaches to synthesize heterocycle compounds,<sup>15</sup> we revealed that H<sub>2</sub>SO<sub>4</sub>/SiO<sub>2</sub> was a high-

efficient and recyclable catalyst for preparing the quinoxaline derivatives in a synthetically practical procedure (stoichiometric ratios of starting materials and short reaction times) with relatively widely functional group compatibility in ethylene glycol at ambient temperature (Scheme 1).



**Scheme 1** Synthesis of quinoxaline derivatives in the presence of H<sub>2</sub>SO<sub>4</sub>/SiO<sub>2</sub>

## RESULTS AND DISCUSSION

To achieve efficient amount of catalyst, the author set up a model reaction using benzil (2.0 mmol), and 1,2-phenylene diamine (2.0 mmol) in ethylene glycol (3.0 ml) without catalyst at room temperature. In this case, the product was obtained in low yield (30%). As shown in table 1, the yield of reaction was increased in the presence of the catalyst (0.1 - 0.3 g) and raising catalyst amount toward 0.4 g did not affect to reaction yield.

**Table 1.** Optimizing of the catalyst amount for the synthesis of quinoxaline derivatives

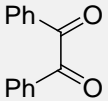
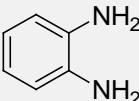
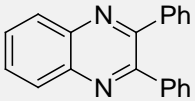
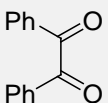
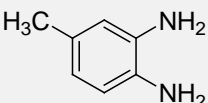
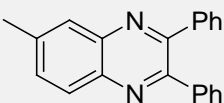
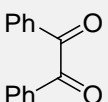
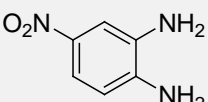
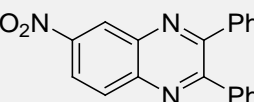
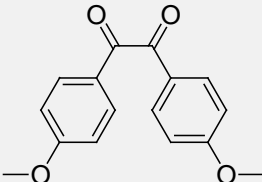
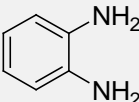
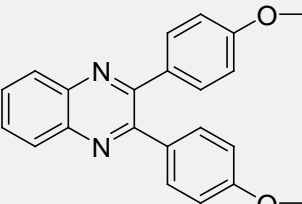
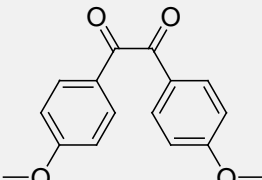
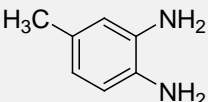
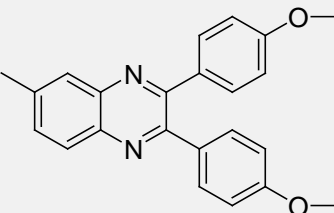
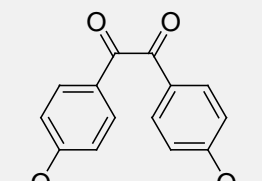
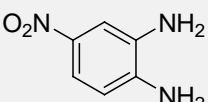
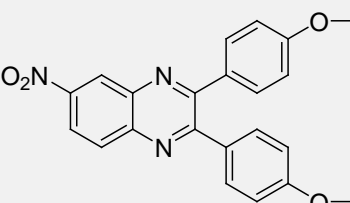
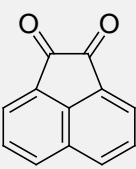
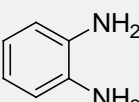
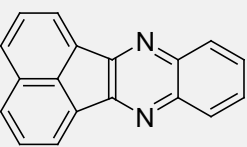
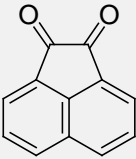
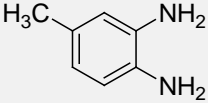
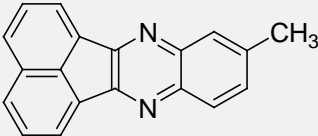
Catalyst g	Yield% <sup>a</sup>
Free	30
0.1	50
0.2	55
0.3	92
0.4	92

<sup>a</sup>Reaction condition: Benzil (2.0 mmol), 1,2-phenylenediamine (2.0 mmol) and catalyst in ethylene glycol (3.0 ml) at room temperature

When we examined model reaction (entry 1, table 2) in the presence of SiO<sub>2</sub>, the desired product was obtained in very low yield (< 10 %), but the product was resulted in 90% using H<sub>2</sub>SO<sub>4</sub> in similar condition as well as sulfuric acid/SiO<sub>2</sub> combination. Therefore, we decided to use sulfuric acid/SiO<sub>2</sub> combination due to its safe, to be solid and its reusability than H<sub>2</sub>SO<sub>4</sub> alone that is dangers and corrosive.

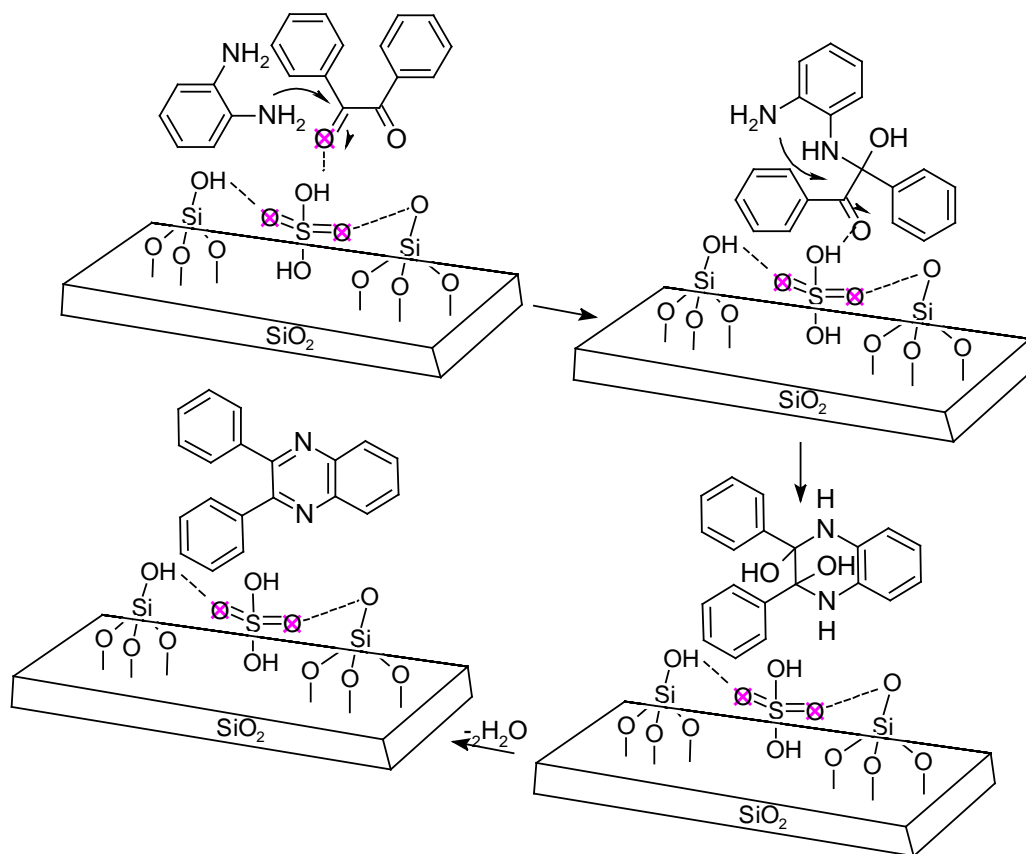
To evaluate the efficiency of this methodology, a number of 1,2-dicarbonyl compounds and 1,2-diamines were further subjected to condensation using very low amount of H<sub>2</sub>SO<sub>4</sub>/SiO<sub>2</sub> (Table 2). When the electron-donating substituents present in diamine part, decreased reaction time, whereas the effect is reverse with the electron withdrawing substituents.

**Table 2.** Synthesis of quinoxaline derivatives in the presence of H<sub>2</sub>SO<sub>4</sub>/SiO<sub>2</sub> in ethylene glycol

1,2-Diketone	Amine	Product	Time, h	Yield, %	m.p., °C
			3.0	92	124-126 <sup>16</sup>
			2.5	88	110-114 <sup>16</sup>
			4.0	85	168-172 <sup>16</sup>
			3.5	88	145-148 <sup>17</sup>
			3.0	90	132-134 <sup>17</sup>
			4.0	85	193-195 <sup>18</sup>
			2.5	92	240-243 <sup>19</sup>
			2.0	90	239-241 <sup>19</sup>

On the other hand, electron-donating substituents with aromatic 1,2-diketone increased reaction time and the effect is reverse with electron withdrawing groups.

Proposed mechanism for the preparation of quinoxaline derivatives in the presence of  $\text{H}_2\text{SO}_4/\text{SiO}_2$  has been shown in Scheme 2.



**Scheme 2.** Suggested mechanism for the synthesis of quinoxaline derivatives using  $\text{H}_2\text{SO}_4/\text{SiO}_2$

## EXPERIMENTAL

Melting points were measured by using the capillary tube method with an electro thermal 9200 apparatus. IR spectra were recorded on Perkin Elmer FT-IR spectrometer did scanning between  $4000\text{--}400\text{ cm}^{-1}$ .  $^1\text{H}$  NMR spectra were obtained on Bruker DRX-300MHz NMR instrument in  $\text{CDCl}_3$ . Analytical TLC of all reactions was performed on Merck precoated plates (silica gel 60F-254 on aluminum). All compounds are known and spectra and physical data were compared with those of authentic samples.<sup>16-19</sup> The catalyst was prepared according to the reported procedure in the literature.<sup>20</sup>

### Preparation of quinoxaline derivatives using $\text{H}_2\text{SO}_4/\text{SiO}_2$ : general procedure:

To a mixture of an appropriate *o*-phenylenediamine (1 mmol, 0.108 g) and a 1,2-dicarbonyl compound (1 mmol) in ethylene glycol (3 ml), a catalytic amount of  $\text{H}_2\text{SO}_4/\text{SiO}_2$  (0.3 g) was added and the mixture was stirred at room

temperature. The progress of the reaction was monitored by TLC (ethyl acetate:n-hexane, 1:3). After completion of the reaction, chloroform (10 ml) was added to the solidified mixture in order to separation of catalyst from the mixture since the catalyst is not soluble in organic solvent. The residue was then diluted with  $\text{H}_2\text{O}$  (15 mL) and the product was extracted with chloroform ( $2 \times 10\text{ mL}$ ). The combined organic layers was dried over  $\text{Na}_2\text{SO}_4$ . The solvent was evaporated under reduced pressure and the pure product was obtained without any further purification.

A variety of substituted *o*-phenylenediamines were condensed with different 1,2-dicarbonyl compounds. The results are shown in Table 2.

### 2,3-Diphenylquinoxaline

White solid, IR (KBr,  $\text{cm}^{-1}$ ): 3055, 1541, 1495, 1477, 1441, 1346, 1315.  $^1\text{H}$  NMR ( $\text{CDCl}_3$ , 300 MHz): 8.16-8.20 (m, 2H), 7.76 -7.79 (m, 2H), 7.56-7.50 (m, 4H), 7.25-7.29 (m, 6H).

**6-Methyl-2,3-diphenylquinoxaline**

Light yellow solid, IR (KBr,  $\text{cm}^{-1}$ ): 3055, 2941, 1619, 1554, 1485, 1444, 1393, 1344.  $^1\text{H}$  NMR ( $\text{CDCl}_3$ , 300 MHz): 2.63 (s, 3H), 7.25-7.35 (m, 5H), 7.45-7.55 (m, 5H), 7.89-8.08 (m, 3H).

**6-Nitro-2,3-diphenylquinoxaline**

Light brown solid, IR (KBr,  $\text{cm}^{-1}$ ): 3433, 3328, 3055, 1658, 1521, 1434, 1398, 1337.  $^1\text{H}$  NMR ( $\text{CDCl}_3$ , 300 MHz): 7.30-7.45 (m, 6H), 7.95 (d, 4H), 8.25 (d, 1H), 8.54 (d, 1H), 9.08 (s, 1H).

**2,3-Bis(4-methoxyphenyl)quinoxaline**

White solid, IR (KBr,  $\text{cm}^{-1}$ ): 3054, 2926, 2871, 2349, 1743, 1441.  $^1\text{H}$  NMR ( $\text{CDCl}_3$ , 300 MHz): 3.85 (s, 6H), 6.89 (d, 4H), 7.5 (d, 4H), 7.74 (q, 2H), 8.14 (q, 2H).

**2,3-Bis(4-methoxyphenyl)-6-methylquinoxaline**

Light yellow solid, IR (KBr,  $\text{cm}^{-1}$ ): 3054, 2922, 1955, 1810, 1735, 1614.  $^1\text{H}$  NMR ( $\text{CDCl}_3$ , 300 MHz): 2.61 (s, 3H), 3.84 (s, 6H), 6.88 (d, 4H), 7.48 (d, 4H), 7.56 (d, 1H), 7.91 (s, 1H), 8.03-8.0 (d, 1H).

**2,3-Bis(4-methoxyphenyl)-6-nitroquinoxaline**

Yellowish brown solid, IR (KBr,  $\text{cm}^{-1}$ ): 3055, 3027, 1950, 1659, 1540, 1477.  $^1\text{H}$  NMR ( $\text{CDCl}_3$ , 300 MHz): 3.73 (s, 6H), 6.98 (m, 4H), 7.56 (m, 4H), 8.24 (d, 1H), 8.49 (d, 1H), 9.1 (d, 1H).

**Acenaphtho[1,2-*b*]quinoxaline**

Yellow solid, IR (KBr,  $\text{cm}^{-1}$ ): 3051, 2926, 1613, 1588, 1528, 1497, 1418, 1343.  $^1\text{H}$  NMR ( $\text{CDCl}_3$ , 300 MHz): 8.37-8.40 (m, 2H), 8.18-8.21 (m, 2H), 8.05-8.08 (m, 2H), 7.78-7.83 (m, 2H), 7.73-7.76 (m, 2H).

**9-Methylacenaphtho[1,2-*b*]quinoxaline**

Light Brown solid, IR (KBr,  $\text{cm}^{-1}$ ): 3051, 2909, 2861, 1719, 1613, 1585, 1483, 1419.  $^1\text{H}$  NMR ( $\text{CDCl}_3$ , 300 MHz): 2.56 (s, 3H), 7.49 (d, 1H, Ar-H), 7.70 (t, 2H, Ar-H), 7.88 (s, 1H, Ar-H), 7.94 (d, 2H, Ar-H), 7.99 (d, 1H, Ar-H), 8.27 (t, 2H, Ar-H).

**Reusability of the catalyst**

At the end of the reaction, the catalyst could be successfully recovered by a simple filtration. The removed catalyst was washed with chloroform, dried at 80 °C for 1 h and reused up to four times in the others reactions without appreciable reduction in the catalytic activity.

**CONCLUSIONS**

In conclusion, an efficient catalytic method for the synthesis of quinoxaline derivatives using sulfuric acid adsorbed on silica gel as catalyst in ethylene glycol at room temperature is reported. The catalyst can be reused after a simple work-up, with a gradual decline of its activity being observed.

**REFERENCES**

- <sup>1</sup>Jaso, A., Zarranz, B., Aldana, I., Monge, A. Synthesis of new quinoxaline-2-carboxylate 1, 4-dioxide derivatives as anti-mycobacterium tuberculosis agents. *J. Med. Chem.*, **2005**, *48*, 2019-2025. <https://doi.org/10.1021/jm049952w>
- <sup>2</sup>Toshima, K., Ozawa, T., Kimura, T., Matsumara, S. The significant effect of the carbohydrate structures on the DNA photocleavage of the quinoxaline-carbohydrate hybrids. *Bioorg. Med. Chem. Lett.*, **2004**, *14*, 2777-2779. <https://doi.org/10.1016/j.bmcl.2004.03.065>
- <sup>3</sup>Sarges, R., Howard, H. R., Browne, R. G., Lebel, L. A., Seymour, P. A. Sarges, R., Howard, H. R., Browne, R. G., Lebel, L. A., Seymour, P. A., & Koe, B. K. (1990). 4-Amino [1,2,4] triazolo[4,3-*a*]quinoxalines. A novel class of potent adenosine receptor antagonists and potential rapid-onset antidepressants. *J. Med. Chem.*, **1990**, *33*, 2240-2254. <https://doi.org/10.1021/jm00170a031>
- <sup>4</sup>Darabi H. R., Tahoori, F., Aghapoor, K., Taala, F., Mohsenzadeh, F.  $\text{NH}_4\text{Cl}-\text{CH}_3\text{OH}$ : an efficient, acid-and metal-free catalyst system for the synthesis of quinoxalines. *J. Braz. Chem. Soc.* **2008**, *19*, 1646-1652. <http://dx.doi.org/10.1590/S0103-50532008000800028>
- <sup>5</sup>Antonioti, S., Dunach E. Direct and catalytic synthesis of quinoxaline derivatives from epoxides and ene-1, 2-diamines. *Tetrahedron Lett.*, **2002**, *43*, 3971-3973. [https://doi.org/10.1016/S0040-4039\(02\)00715-3](https://doi.org/10.1016/S0040-4039(02)00715-3)
- <sup>6</sup>Marziano N. C., Ronchin L., Tortato C., Ronchin S., Vavasori A. Selective oxidations by nitrosating agents: Part 2: Oxidations of alcohols and ketones over solid acid catalysts. *J. Mol. Catal. A-Chem.*, **2005**, *235*, 26-34. <https://doi.org/10.1016/j.molcata.2005.03.008>
- <sup>7</sup>Du Z., Si C., Li Y., Wang Y., Lu J. Improved synthesis of 5-substituted 1H-tetrazoles via the [3+2] cycloaddition of nitriles and sodium azide catalyzed by silica sulfuric acid. *Int. J. Mol. Sci.*, **2012**, *13*, 4696-4703. <https://doi.org/10.3390/ijms13044696>
- <sup>8</sup>Marziano N. C., Ronchin L., Tortato C., Vavasori A., Badetti C. Catalyzed Beckmann rearrangement of cyclohexanone oxime in heterogeneous liquid/solid system: Part 1: Batch and continuous operation with supported acid catalysts. *J. Mol. Catal. A-Chem.*, **2007**, *277*, 221-232. <https://doi.org/10.1016/j.molcata.2007.07.046>
- <sup>9</sup>Zhou J. F., Chen X. A., Wang Q. B., Zhang B., Zhang L. Y., Yusulf A., Wang Z. F., Zhang J. B., Tang J.  $\text{H}_2\text{SO}_4\text{-SiO}_2$ : Highly efficient and novel catalyst for the Ferrier-type glycosylation. *Chin. Chem. Lett.*, **2010**, *21*, 922-926. <https://doi.org/10.1016/j.ccllet.2010.03.013>
- <sup>10</sup>Zhang Y., Liangv, Shang Z. Fast and Eco-friendly Synthesis of Dipyrromethanes by  $\text{H}_2\text{SO}_4\text{-SiO}_2$  Catalysis under Solvent-free Conditions. *Chin. J. Chem.*, **2010**, *28*, 259-262. <https://doi.org/10.1002/cjoc.201090063>
- <sup>11</sup>Chakraborti A. K., Singh B., Chankeshwara S. V., Patel A. R. Protic acid immobilized on solid support as an extremely efficient recyclable catalyst system for a direct and atom economical esterification of carboxylic acids with alcohols. *J. Org. Chem.*, **2009**, *74*, 5967-5974. <https://doi.org/10.1021/jo900614s>



- <sup>12</sup>Elvia R., Cahyana A. H., Wibowo W. Catalytic acetylation of (+)-cedrol with heterogeneous catalyst H<sub>2</sub>SO<sub>4</sub>/SiO<sub>2</sub> under solvent free conditions. *Chem. Inter.*, **2015**, *1*, 196-201.
- <sup>13</sup>Maleki, B., Shirvan, H. K., Taimazi, F., & Akbarzadeh, E. (2012). Sulfuric acid immobilized on silica gel as highly efficient and heterogeneous catalyst for the one-pot synthesis of 2,4,5-triaryl-1H-imidazoles. *Int. J. Org. Chem.*, **2012**, *2*, 93-99. <http://dx.doi.org/10.4236/ijoc.2012.21015>
- <sup>14</sup>Kaur M., Sharma S., Bedi P. M. S. Silica supported Brönsted acids as catalyst in organic transformations: A comprehensive review. *Chin. J. Catal.*, **2015**, *36*, 520-549. [https://doi.org/10.1016/S1872-2067\(14\)60299-0](https://doi.org/10.1016/S1872-2067(14)60299-0)
- <sup>15</sup>Behbahani, F. K., Naeini, S., Suzangarzadeh, S. FePO<sub>4</sub>-catalyzed synthesis of β-amido carbonyl compounds, *Eur. Chem. Bull.*, **2013**, *2*(11), 832-835; <http://dx.doi.org/10.17628/ecb.2013.2.832-835>; Behbahani, F. K., Mohammadlo, M. L-Proline-catalyzed synthesis of fused dihydropyridines through Hantzsch. *Eur. Chem. Bull.*, **2013**, *2*(11), 916-919; <http://dx.doi.org/10.17628/ecb.2013.2.916-919>; Behbahani, F. K., Mohammadi Ziarani, L. One pot three-component Mannich reaction Promoted by iron (III) phosphate. *Eur. Chem. Bull.*, **2013**, *2*(10), 782-784; <http://dx.doi.org/10.17628/ecb.2013.2.782-784>. Behbahani, F. K., Lotfi, A. Catalytic performance of SiO<sub>2</sub>-supported Fe(ClO<sub>4</sub>)<sub>3</sub>·6H<sub>2</sub>O in synthesis of 2-substituted benzimidazoles. *Eur. Chem. Bull.*, **2013**, *2*(9), 694-697. <http://dx.doi.org/10.17628/ecb.2013.2.694-697>.
- <sup>16</sup>Cai J. J., Zou J. P., Pan X. Q., Zhang W. Gallium (III) triflate-catalyzed synthesis of quinoxaline derivatives. *Tetrahedron Lett.*, **2008**, *49*, 7386-7390. <https://doi.org/10.1016/j.tetlet.2008.10.058>
- <sup>17</sup>Hasaninejad A., Zare A., Mohammadzadeh M. R., Shekouhy M. Oxalic acid as an efficient, cheap, and reusable catalyst for the preparation of quinoxalines via condensation of 1, 2-diamines with α-diketones at room temperature. *ARKIVOC*, **2008**, *13*, 28-35. <https://doi.org/10.3998/ark.5550190.0009.d04>
- <sup>18</sup>Mohammadi Ziarani G., Badiei A., Haddadpour M. Application of sulfonic acid functionalized nanoporous silica (SBA-Pr-SO<sub>3</sub>H) for one-pot synthesis of quinoxaline derivatives. *Inter. J. Chem.*, **2011**, *3*, 87. <https://doi.org/10.5539/ijc.v3n1p87>
- <sup>19</sup>Niknam K., Saberi D., Mohagheghnejad M. Silica bonded S-sulfonic acid: a recyclable catalyst for the synthesis of quinoxalines at room temperature. *Molecules*, **2009**, *14*, 1915-1926. <https://doi.org/10.3390/molecules14051915>.
- <sup>20</sup>Montazeri N. Sulfuric Acid Impregnated on Silica Gel (H<sub>2</sub>SO<sub>4</sub>/SiO<sub>2</sub>): A Versatile and reusable Catalyst for the Synthesis of 1, 2, 4-Triazolo [5, 1-b][1, 3] thiazin-7-ones. *Asian J. Chem.*, **2010**, *22*, 7432-7434.

Received: 26.07.2019

Accepted: 11.11.2019.